Diode laser modules based on laser-machined, multi-layer ceramic substrates with integrated water cooling and micro-optics

Alberto Campos Zatarain

Submitted for the degree of Doctor of Philosophy

Heriot-Watt University

School of Engineering and Physical Sciences

May, 2012

ABSTRACT

This thesis presents a study on the use of low temperature co-fired ceramic (LTCC) material as a new platform for the packaging of multiple broad area single emitter diode lasers. This will address the recent trend in the laser industry of combining multiple laser diodes in a common package to reach the beam brightness and power required for pumping fibre lasers and for direct-diode industrial applications, such as welding, cutting, and etching. Packages based on multiple single emitters offer advantages over those derived from monolithic diode bars such as higher brightness, negligible thermal crosstalk between neighbouring emitters and protection against cascading failed emitters. In addition, insulated sub-mounted laser diodes based on telecommunication standards are preferred to diode bars and stacks because of the degree of assembly automation, and improved lifetime. At present, lasers are packaged on Cu or CuW platforms, whose high thermal conductivities allow an efficient passive cooling. However, as the number of emitters per package increases and improvements in the laser technology enable higher output power, the passive cooling will become insufficient. To overcome this problem, a LTCC platform capable of actively removing the heat generated by the lasers through impingement jet cooling was developed. It was provided with an internal water manifold capable to impinge water at 0.15 $lmin^{-1}$ flow rate on the back surface of each laser with a variation of less than 2 °C in the temperature between the diodes. The thermal impedance of 2.7°C/W obtained allows the LTCC structure to cool the latest commercial broad area single emitter diode lasers which deliver up to 13 W of optical power. Commonly, the emitters are placed in a "staircase" formation to stack the emitters in the fast-axis, maintaining the brightness of the diode lasers. However, due to technical difficulties of machining the LTCC structure with a staircase-shaped face, a novel out-plane beam shaping method was proposed to obtain an elegant and compact free space combination of the laser beam on board using inexpensive optics. A compact arrangement was obtained using aligned folding mirrors, which stacked the beams on top of each other in the fast direction with the minimum dead space.

A mis padres y hermanas

ACKNOWLEDGEMENTS

I would like to thank all the wonderful people who helped, supported and motivated me during the preparation of this doctoral thesis.

First of all, I would like to thank my supervisor Professor Howard J. Baker for his support, guidance and patience during this project. I am also grateful to Professor Denis R. Hall for his valuable comments. I thank Dr. Roy McBride for his help during the first stage of the project. I express my sincere thanks to Dr. Aaron M. McKay for his support without which this work would not have been successful. Finally, I thank The National Council on Science and Technology (CONACYT) of Mexico for providing the funding for my studies.

I wish to thank my parents, Manuel Alberto y María Del Carmen, and sisters Claudia, Karla and Lorena for their love, support and encouragement throughout this challenging journey. I love you.

Thanks to my friends Berenice, Edith, Gabriela, Irina, Karina, Marine, Nadezhda, Natalia, Paola, Antonio, Carlos, Daniel, Jesus, Omar and Roberto who are always there when I need them. Thank you for the good times. Finally, I would like to thank Morag for her moral support.

DECLARATION STATEMENT

(Research Thesis Submission Form should be placed here)

TABLE OF CONTENTS

LIST OF ACRONYMS

AOM: Acousto-Optic Modulator

BA: Broad Area

BPP: Beam Parameter Product

CAD: Computer-Aided Design

CCP: Conduction-Cooled Package

CNC: Computer Numerical Control

COD: Catastrophic Optical Damage

CTE: Coefficient of Thermal Expansion

CVD: Chemical Vapour Deposition

CW: Continuous Wave

DH: Double Heterostructure

DXF: Data Exchange File

EFL: Effective Focal Length

FAC: Fast-Axis Collimator

FEA: Finite Element Analysis

FL: Focal Length

FW: Full Width

FWHM: Full Width at Half Maximum

HAZ: Heat Affected Zone

HPDL: High Power Diode Laser

HR: High-Reflection

HTCC: High Temperature Co-fired Ceramic

IC3: ICE-CUBED

IMAPS: International Microelectronics and Packaging Society

IR: Infrared

LTCC: Low Temperature Co-fired Ceramic

MBE: Molecular Beam Epitaxy

MCC: Micro-Channel Cooler

MDS: Modular Diode Laser Systems, research program in Germany

MEMS: Micro-Electro-Mechanical Systems, Heriot-Watt University

MISEC: MicroSystems Engineering Centre

MOCVD: Metal Organic Chemical Vapour Deposition

MOVPE: Metal Organic Vapour Phase Epitaxy

NIR: Near Infrared

NOVALAS: Innovative Laser Systems Based on Diode Lasers, research program in Germany

OXC: Optical Cross-Connect

PAS: Pressure Assisted Sintering

PIB: Power-in-the-Bucket

PID: Proportional-Integral-Derivative

PLAS: Pressureless Constrained Sintering

PSO: Position Synchronized Output

PSU: Power Supply Unit

QCW: Quasi Continuous Wave

QW: Quantum Well

SHEDS: Super High Efficiency Diode Sources, research program in USA

SMA: Sub Multi Assembly

SVM: Sacrificial Volume Material

TEA: Transversely Excited Atmospheric

TFM: Thick Film Multilayer

UV: Ultraviolet

PUBLICATIONS

A. Campos-Zatarain, A. McKay, H. J. Baker, D. R. Hall, and M. Desmulliez, "High-Quality CO_2 Laser Machining of LTCC Structures for Thermal Management of a Group of Single-Emitter Laser Diodes," in Proceedings of IMAPS 2009 42nd International Symposium on Microelectronics, San Jose, CA, USA, 2009, pp. 452-458.

A. Campos-Zatarain, A. M. McKay, and H. J. Baker, “Design, Fabrication and Characterization of a LTCC Cooling Structure Suitable for Diode Laser Technology”, to be submitted to International Journal of Applied Ceramic Technology.

A. Campos-Zatarain, A. M. McKay, and H. J. Baker, “Beam combining of single emitter diode lasers placed on multi-layer ceramic substrate with integrated water cooling and micro-optics”, in preparation.

CHAPTER 1
INTRODUCTION

1.1 Motivation

A recent trend in industry is to fabricate high-power laser diode modules, to achieve the beam brightness and power required for pumping fibre lasers and material processing. For this, groups of single-emitter broad-area (BA) laser diodes which are passively cooled in a common package are used. Insulated, sub-mounted BA laser diodes based on telecommunication standards are preferred to diode bars and stacks because of the degree of assembly automation, and improved lifetime. Single-emitter laser diodes are limited to low powers, typically less than 15 W. However further brightness and output power improvements in BA diodes mean that current passive cooling methods will be insufficient and the challenge becomes to efficiently deal with the localised heat sources by an active cooling approach.

1.2 Objective

To build a platform in low temperature co-fired ceramic *(LTCC*), which is a material recently used for optical packaging, but known for more than 20 years in the electronics industry. This platform should be capable of accommodating multiple BA diode lasers and passive optical components, as lenses and mirrors. It must provide metallization for high current and effective localized water cooling for removing the heat generated by the BA diode lasers.

1.3 Review of High-Power Diode Laser Technology

Single emitter diode lasers with a continuous wave (*CW*) output powers greater than 0.5 W are referred as high power diode lasers (*HPDLs*). First diode lasers were simple homojunction devices consisting of GaAs with an active region determined by the diffusion length, typically 2 µm thick [1]. Modern commercial diode lasers consist of a double heterostructure (DH) with quantum wells (*QWs*) as active region; commonly, the QW is a thin layer of InGaAs with a thickness of 10 nm. The insertion of quantum wells in the structure allows low threshold current densities, high efficiencies, high output power, and low temperature dependence [1]. InGaAs is embeded in AlGaAs layers which provide optical confinement and have a larger band gap but almost the same lattice constant as GaAs. The band gap offsets provide enough confinement, normally >100 meV, to reduce the leakage of carriers due to thermal excitation.

During the last 20 years improvements in the design and manufacturing process of diode lasers have allowed higher outputs and higher power-conversion efficiencies. This has permitted their transition from being a scientific device to a powerful industrial tool. HPDLs evolved from low-power diode lasers, which were conceived for data-storage and communication purposes in the 1980's. In the 1990's, improvements in the two main epitaxial growth techniques, molecular beam epitaxy (*MBE*) and metal organic vapour phase epitaxy (*MOVPE*), allowed the fabrication of diode bars with output powers greater than 20 W and 10,000 hours of lifetime [2]. But it was not until the last decade, that advances in diode laser technology, specially under the projects SHEDS (Super High Efficiency Diode Sources) [3] in USA and NOVALAS (Innovative Laser Systems Based on Diode Lasers) [4] and MDS (Modular Diode Laser Systems) [5] in Germany, allowed the HPDL to become a fundamental part in laser systems used in materials processing, medical and pumping applications. The main advantages of systems based on HPDL are a low cost per watt, high efficiency and compact size.

The increase of output power of single emitters and the arrangement of multiple emitters in a monolithic semiconductor bar (*diode bar*) have been the main directions in high power diode technology to reach higher output powers. According to Strohmaier [6] state of the art HPDL broad area single emitters can produce a maximum power greater than 20 W with reliable powers in the range 10-12 W. On the other hand, diode bars are capable of delivering several hundreds of watts. For example Knapczyk [7] in 2011 reported an output of 960 W with an efficiency of 70 %, the maximum output powers in commercial products are 200 W in CW and 320 W in QCW. If output powers in the order of kW are required, multiple bars are stacked.

1.4 Broad Area Single Emitters

According to Paschke [8], the preferred HPDL for pumping is the broad area (*BA*) single emitter because of its high efficiency and non complex manufacturing process. BA single emitters are edge-emitting diode lasers with a wide emitting region, typically, in the order of 100 µm and optical confinement layers in the range of 1 to 4 µm. Because of this geometry, the beam divergence is completely different in each direction, typically, 5 to 10° (*full-width half-maximum*) in the long direction (*slow-axis*) and 20 to 30° in the short direction (*fast-axis*). To correct the large divergence in the fast-axis, commonly, a cylindrical lens with high numerical aperture is placed close to the

emitting region. A second cylindrical lens could be used to correct the divergence in the slow direction.

The key factor in the development of high power fibre lasers, a market pioneered and dominated by IPG Photonics, was the continuous advancement of BA diode laser pump technologies. Fibre lasers can provide diffraction-limited powers in the orders of kW's with pump efficiencies as high as 80 %. The current trend is the use of high power fibre lasers for industrial materials processing applications, such as bending, cutting and welding; this boom has increased the demand for BA single emitter diode lasers. An analysis done by Strategies Unlimited predicted that the laser market for kilowatt materials processing will grow to more than $1 billion USD by 2013.

1.5 Diode Bars

As mentioned in Sec. 1.3, for higher output power, multiple emitters are fabricated monolithically in the same substrate. Normally, a diode bar with dimensions 10 mm × (0.8-2mm) × (0.1-0.15 mm) contains between 10 and 70 broad area emitters side by side. The spacing between them depends upon the thermal load and the operating requirements [9]. A typical diode bar emitting at 808 nm, which is based in the structure reported by Sebastian in 2001 [10], is fabricated using a 17 nm GaAsP QW embedded in two confinement or waveguide layers of $Al_{0.45}Ga_{0.55}AS$ with a thickness of 1.0 µm each. Surrounding the confinement layers are two cladding layers of $Al_{0.70}Ga_{0.30}AS$ with a thickness of 800 and 500 nm, respectively. On the top, a *p* doped layer of GaAs (*p*-side) with a thickness between 500 and 1000 nm is grown. The complete structure is grown on the top of a 120 µm *n* doped GaAS substrate using metal organic chemical vapour deposition (*MOCVD*) at low pressure.

Although diode bars show efficiencies higher than 55 %, heat flux densities in the order of few kW/cm^2 can be generated. For example, an 808 nm 200 W bar containing 47 emitters, 100 µm width and length of 2 mm, and an efficiency of 55 % could generate a heat flux $q \approx 1.75$ kW/cm^2. This becomes an issue due to the fact that high rises in temperature decrease the reliability and the life time of diode bars [11]. To limit the rise in the temperature, low thermal impedance between the diode bar and the heat sink is necessary.

1.6 Packaging and Cooling of Diode Bars

Commonly, the *p*-side, previously metalized with a Ti-Pt-Au layer, is soldered onto a heat sink. In this way the thermal impedance between the junction and the heat sink is lower. In the past, copper was the preferred material for heat sinks because of its high thermal conductivity, which maximizes the heat flow from the diode. The problem with copper heat sinks was the strain added to the diode bar during the soldering process due to the mismatch between the thermal expansion coefficients (*CTE*) of copper (16.7 ppm/°C) and gallium arsenide (5.8 ppm/°C). Strain produces curvature or vertical bowing ("*smile*") of the laser chip and is also believed to reduce the lifetime of the diode bar. In the past, soft indium solder was used to bond the two materials. It helped to reduce the mounting stress during the cooling down after soldering due to its plastic deformation. Indium solder shows a good performance for continuous-wave (*CW*) and quasi-continuous-wave (*QCW*) operation. However, indium solder has been found to crack or migrate into the facet when it is exposed to ON/OFF cycles or long pulses (>500 µs), such as used for direct-diode processing applications This migration, which leaves a void in the solder layer, tends to block the emitter facet; therefore a hot spot is created. This hot spot can lead to the melting and recrystallization of the semiconductor material on the facet, which is known as Catastrophic Optical Damage (*COD*); this limits the life time and reduces the peak power. Excellent reviews in the problems associated with Cu heat sinks and soft solders have been presented by Stephens [12] and Yuen [13].

To avoid the problems associated with soft solders, HPDL manufacturers have decided to implement telecommunications laser-packaging techniques. The telecommunications industry approach was to use hard solder with a heat sink with similar thermal expansion characteristics. One of the first HPDLs manufacturers which implemented it successfully was Coherent. Their process, named PulseLife™ solder technology with conduction-cooled package (*CCP*), involves the positioning of the bar on a copper-tungsten (*CuW*) heat sink with the Cu:W ratio chosen to match the CTE of GaAS. They are soldered using Gold-tin (*AuSn*) solder, which is harder than indium and has a higher melting point. Other CTE matched heat sink materials used by manufacturers are copper- molybdenum (*CuMo*), beryllium oxide (*BeO*) and aluminium nitride (*AlN*).

However, there is a trade-off to be made in these materials between matching CTE and thermal conductivity, as materials have lower thermal conductivity than Cu. By

example, AlN and BeO thermal conductivities are 140-180 W/mK° and 260 W/mK° respectively, while copper is 385 W/mK°. This reduction leads to an increment in the total thermal resistance of the package. Consequently, the diode bar will be working at higher temperature which could reduce the lifetime of the diode bar. For this reason, new heat sink materials with lower CTE and thermal resistance have been explored; some of these materials are chemical vapour deposition (*CVD*) diamond, carbon-carbon composites and metal matrix composites [14].

Another problem in diode bars, especially with powers greater than 50 W is thermal rollover. According to Crump [15], thermal rollover occurs when the temperature in the bar increases causing a jumping of the carriers from the junction or quantum well into the contacts. This leads to a reduction in the peak power. To limit the thermal rollover at high output powers, the use of active cooling is needed.

1.6.1 Micro- channel coolers (MCC's)

The most common active method to remove the heat generated by the bar is the use of metallic micro-channel/fin coolers. The first report of the use of a Cu MCC was done by Krause [16] in 1994, it was a design based on the silicon MCC presented by Beach [17] in 1992. Commonly MCC's are made of several sheets of copper (*Cu*) or copper alloy (e.g. tungsten-copper or molybdenum-copper). Every sheet is machined or etched precisely with tolerances less than 10 µm. Later, the sheets are bonded together at high temperature to form the internal channel/fin geometry and manifolds. Typically, channel/fin widths are in the range of some 100 µm and located around 100 µm below the top surface of the cooler [18].

The main problem associated with the use of metallic MCC's in high power systems is the electrolytic or galvanic corrosion and erosion of the internal structure. They are produced by the use of deionised water which is needed to avoid the electrical contact between the coolant and the diode bars when they are stacked. In 2005 Haake [19] presented a paper explaining how the water chemistry impacts the erosion and corrosion of Cu MCCs. Also in 2005, Treusch [20] presented a paper explaining how the corrosion of the MCCs affects the reliability of the diode bar. He reported that as a result of the loss of material, an increase in the thermal impedance will appear due to the reduction in the heat transfer region. This will lead to a reduction in the output power and wavelength shifting; additionally, there will be a pressure drop due to a

change in the cross section of the channel. Another mechanism of erosion is the excessive water flow, which is required to improve the thermal performance of the cooler. Finally, particles detached by erosion can produce blockage of the microstructures which could lead to a sudden catastrophic failure of the diode bar. To minimize these effects, a chiller equipped with ways to control the resistivity, pH of the coolant and capable of filtering particles below 20 μm is needed, therefore increasing the price of the system.

In 2003, Miyajima [21] reported the fabrication of a jet water-cooled heat sink, in which simpler structure reduced some of the MCC's drawbacks such as the blocking of channels by detached particles, high fabrication costs and high pressure flows. However, jet coolers are still made of copper; therefore, the use of deionised water is still needed.

1.6.2 LTCC jet coolers

In 2008, Feeler [22] reported a ceramic jet cooler in which the coolant is not in electrical contact with the diode bar. As a result of this, deionised water is no longer needed, eliminating with this the problems and cost associated with the use of deionised water. The material used for this was low temperature co-fired ceramic (*LTCC*), a mature technology in the electronics industry.

1.6.3 Double-sided cooling

Double-sided cooling (*N-contact*) packages are typically used in laboratories to obtain the maximum optical output power of diode bars. In 2010 Leers [23] presented a deeper study about the benefits of the permanent use of double-sided cooling for high power diode laser bars. Leers reported a reduction in the thermal resistance by more than 25 %. However, the relatively short life span of the micro-channel heat sinks and the high installation and mounting costs are the main drawbacks of double-sided cooling [24].

1.7 Multiple Broad Area Single Emitters

In recent years, the need for fibre coupled lasers with higher brightness for direct applications and fibre laser pumping has increased. As mentioned before, BA single emitter diode lasers are preferred for pumping applications. Traditionally, pumping sources consisted of several BA single emitters, each one mounted in a pigtailed

telecom grade package, multiplexed into a single fibre using single or multi stage fused-tapered fibre combiners. In recent years the numbers of BA's per package have increased from one to three. Although BA's can deliver a high level of brightness, when they are coupled into the fibre the brightness is reduced due to the fact single emitter under fills the fibre in the fast-axis direction. Moreover, the use of multiple fibre combiners to reach high powers reduces the quality of the beam. Because of this, a new approach is to combine, in a module, multiple BA emitters in free space and couple into a fibre. In this manner, the brightness of individual emitters is kept and power levels of diode bar systems are reached. This technology has been patented by nLIGHT and commercialized under the name Pearl™ [25].

In Pearl™ modules every BA is sub mounted on a CTE matching substrate using hard solders such as AuSn, allowing high reliability under the extreme thermal fatigue associated with the pulsed mode needed for material processing. The BA's are arranged in a stair-step configuration providing an excellent thermal path between the diode and the cooling plate; this maintains a low junction temperature avoiding the use of active cooling. Also, the use of very complex optics is not needed. Because of all these advantages, a reliable and very compact high power laser system is achievable.

As the number of emitters per module increases to reach higher powers, and advances in laser diode technology allow higher output powers in BA single emitters, conductive cooling will become insufficient. Even though LTCC technology is used by Northrop Grumman to fabricate MCC's for diode bars, it has never been considered as a substrate for multichip modules. The purpose of this thesis is to explore the use of LTCC technology for the fabrication of modules capable of accommodating multiple BA's on AlN submounts and optical components. As well, the modules must be capable of providing localized cooling. Some of the characteristics that make LTCC an attractive material for the fabrication of coolers are similar CTE to aluminium nitride, electrical insulation which allows the use of non-deionised water and serial connection of the diode lasers and feasibility to create complex internal structures.

1.8 LTCC Technology

Green state LTCC is a composite consisting of alumina particles, about 20-40 % of weight after sintering, and glass particles. This mixture is held together by an organic binder. LTCC has been widely used in radio frequency and automotive electronics

because of its characteristics, such as feasibility of easily machining detailed structures in single layers to form very complex 3D structures, embedding of passive elements, such as resistors, capacitors and inductors, hermeticity, dielectric properties and, finally, it allows the co-firing of highly conductive materials.

Recently, according to Horowitz [26], there has been much interest in the use of LTCC as a platform for optical integration of both active and passive components because of its mechanical, thermal and environmental stability, and its cost effectiveness. For example, Nowak [27] reported the accurate placement of passive optical components in U-grooves in LTCC by using laser machining, attaining less than 1 dB losses in fibre-to-fibre coupling.

1.9 Structure of the Thesis

Chapter 2: LTCC as platform for diode laser technology. This chapter gives an introduction to LTCC technology. It will give a review of the LTCC process, emphasizing the machining and lamination parts. Traditional methods for machining will be compared with the CO_2 laser machining technique developed by our group. Issues associated with the fabrication of internal cavities in LTCC, during lamination, and our solution to minimise them using nanocarbon layers will be explained. A general overview of the use of LTCC in microfluidics and optical integrations will be given. Finally, the reasons why LTCC is an excellent platform for high power diode lasers systems will be given.

Chapter 3: Micromachining of LTCC and nanocarbon layers with CO_2 laser. Details of the in-house custom CO_2 system will be given. Its capabilities will be shown with examples of cuts. As well, the suitability of our system for cutting nanocarbon sheets will be demonstrated. Finally, examples of the excellent fitting between LTCC and nanocarbon layers will be shown.

Chapter 4: Fabrication and testing of a laminated structure in LTCC for cooling a high power broad area single emitter diode laser. This chapter describes the design and manufacturing steps used to build a structure capable of cooling a BA diode laser. It describes the problems that arose during the fabrication process and the proposed solutions to overcome them. Performance parameters of the jet coolers such as flow per

jet, pressure drop, water jet velocity and Reynolds number are presented. The process for mounting the laser on sub mount on the top of the LTCC cooler is described as well. Finally, to check the efficiency of the cooling structure the thermal impedance is calculated; the setup of the experiment and the results are explained.

Chapter 5: Placement of optical elements onto LTCC structures. This chapter addresses the need of mounting a fast-axis collimation (*FAC*) lens on the LTCC cooler for the correction of the high divergence of the Bookham laser. The mounting process is explained. The resulting beam after correction in the far field is shown. Finally, the divergence and pointing stability of the corrected beam as a function of the power dissipated through the cooling structure are reported.

Chapter 6: Beam combining of 4 single emitter diode lasers placed on a LTCC structure. This chapter presents and discusses the design of a module capable of accommodating 4 BA single emitter diode lasers, with integrated active cooling and micro-optics on board. It addresses the recent trend of combining multiple BA's in a common package to reach the beam brightness and power required for pumping fibre lasers and direct-diode diode industrial applications. To reach power scaling while simultaneously maintaining the high brightness, a novel out-of-plane beam shaping method using inexpensive optics will be presented.

Chapter 7: Conclusions. This chapter summarizes the completed work and gives ideas to work out the problems which could not be solved during the realization of this project.

CHAPTER 2

LTCC AS A PLATFORM FOR DIODE LASER TECHNOLOGY

2.1 Introduction

Next-generation packaging for photonics and MEMS (*Micro-Electro-Mechanical Systems*) modules will require a low-cost, high-performance technology for hybrid integration of electrical, optical and mechanical functions. In addition, these features must be delivered to the market faster and at a low price. Low temperature co-fired ceramic (LTCC) materials, effective in harsh-environment military and high-volume automotive and wireless applications possess the attributes to satisfy these requirements. Characteristics such as non corrosive material, similar CTE to aluminium nitride, hermeticity, possibility of co-firing metals and feasibility of easily machining detailed structures in single layers to form very complex 3D structures make LTCC an attractive option for diode laser technology.

Multilayer ceramic packaging technology has been used in the electronics industry for more than forty years. It was developed by RCA Corporation in the late 50's and patented by them in 1965 [28]. However, it became a premiere packaging technology thanks to its introduction by IBM in its computer and microelectronics programs, specifically in mainframes in the late 60's.

Three ceramic based technologies have been used for substrate/package applications:

Thick Film Multilayer (*TFM*). This technology utilizes ink or pastes, which are screen printed onto ceramic substrates. Normally, this ink is a combination of metal or dielectric powder, vitreous or oxide powder, and an organic binder. Using the right combination of compounds in the ink, conductors, capacitors, resistors or inductors can be formed over the substrate. After ink is applied over the substrate, it must be dried and fired, typically between 850°C and 1000°C. The main problem of TFM is that it is a sequential process. Multiple levels of conductors and vertical electrical connections between layers (*via*) must be formed one layer at a time, and separated by dielectric material. In addition, it requires a substrate to support these layers. If a complex circuit needs to be fabricated, it will require a large number of processing steps, thus increasing the final cost of the product. In addition, they suffer from poor planarity, making the

thickness control of dielectric layers very difficult. Another disadvantage of TFM is that it only allows low to medium packaging density. Finally, vias through the base substrate are relatively large and must be pre-cut with laser.

High Temperature Co-fired Ceramic (*HTCC*). It was created to increase the packaging density. It involves the lamination of single conductor/dielectric layers by firing under pressure at high temperatures (1600°C-1800°C) in a hydrogen atmosphere. The advantage of this technology is that individual layers are formed in parallel by screen printing conductor material over sheets of dielectric tape. This tape is a slurry mixture of alumina and an organic binder. Normally, vias are created using mechanical methods like punching; after the holes are formed, they are filled with a conductive material before printing the conductor traces. The main disadvantage of HTCC is that due to the high firing temperature, only metals like tungsten and molymanganese, which have low conductivity, can be used as conductors. Moreover, it presents a high dielectric constant, and a poor coefficient of thermal expansion (*CTE*) match to silicon. Finally, HTCC suffers from size shrinkage due to firing and the cost of the tooling is very high.

Low Temperature Co-fired Ceramic (*LTCC*). LTCC is a hybrid that combines the advantages of HTCC and TFM technologies. LTCC was developed due to the necessity to use materials with higher electrical conductivity, like in TFM, on cofired dielectric tapes, like in HTCC. In this technology, the lamination firing temperature was reduced to around 850 °C, allowing the use of materials like gold, silver and copper, which have higher conductivity. The reduction in the firing temperature was obtained using a mixture of alumina-filled glass or crystallisable glass in an organic binder. Changing the compounds in the tape made it possible to have a wide range of dielectric constants. Also, the coefficient of thermal expansion can be modified to match alumina, gallium arsenide or silicon. LTCC allows high density packaging at low cost for medium to high volume. It has a relatively low cost of tooling for low volume production. LTCC technology meets many of the requirements necessary for next generation packaging. It could become an enabler for fibre optic and MEMS packaging.

2.2 Review of LTCC

The first LTCC based system was introduced in 1983 by DuPont Electronic Materials Division and Hughes Aircraft for military purpose [29]. LTCC technology was

developed combining the advantages of TFM and HTCC technologies, as shown in Fig. 2.1, with the purpose of achieving high speed, high density packaging and low loss material.

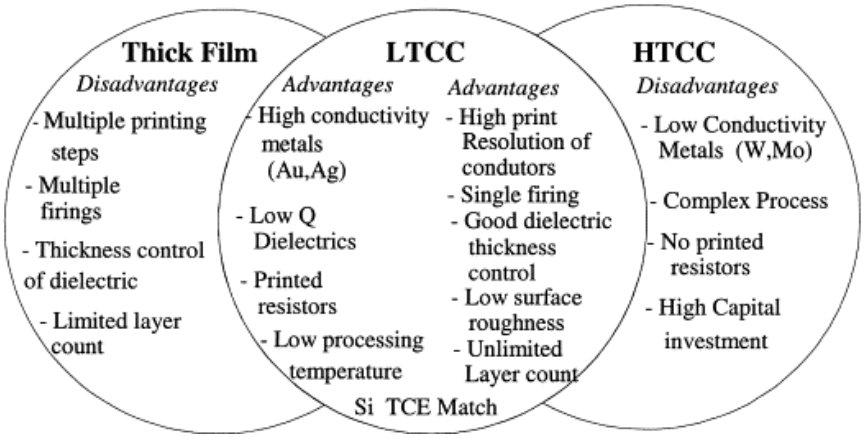

Figure 2.1 Advantages of LTCC technology [30]

In the beginning, LTCC technology was used mainly in military systems due to the high cost of fabrication, principally because of the use of gold as a conductor. It was not until the developments in conductor pastes allowed the incorporation of silver, the least expensive and most conducting air fireable metal, that LTCC was incorporated in commercial and consumer applications [31].

The key component in LTCC technology is the unfired dielectric ceramic layer also known as Green Tape™ or ceramic in green state. The green tape is produced by tape casting of ceramic and/or glass slurry, typically onto a polyester (*Mylar*) carrier at varying thickness (30-350 μm). Tape casting using a doctor blade method is the best option for creating thin and flat ceramics with an excellent surface finish and thickness tolerance [32].

In commercial tapes, the slurry is a mixture of glass-ceramics (crystallizable glass) or glass+ceramics (multiphase ceramics), organic binder, plasticizer, solvent and dispersant materials, as shown in Fig. 2.2. Normally, powders are manufactured by conventional ceramic process. Glass and ceramic materials are produced by weighting the starting materials and mixing them in a pot mill. Then, the mix is pressed into pellets, which are melted at the right temperature. Any further reaction is stopped by

quenching the melt in distilled water. After this, the melt is pulverized in a ball mill. Finally, the right amount of ceramics and/or glasses are mixed in the ball mill [33].

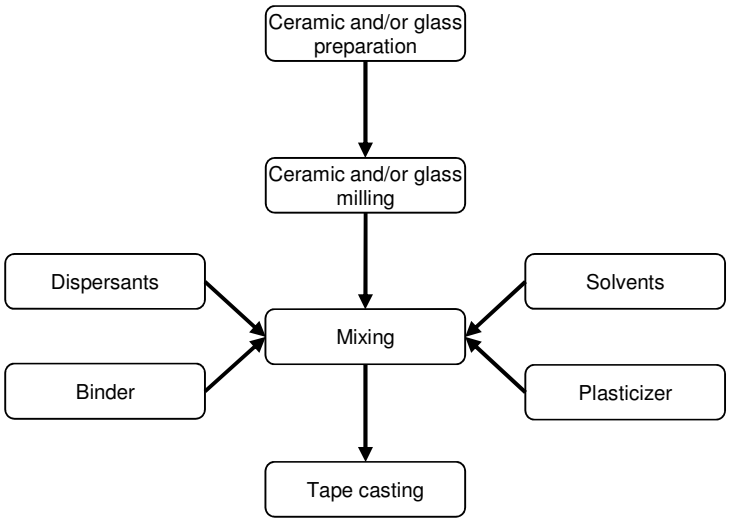

Figure 2.2 Production process of cast ceramic tapes

Glass-ceramics are the most frequent system in the fabrication of LTCC tapes. Here, amorphous glass, containing a small amount of crystalline phase which acts as nucleating agent, crystallizes and densifies during firing [34]. The glass+ceramic is a mixture of low-softening glass and ceramic filler powders. Here, the low softening glass becomes a viscous liquid during sintering, promoting the densification of glass+ceramic at lower temperature than that required just for the ceramics. The ceramic fillers, which are uniformly disposed in the glass matrix, are used to adjust the physical properties of the composite [35]. The densification occurs in a three-stage liquid-phase process, particle rearrangement, dissolution and precipitation, and solid state sintering [36]. Depending on the reactivity between the filler and the glass the densification can be classified in non-reactive, partially reactive and completely reactive and will occur in any of the stages. In the case of non-reactive systems no dissolution and precipitation is observed. As the liquid phase appears, the redistribution of the liquid fills the pores, and the particles are rearranged until they reach densification. In the partially reactive system, the dissolution of the filler in the glass is limited and occurs in localized places. Here, no particle growth or shape accommodation is observed. Finally, for completely reactive systems, the dissolution of refractory filler is extensive and shape accommodation is observed [37]. For further information on liquid phase sintering consult the extended review on the topic done by German [38].

After the ceramics and/or glasses are mixed, different organic materials, such as binders, plasticizers, dispersing agents, antifoaming agents and surface treatment agents, are added to facilitate the casting of the composite. The functions of the binder are to provide strength to the green tape and keep the ceramic/glass powder particles together by organic bridges [39]. Normally the binder is a mix of polyvinyl butyral (PVB) or any acrylic plastic with a non-aqueous solvent. Another important role of the binder is to bond the green sheets together in the heat pressing steps. As the amount of binder is related to the shrinkage of the tape during firing [40], it is desirable to keep it at a minimum without compromising the tape handling properties, such as delamination of the green sheets before sintering or brittleness. Plasticizer, such as butyl stearate, is added to lower the glass transition temperature (Tg) and melting point of the binder. This prevents tape cracking and provides flexibility to the tape, making it easy to shape [41]. Dispersant or wetting agent avoids agglomeration of small particles by steric and/or electrostatic repulsion providing a stable suspension. This helps to produce a homogenous and uniform tape. Solvents are added to dissolve organic additives (dispersant, binder and plasticizer) and distribute them uniformly throughout the slurry. Solvents are removed immediately, by evaporation, after the casting process leaving a dense tape on the carrier [39]. Once the slurry is ready, it is pumped directly to a tape-casting machine and made to pass under the edge of a smooth knife set at a fixed height, on to a plastic carrier moving at a precise velocity. The slurry subsequently dries to form a tape of leather-hard consistency. The process is depicted in Fig. 2.3.

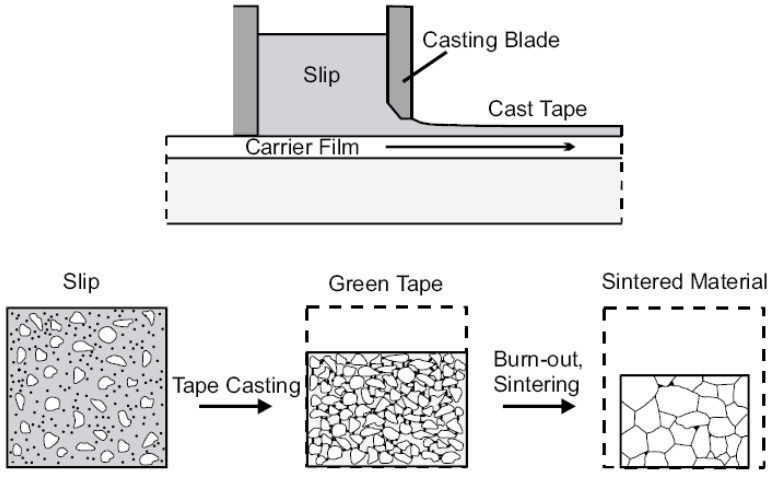

Figure 2.3 Tape casting of the slurry onto carrier film

Different glass systems are used for commercial tapes. For example, the Ferro A6 is based on an amorphous calcium borosilicate glass which after firing produces a dense Wollastonite ($CaSiO_3$) and calciborite (CaB_2O_4) structure. Other manufacturers use alumina (Al_2O_3) as the main chemical addition in the unfired tape. For example Heraeus CT700/CT800 are based on Celsian phase, barium aluminum silicates which produce alumina and $BaAl_2Si_2O_8$. Motorola T2000 after firing produces Anorthite ($CaAl_2Si_2O_8$) and alumina. An excellent review of the chemical properties of commercial tapes was done by Jones [40].

In our case, we are interested in a unique tape from Heraeus called HeraLock® HL2000, which is self-constraining, allowing near zero shrinkage in the X-Y directions. In green state its composition is alumina, TiO_2 and glass, and after firing corundum (Al_2O_3), sanidine ($(K,Na)(Si_3Al)O_8$), alumina, $Ca(Ti,Mg,Al)(Si,Al)_2O_6$, $BaTiAl_6O_{12}$ and $NaTiSi_2O_6$ phases are formed.

2.3 Process for Manufacturing Multilayer Ceramic Structures

The manufacturing process for LTCC starts with the preparation of the green tape, as explained in the previous section, and terminates with the inspection or testing of the finished module; the multistep process is summarized Fig. 2.4. Details of each step will be given below.

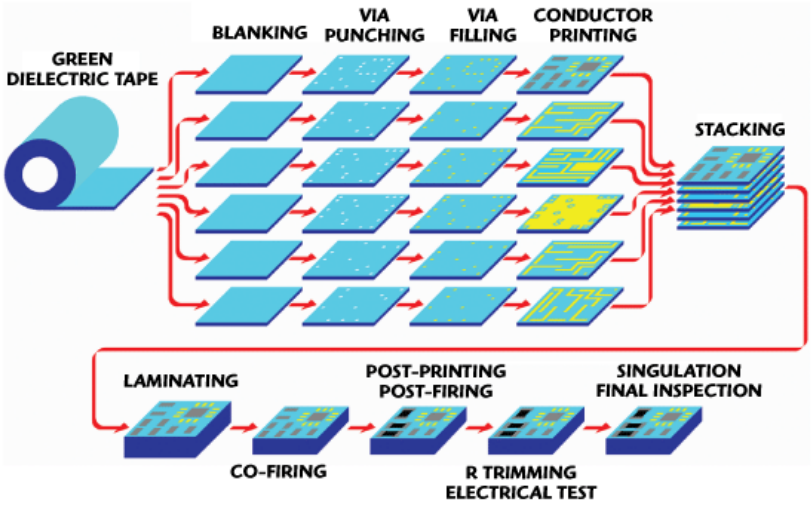

Figure 2.4 Manufacturing steps of LTCC substrates [42]

2.3.1 Blanking or shape forming

In this part the green tape is unrolled onto a stainless steel table and cut to the ideal size with a laser, hot knife or die cutter; the cut pieces should be used within 2 weeks.

2.3.2 Preconditioning

Some tapes must be preconditioned. In this step, the green tape has to be baked for about half an hour at 120 °C followed by stabilization at room temperature. Another mechanism for preconditioning is to allow the tape to stand for 24 hours in a nitrogen box.

2.3.3 Forming of vias and 2D structures

Vias and 2D structures in the tape are punched or machined by mechanical methods or laser. Here, the processed surface must be smooth with satisfactory accuracy and have no process scrap attached to it. For this, parameters such as cutter speed, punch pressure or laser power must be carefully selected; for a more detailed explanation see Sec. 3.4.

2.3.4 Via filling

Via filling is the process in which via holes formed in the green sheet, for Z-axis electrical interconnection, are filled with conductors such as gold or silver. The most common method for via filling is conventional thick film screen printing. Here, conductive paste is applied on a stencil, with apertures above the vias according to the design, and it is drawn with a vacuum pump into the holes to fill them. The tape has to be placed on a sheet of non-spread paper which is placed on a porous stone to avoid the leakage of the paste as seen in Fig. 2.5.

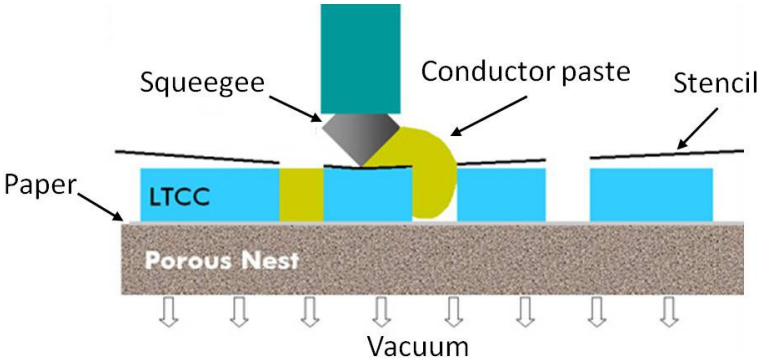

Figure 2.5 Via filling by screen printing

2.3.5 Screen printing

Co-fireable conductors are printed using a conventional thick film screen printer. The screen is a highly tensioned mesh structure woven from fine stainless steel or polyester wire over a frame, and the parts other than the openings are covered in emulsion as seen in Fig. 2.6. Mesh is characterized by material, orientation, size and density, and tension. As in via filling, vacuum through a porous stone is used to hold the tape in position. Due to the flatness of the green tape, printing of the conductor tends to be easier and of higher resolution than standard thick film on alumina. After printing, the conductors and vias are dried in an oven at 80 °C to 120 °C for 5 to 30 minutes depending on the material.

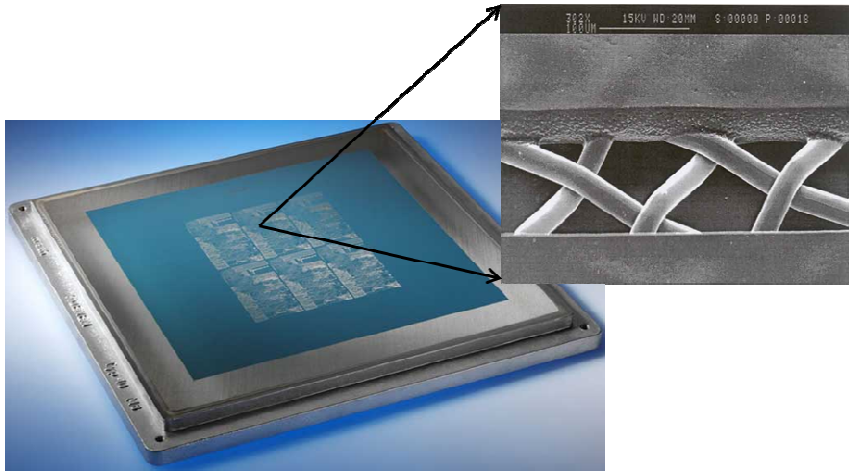

Figure 2.6 Screen with emulsion coating

Various process parameters, such as speed, pressure and angle of the squeegee must be considered to reach a high transfer quality. The speed of the squeegee is determined by the printing time and the viscosity of the paste. Slow speed increases printability but increases the time of process. However, when the speed is increased the viscosity of the paste is lower allowing a better fluidity through the orifices in the screen. In the process in which the paste is transferred to the tape, the squeegee presses down the screen until it touches the tape. The appropriate pressure depends on the amount of deformation of the screen and the gap between it and the tape. In general high pressure causes bleeding easily, but low pressure could result in blurring. Finally, if the adjustment of pressure or speed does not produce a good printing, the angle of the squeegee can be modified to reduce the defects [43].

2.3.6 Stacking and lamination

Once the tapes are cut and printed, they must be stacked and aligned precisely to form the 3D structure. For this, layers are registered (stacking holes) and stacked on a pin fixture as seen in Fig. 2.7.

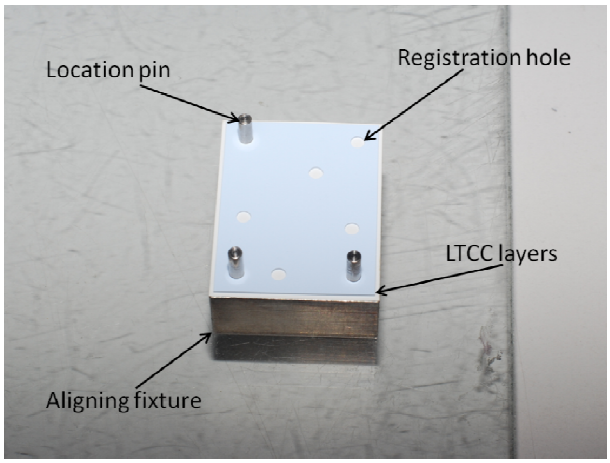

Figure 2.7 Stacking of LTCC layers on pin-alignment fixture

Once the layers are stacked, layers are laminated. Lamination and firing are the most critical steps in the fabrication process due to the fact that they determine the quality of the final LTCC structure. The most common method for lamination is bonding by thermo-compression of the LTCC layers at temperatures above the binder's glass transition point. To obtain homogenous bonding, it is necessary to have a good interpenetration of the powder particles as seen in Fig. 2.8.

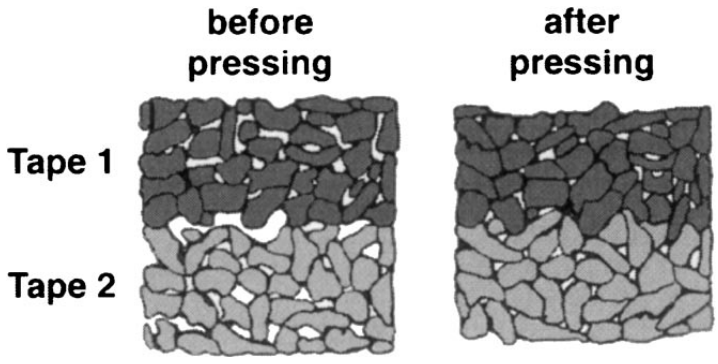

Figure 2.8 Arrangement of particles before and after the lamination process [44]

For this, the ratio between binder and powders during tape production must be considered to produce a smooth movement of the particles, to facilitate the

interpenetration of the tapes [44]. Normally the layers are joined together at high pressures in the range of 10-30 MPa and temperatures in the range of 50-80 °C for 1-20 minutes. Two approaches can be used for the thermo-compression. In the first one, known as uniaxial lamination, the stack is typically pressed between two heated plates. The second approach is to use an isostatic press which uses a hot fluid as a means of applying pressure in all directions. The stacked sheets are vacuum sealed in a plastic bag, to avoid the fluid from contacting the sheets. Pressure, temperature and time are similar to the those used in uniaxial pressing. Although thermo-compression allows the lamination of a considerable number of layers (> 40) and a strong bonding between them, the temperature and pressure produce mass flow which can lead to deformation or collapsing of internal structures as seen in Fig. 2.9.

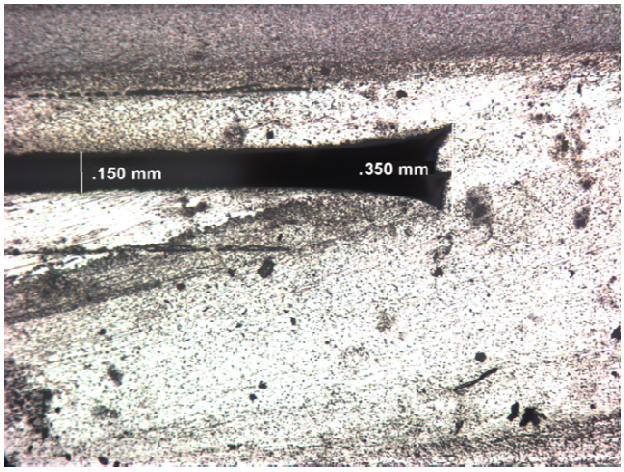

Figure 2.9 Example of water channel collapse caused by unsupported isostatic lamination

To overcome this, new techniques for bonding have been developed. By example, Roosen [45] developed a technique in which LTCC layers are bonded using a double-sided adhesive tape. Acrylate is used as adhesive which is carried on a polyethylene terephthalate (*PET*) layer. During the burnout cycle the organic components of the tape melt and diffuse into the LTCC layers, leading to a complete elimination of the tape. This technique enables the lamination at room temperature with low pressure. The main disadvantage of the use of tape is that fabrication of closed chambers cannot be done. Jurkow [46] developed a solved-based lamination technique. Here, a chemical agent is used to melt the surface of the LTCC layers allowing the bonding of them a room temperature with a pressure below 0.5 MPa. They claimed that the fabrication of closed structures with no deformation is possible with this technique. However, as the layers

become soft after bonding and must be dried to avoid the collapsing or deformation of the internal structures, progressive lamination is recommended. Another way to prevent deformation or collapsing of internal structures, in a single lamination, is the use of a sacrificial volume material (*SVM*) to provide mechanical support during lamination. Different materials have been used as SVM, for example, Jones [47] used wax to minimize the deformation of micro heat pipes. Smetana [48] has proposed the use of a polymer-based SVM for the fabrication of a fluidic heat exchangers. On the other hand, Birol [49] proposed the use of a graphite powder-based sacrificial layer for the fabrication of microfluidic structures. Whatever the material used, this should not interact with the LTCC ceramics and should be removed during the firing process.

2.3.7 Co-firing

Co-firing is the process in which the laminated structure is heated at high temperature so the conductor paste and the ceramic are fired at the same time. The co-firing process could be seen as a two-steps process; organic burnout and sintering at peak temperature. According to Schultze [50], organic burnout is a complex process which includes vaporization, decomposition and depolymerisation, and oxidation of the organic matrix (binder, plasticizer, dispersant and residues of organic solvents). It takes place between the temperatures 120 °C and 500 °C. It is recommended that the structure soak in this temperature range at least half an hour. Peak temperatures are between 850 °C and 900 °C, depending on the metals and tape composition, and should be held for more than 15 minutes. An example of a firing profile is shown in Fig. 2.10.

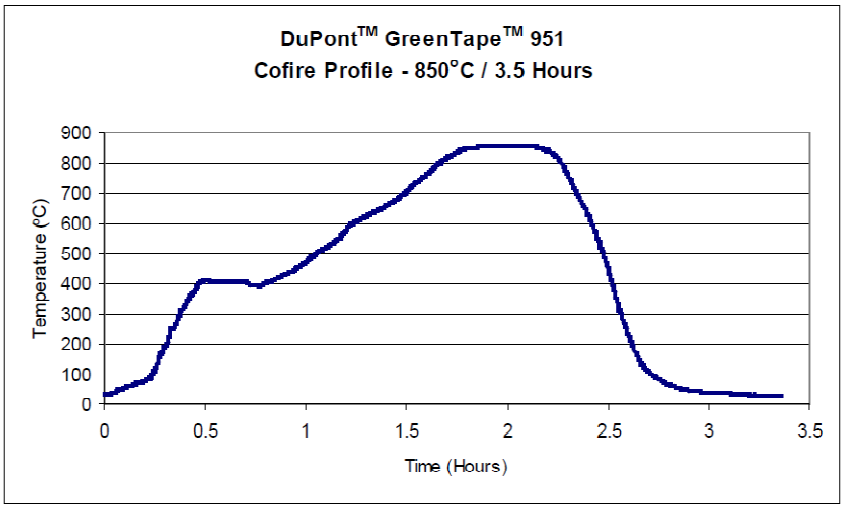

Figure 2.10 Firing profile for DuPont 951 green tape

As explained before, the firing of the conductors must be done below the melting point of each metal ingredient. Conductive paste is a mixture of metal powders and an organic vehicle. The bonding between the conductor and the LTCC substrate is the result of the dissolution of the metal in the glass of the ceramic tape during sintering [51]. To improve the adherence of the conductive material to the structure, powders with the same or similar ceramic composition to those used in LTCC are added to the conductive paste. Further information can be found in [52]. A problem observed during co-firing of conductors is the migration of un-reacted glasses to the top of the conductor surface [53]. This will make the soldering of surface mount-components difficult or will provide inadequate bond strength for gold wire bonds, as well, it will modify its resistivity.

A disadvantage of standard LTCC tapes is the variable shrinkage of the structure during firing. Normally, the dimensions of the structure after sintering are about 84% to 87% of the size in green state, with tolerances up to ± 0.5%. This positional uncertainty has created many difficulties in automatic assembly operations, such as wire bonding and die placement, where a significant variation from the intended nominal position could lead to an increment of defects, therefore increasing the production costs [54].

To limit the x/y shrinkage during sintering different constraining mechanisms have been explored. Two examples of these techniques are Pressureless Constrained Sintering (*PLAS*) and Pressure Assisted Sintering (*PAS*). In both methods, a laminated release tape is used on the external layers of the structure to constrain it during sintering. The release tape is based on ceramic particles with a higher sintering temperature than those in the LTCC; therefore they don't shrink during sintering. This, prevents the shrinkage of the rest of the structure [55]. A post-process, such as brushing, sand-blasting or water jet, is needed to remove the release tape. The use of the release tape often obligates a post-firing printing of conductors because the contact of them with the tape, during co-firing, changes their properties. This produces a change in the resistivity and makes the bonding and soldering on them difficult. Although these methods can allow the control of shrinkage below 0.1%, the need of a hot pressure furnace in the case of PAS and the increase of the post-firing processes make them an unattractive option for the manufacturers.

In 2002 Lautzenheiser [56] presented a self constrained LTCC tape which eliminated the cost of adding and removing of the release tape and kept the manufacturing process simple. The HeraLock™ tape consists of one self-constraining layer sandwiched between two glass+ceramic layers as seen in Fig. 2.11.

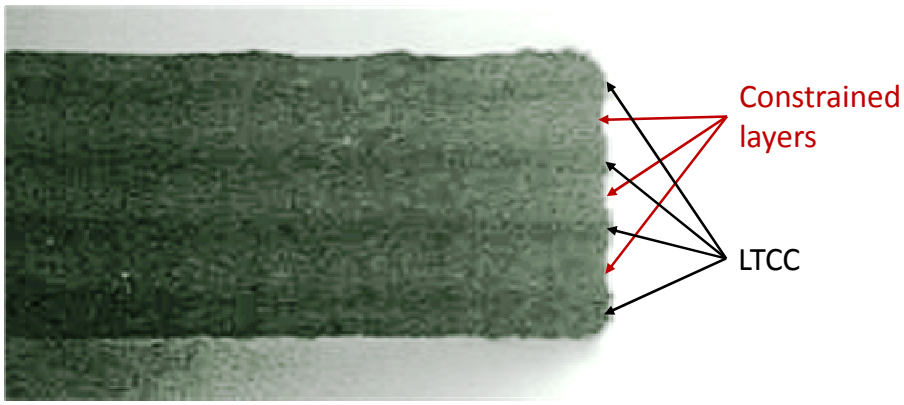

Figure 2.11 HeraLock stacked tape [56]

The constraining layer consists of a refractory ceramic, binder and a wetting agent. Similar to the release tape, the refractory ceramic will not sinter at the temperature of the glass+ceramic layer and will partially fuse with the glass contained in it. The purpose of the wetting agent is to improve the penetration of the glass into the refractory ceramic. As a result, the layers will densify in the z direction with shrinkage less than 1% in the X-Y direction. For further information on the mechanism of the self-constrained tape consult [57].

2.3.8 Post-firing

Due to the fact that values of resistors or capacitors can exceed the capacity of thick film processing, surface mount components are integrated on the top or bottom layer. For this, surface mount pads and tracks are printed as a post fire process [58].

2.3.9 Inspection and testing

After the firing process has been completed, the module is 100 % tested for electrical opens and shorts. Subsequently, the structure will be cut to the right size.

2.4 Laser Machining

In order to obtain vias for electrical interconnection between layers, LTCC tapes are usually machined by drilling, punching or stamping methods; due to their low hardness, ceramic foils are normally machined in green state. High speed drilling machines with hard metal drilling tools are used to drill holes and larger slots in LTCC tapes. Due to the strong wear, drilling can only be used effectively when the number of holes per tapes is low. Also, mechanical drilling of vias becomes more difficult as the hole size decreases because of the corresponding decrease in the mechanical strength of the hole punch. Punching can be applied for cutting the shape as well as for realizing holes and cavities. The holes are used for the alignment of LTCC sheets (registration holes) and for interconnecting layers (microvias). However, mechanical methods are limited in hole\diameter and density and are subject to wear due to tool/workpiece physical contact. The laser has become, in recent years, an important tool for machining LTCC; it has replaced some mechanical methods in the LTCC process.

In 1999 Imen and Allen [59] reported the use of a TEA CO_2 laser to machine green alumina sheets. They found that drilling in air was inefficient due to the fact that electrical breakdown of air at the beam focus drastically reduced the laser energy at the substrate surface. To overcome the problem, working at reduced pressures was needed. Images of pulse drilled holes by two different fluences are shown in Fig. 2.12.

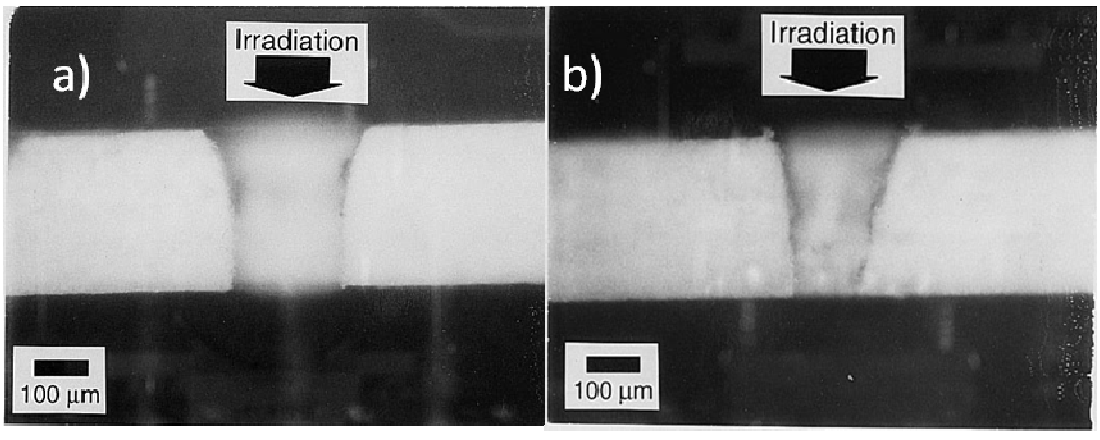

Figure 2.12 Via holes drilled at 9.5 um: a) 24 40-mJ pulses and b) 40 10-mJ pulses [59]

Diode laser machining has poor performance due to low absorption of the green state material in the near-infrared region (*NIR*) as reported by Slocombe [60]. To increase the absorption of the polymer/alumina composite at the laser diode wavelength (852 nm),

Slocombe reported the introduction of dry black powder paint in the composite. This increased the laser absorption from 12 to over 90 %. Diode laser machined grooves in alumina/polymer with black powder paint pigment are shown in Fig. 2.13.

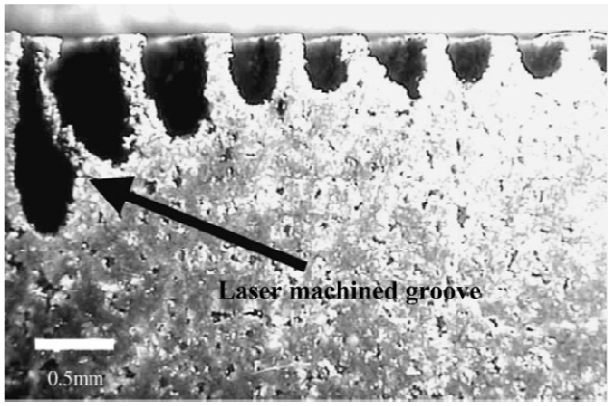

Figure 2.13 Laser machined grooves in alumina/polymer with black powder paint pigment [60]

Kita [61] in 2002 reported the use of Nd:YAG lasers for the drilling and cutting of LTCC tape. The machining had a reasonable quality but it had a strong dependency on the content of glass in the tape. The via made in a LTTC tape with high content of glass, showed in Fig. 2.14, is filled with melted glass. Even when it is possible to remove the melted glass, the shape becomes irregular.

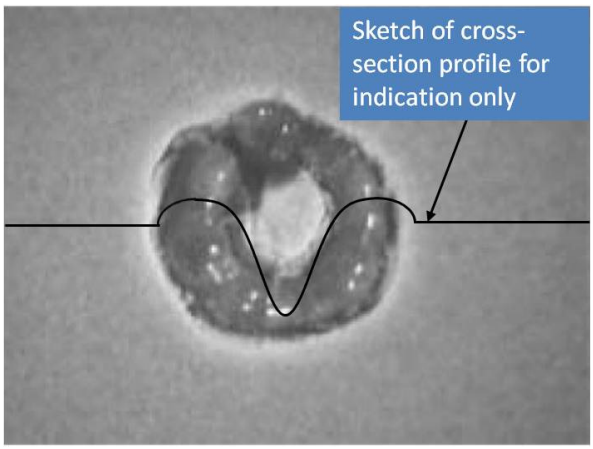

Figure 2.14 Vias filled with melted glass [61]

In 2006 Rebenclau [62] compared the fabrication of vias in LTCC tapes using mechanical punching and lasers drilling. For laser drilling CO_2, Nd-YAG and UV lasers were used.

In order to avoid the problems associated with the previous laser machining techniques, Nowak [63] developed in our research group a novel "cold" self-cleaning technique for processing LTCC in "green" state. With this technique the deposition of vaporized material or the vitrification of glass and ceramic in the drilling site due to high temperature were eliminated. This technique employs a low-power CO_2 laser, which results in high-speed cutting with negligible thermal effects at the interaction site. This is a three stage "cold" process in which the first stage is characterized by the strong, localized absorption of 10.6-µm laser radiation on the ceramic and glass producing an increment of the temperature. The generated heat is transferred immediately to the surrounding binder producing a rapid but controllable polymer pyrolysis at 200–400°C, finally, the transport of un-sintered ceramic particles from the site by the polymer decomposition of gases. This technique has several advantages: no molten ceramic is produced, so avoiding heat affected zone, it is self cleaning, machining is done at low power and it is independent of the differences in the composition between different types of tapes. As seen in Fig. 2.15, it has the capacity to process arbitrary shapes with lateral resolution comparable to spot size (50 µm) and depth resolution comparable to the ceramic grain size. For a model of the "cold" ablation process, consult [64].

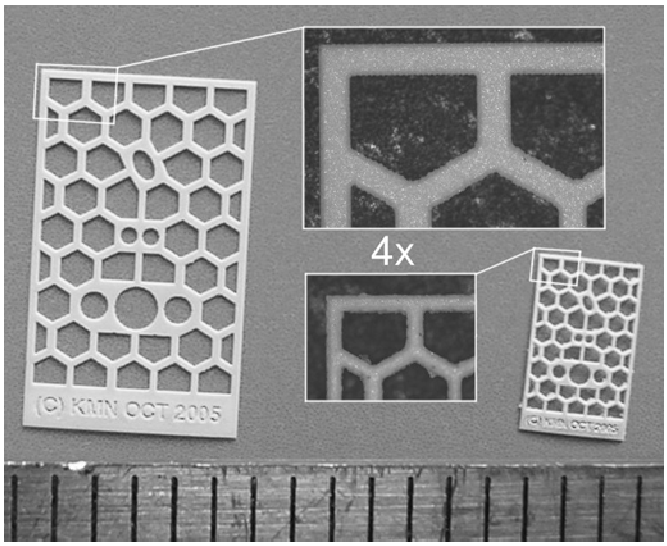

Figure 2.15 Demonstration of the process capabilities, structures fabricated by raster scanning [63]. Ruler division 1 mm

2.5 New LTCC Applications

Even though LTCC technology was well-established for the electronic circuit industry, the feasibility to fabricate vias, channels and cavities made LTCC technology an

attractive platform for new applications, such as microfluidic systems, fibre optic and electro-optic packaging [26, 65].

In 2003 Low [66] explored the capabilities of LTCC technology for the packaging of optical MEMS. He designed a LTCC package for an optical cross-connect (*OXC*) switch device, as depicted in Fig. 2.16.

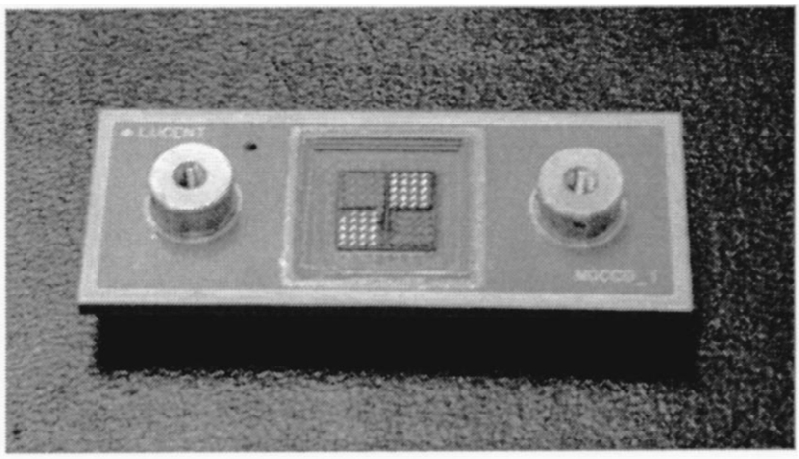

Figure 2.16 The optical cross-connect switch LTCC package [66]

The fabrication of grooves in LTCC, a step toward electro-optic integration, for passive alignment of optic fibres has been reported by Heilala [67] and Nowak [27]. Heilala reported the fabrication of passive alignment grooves for multimode fibre-to-edge emitting laser alignment in 2005. For this, two methods of fabrication were used: punching (Fig. 2.17a) and screen printing of photoimageable glass (Fig.2.17b).

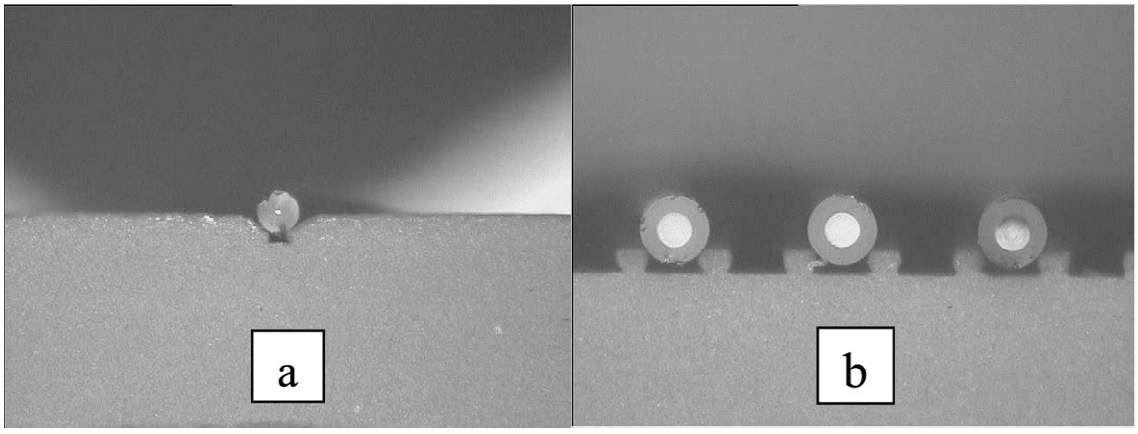

Figure 2.17 Passive alignment grooves a) Punching b) Screen Printing [67]

Using the “cold” machining process, Nowak et al. also reported the fabrication of grooves, as shown in Fig. 2.18. They achieved low-loss butt coupling of <1dB for single-mode fibres using laser written grooves.

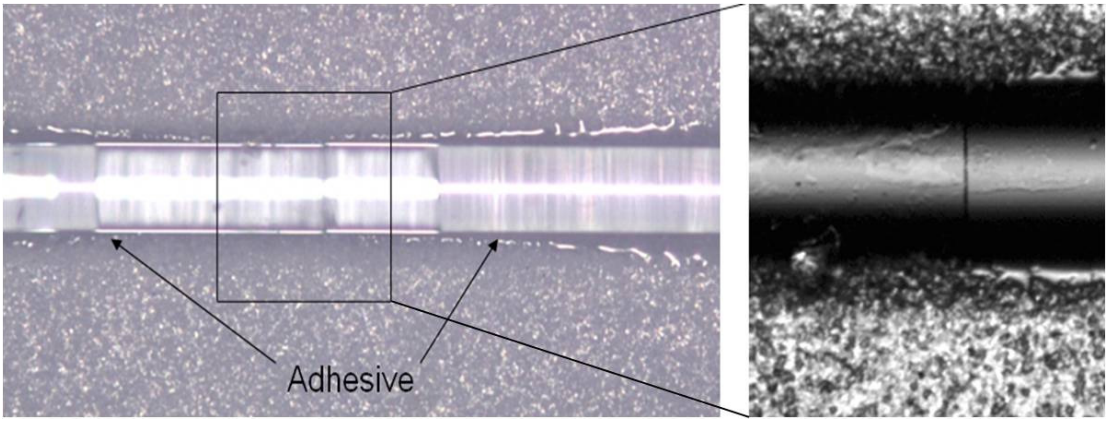

Figure 2.18 View from the top of the grooves and butt-coupled fibres on LTCC [27]

In 2006, Youngsman [68] reported several LTCC blocks for lab-in-packages devices. Different techniques for the fabrication of fundamental features required in fluidic packaging were used, for example the use of a sacrificial carbon material to fill mechanical machined channels, therefore avoiding their collapsing during lamination (Fig. 2.19a). Inlet/outlet ports were realized by embedding sapphire tubes in the structure taking advantage of the natural shrinkage of LTCC (Fig. 2.19b). Finally, different methods to incorporate sapphire lenses in the structures were explored.

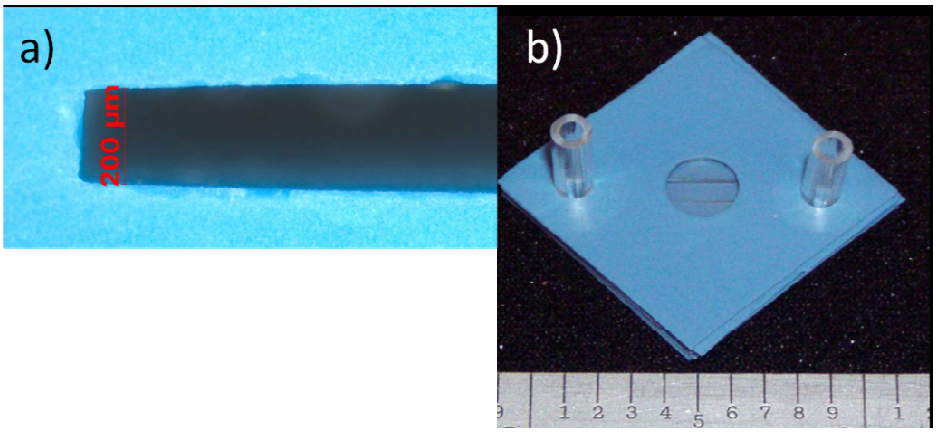

Figure 2.19 a) Cross section of a channel created by machining and filling with carbon b) Simple channel with sapphire tubes fired into LTCC [68]

2.6 LTCC Coolers for Diode Bars

Because the feasibility to fabricate complex embedded structures, its dielectric properties, hermeticity and being a harder material than copper after firing, LTCC was incorporated in a cooling system for high power diode laser bars. In 2008, Feeler [22] reported a LTCC jet cooler in which the coolant is not in electrical contact with the diode bar. To avoid the electrical contact between the diode bar and the coolant, and remove the heat generated, the diode bar was mounted on a thermal window, as shown in Fig. 2.20. AlN, BeO or CVD diamond materials were used for the thermal windows. The main advantage of these materials is the similar CTE to LTCC and GaAs which allows the use of hard solders, such as AuSn.

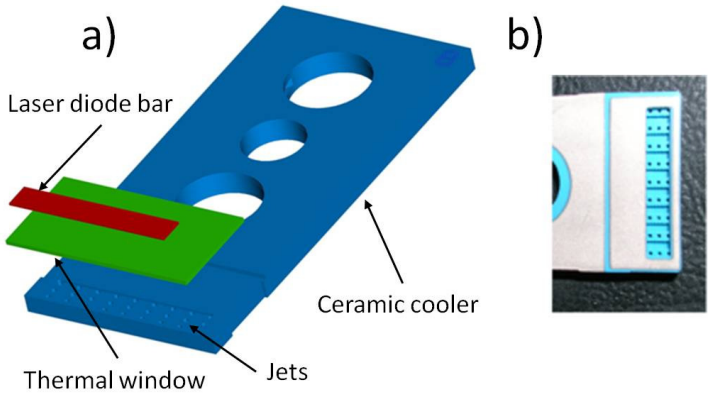

Figure 2.20 a) Exploded view of a ceramic cooler, thermal window, and laser diode bar [22] b) A prototype assembly with metallized LTCC illustrating a window in the LTCC surface and array of jets [69]

In terms of fabrication, LTCC was machined in green state by punching. To avoid the use of SVMs, cavity formation was done using sequential lamination at reduced pressure. Finally, metallization was done by standard screen printing [69]. This concept has been commercialized by Northrop Grumman under the name ICE-CUBED (*IC3*) technology for cooling HPDL bars. Their plan is to replace copper cooling systems by IC3 technology. Figure 2.21 shows LTCC microchannel-cooled packages for 1 and 3 HPDL bars.

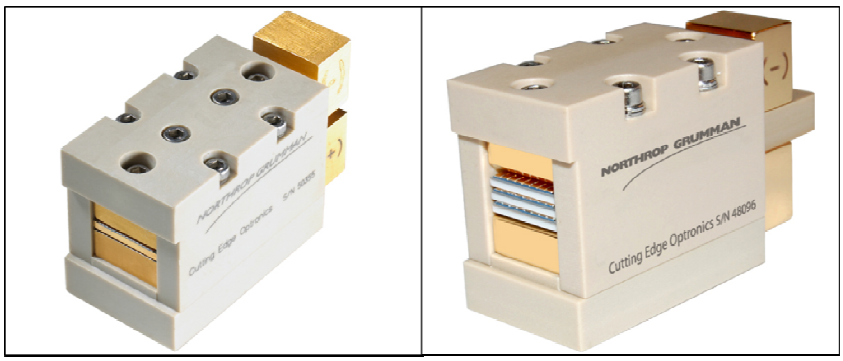

Figure 2.21 The microchannel-cooled packages for 1 and 3 HPDL bars

As mentioned before, in recent years the need for fibre coupled lasers with higher brightness for direct applications and fibre laser pumping has increased. A new approach is to combine, in a module, multiple BA emitters in free space and coupled into a fibre. In this manner, the brightness of individual emitters is kept and power levels of diode bar systems are reached.

In our case, our objective is to apply LTCC technology for the fabrication of modules capable of accommodating multiple BA diodes on AlN submounts. Modules must be capable of providing localized cooling on board and supporting the placement of optics. In terms of fabrication, a different approach to Grumman will be used. Machining of LTCC tapes will be done using the "cold" technique developed by Nowak. To avoid the collapsing of internal structures, such as, channels and reservoirs, nanocarbon sacrificial layers will be used as SVM. Heralock™ 2000 self-constrained LTCC will be used; therefore only shrinkage in the Z-direction must be considered in the design and the positional uncertainty which could create difficulties during the automatic wire bonding operation will be eliminated. In addition, the feasibility of machining the nanocarbon layers using the "cold" technique will be studied. All these changes will lead to a faster manufacturing process.

CHAPTER 3

MICROMACHINING OF LTCC AND NANOCARBON LAYERS WITH CO_2 LASER

3.1 Introduction

In this chapter, the description of the more important characteristics, such as control signals, power stability and control of power on target using an acousto-optic modulator, of the new in-house custom CO_2 system developed by PowerPhotonic Ltd in collaboration with our research group for machining LTCC are presented. The obtained etching rates of HeraLock® HL2000 and CeramTape GC tapes using the custom CO_2 system are reported. The capability of the system for cutting 250 µm nanocarbon layers, which will be used as SVM for inner structures, is demonstrated. Finally, the matching between LTCC and SVM features, which is necessary to obtain a defined inner structure, is shown.

3.2 Set Up for "Cold" Ablation of LTCC

As mentioned in Section 2.4, Nowak [63] developed a novel "cold" self-cleaning technique for processing LTCC in "green" state. This technique uses a low-power CO_2 laser, which results in high-speed cutting with negligible thermal effects at the interaction site; therefore, the machining of precise 2D structures can be achieved. Because of the advantages of the "cold" technique, the MicroSystems Engineering Centre (*MISEC*) at Heriot-Watt University decided to incorporate this technology in the fabrication of LTCC micro-devices. For this, a CO_2 micromachining laser system was developed by PowerPhotonic Ltd in collaboration with our research group (Laser and Photonics Applications). A diagram of the designed system and the one built are shown in Fig. 3.1 and Fig 3.2, respectively.

The key element of the system is a CO_2 slab laser from Rofin-Sinair UK Ltd. The SC x10 laser is a high-frequency excited diffusion cooled slab laser, designed for industrial use as a cutting, welding, drilling or marking tool. At 20 °C coolant temperature with a frequency of 20 kHz and 50 % duty cycle it can deliver 100 W average and peak power of 240 W with a stability of ±7%. The output beam is slightly elliptical with a near-Gaussian profile with a M^2<1.2 and diameter ($1/e^2$) of 7.5±0.5mm.

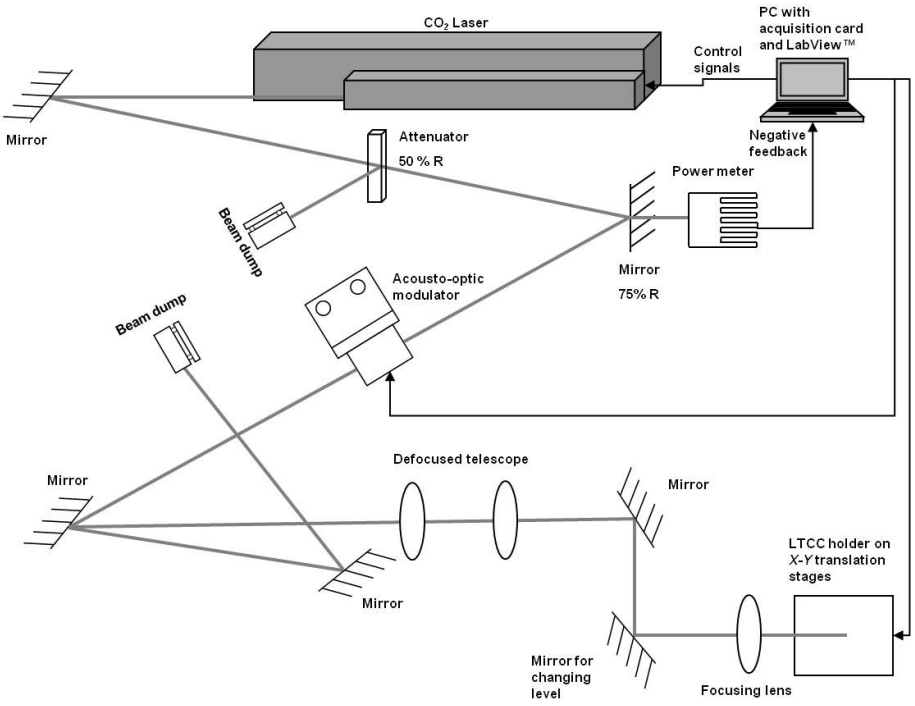

Figure 3.1 Schematic of the CO_2 system for micromachining LTCC in green state

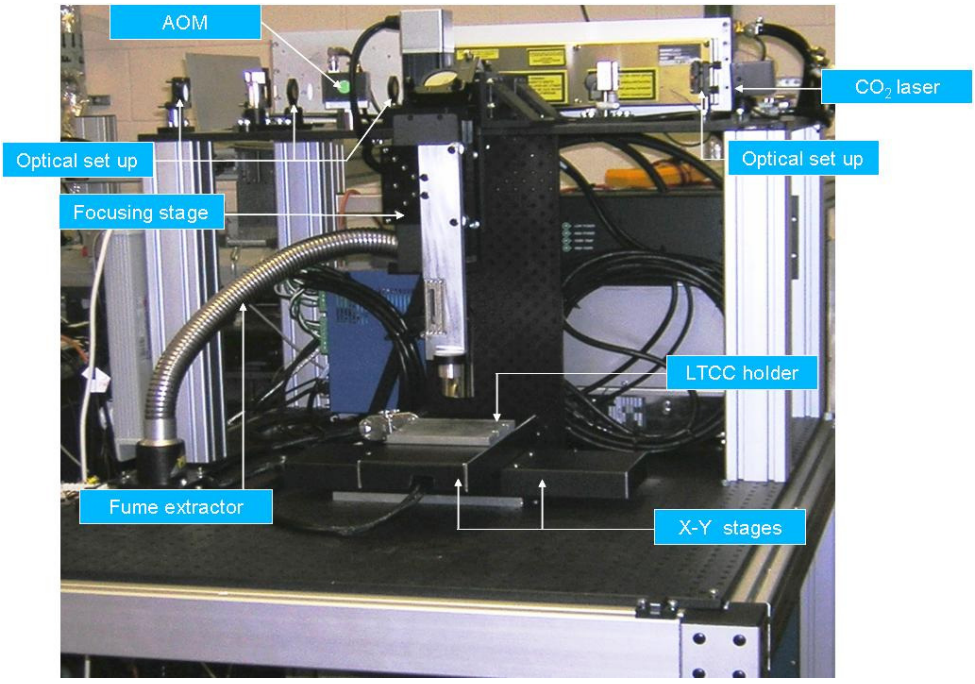

Figure 3.2 CO_2 laser micro-machining system for LTCC

The laser is used in a quasi-CW mode, controlling the RF power supply is a 5V rectangular signal with a frequency of 20 kHz and duty cycle of 20 % as seen in Fig. 3.3; these conditions result in an average output power of ≈50 W.

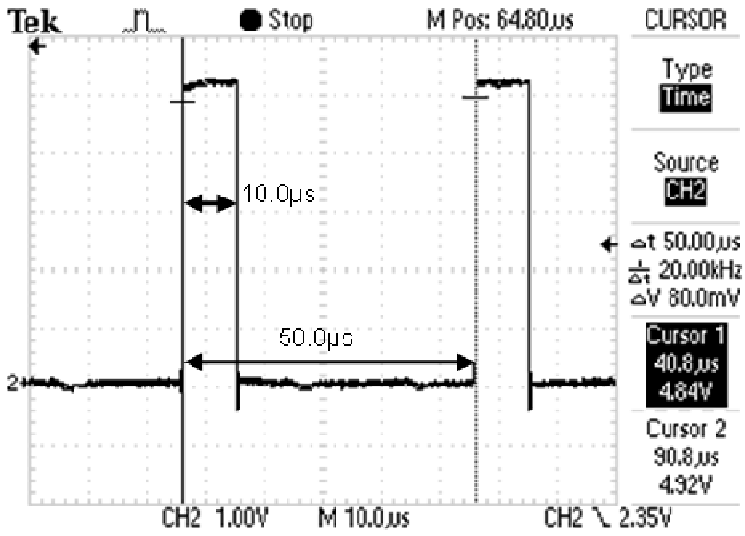

Figure 3.3 20% duty cycle laser control signal

As seen in Fig. 3.1, a germanium acousto-optic modulator *AOM* (NEOS Technology, USA) was used in the optical set-up. The AOM had restrictions in the beam size and incident optical power. Optical beam diameter on the AOM must not exceed the 5.0 mm height of the acoustic aperture to avoid distortion of the beam. The beam was reduced from 7.5 mm to 5 mm using a gold coated concave mirror with a radius of curvature of 10 meters. Power was reduced from 50 W to 18.75 W to avoid thermal lensing in the germanium crystal and possible damage of the modulator. For this, a 50:50 beam splitter and a 75 % reflectivity mirror were used, as shown in Fig. 3.1.

The 25 % of power transmitted by the mirror was measured at rate of 10 Hz by a thermopile-based power detector (Gentec-EO, Canada). The measurement was used to stabilize the output power of the laser using a proportional-integral-derivative (*PID*) feedback loop implemented in a LabView program, which modifies the duty cycle of the RF power supply control signal. Less than 0.4% peak-to-peak power variation with 26 dB S/N ratio was obtained, as shown in Fig. 3.4.

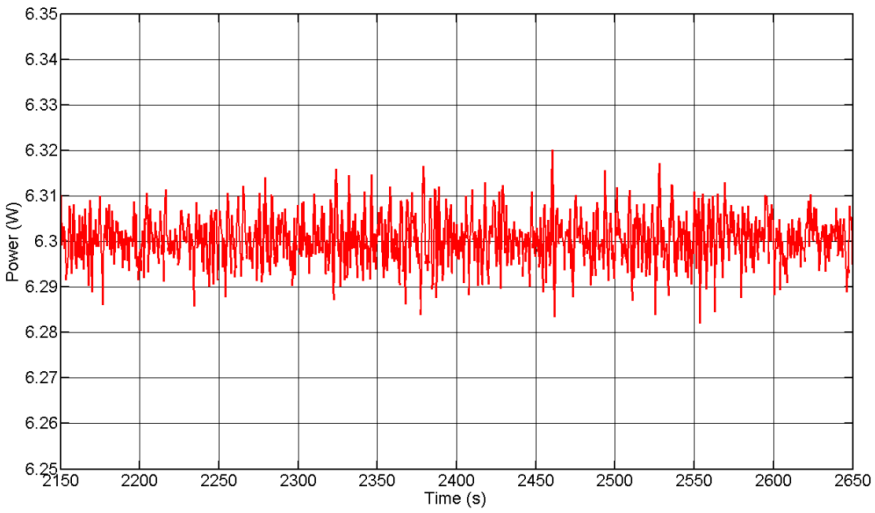

Figure 3.4 Output power stability

The 75% reflected power was directed to the AOM. The AOM is used to provide rectangular pulses of controlled duration and power to the LTCC tape without disturbing the laser output stability. It is capable of providing single pulses for via drilling and power control for continuous cutting or machining at different levels of one LTCC layer (grey-scale). The AOM deflects radiation into the first diffraction order with the desired power; meanwhile, the zero order is guided to a beam dump. The AOM is controlled by pulses with a minimum duration of 100 µs with increments equal to the period of the laser control signal. Pulses are synchronized with the control signal of the laser, as shown in Fig. 3.5.

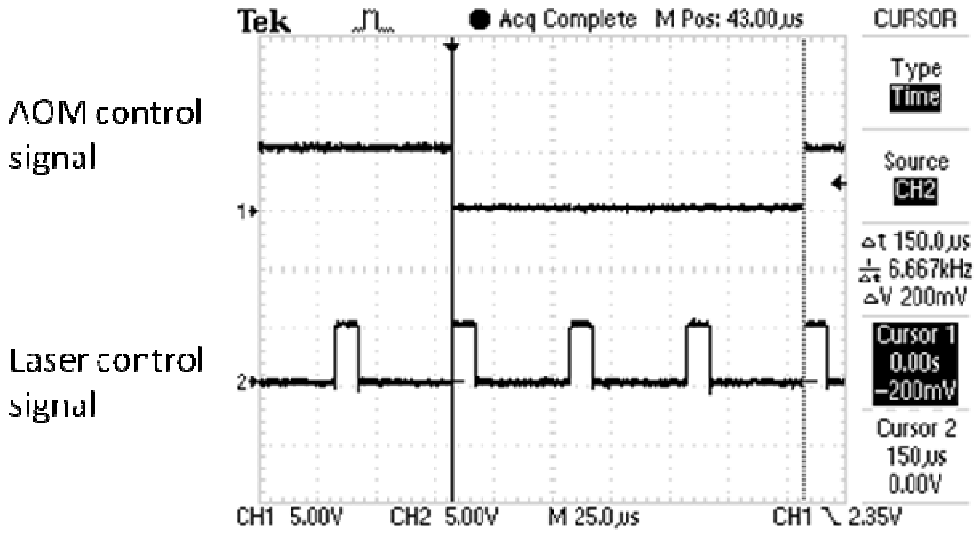

Figure 3.5 150 µs AOM control pulses synchronized with laser control signal

To achieve an approximately 100 µm machining spot size, the deflected beam must be re-expanded ≈ 1.8 times before reaching the final lens, a 2.5″ (63.5 mm) focal length ZnSE meniscus mounted on a motorized vertical translation stage. For this, a telescope defocused by 1″ (25.4 mm) was used. The telescope was formed by two ZnSe lenses with 2″ (50.8 mm) and 5″ (127 mm) focal lengths.

LTCC tape to be machined was held in position using a 6″ (152.4 mm) × 6″ (152.4 mm) porous ceramic vacuum chuck with pore size of less than 20 µm and ±1 mil (25.4 µm) flatness. The handling of pieces up to 6″ × 6″ was necessary because the commercial equipment for LTCC, such as stacker, laminator and screen printer, used by the MISEC group have been designed to work with pieces of this size. Vacuum chuck was mounted on two ALS130 (Aerotech, USA) mechanical bearing, linear motor stages configured as an *XY* assembly with travelling distances of 150 mm, resolution of 10 nm and non-contact encoders. Both were controlled using Ndrive 10B-MXH-AUXPWR drivers. The Ndrive included a Position Synchronized Output (*PSO*) or Laser Firing option which was programmed to generate an output signal synchronized to the *X* axis position. The PSO signal was programmed to trigger the AOM control signal, as shown in Fig. 3.6.

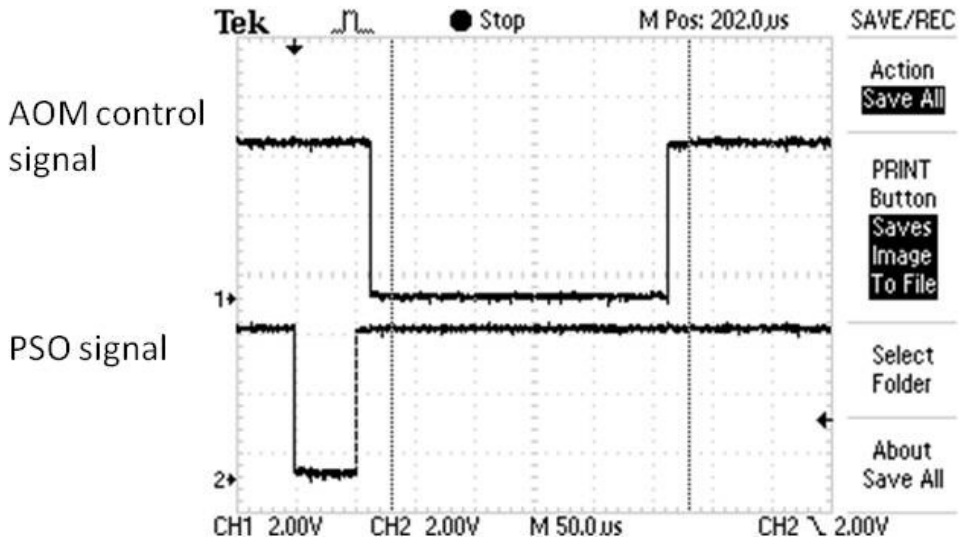

Figure 3.6 PSO signal triggering a 250 µs AOM control signal

Figure 3.7 shows the triggering of 250 µs AOM control pulses every 50 µm during the travelling of the *X* axis stage at speed of 10 mm/s.

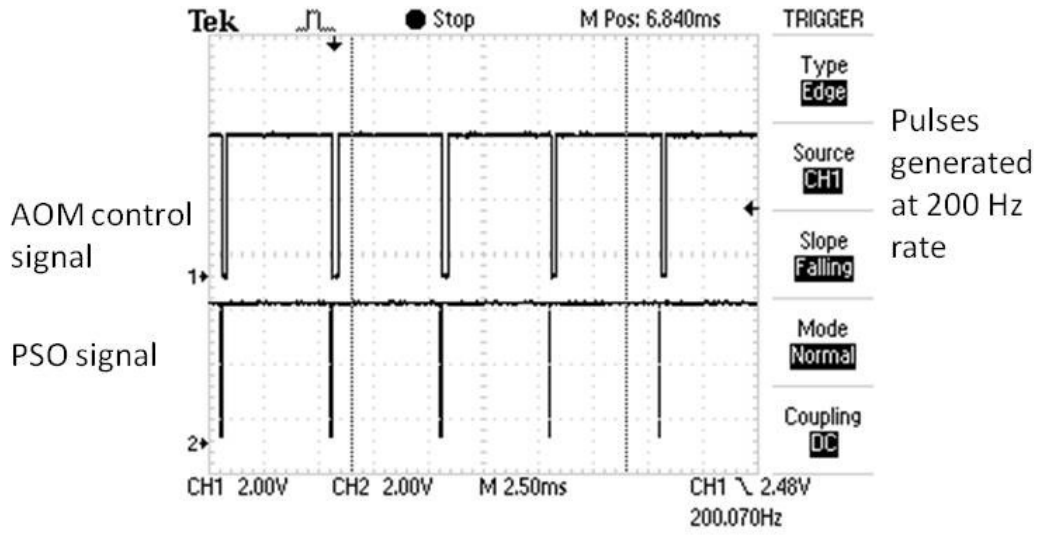

Figure 3.7 Train of 250 µs AOM control pulses generated every 50 µm during the travelling of the X axis stage at speed of 10 mm/s

To verify the machined features off-line, without removing the tape from the vacuum chuck, the laser system was equipped with a 4x magnification and 3 µm resolution video microscope mounted on the focusing translation stage.

Finally, the system was equipped with a recirculating chiller (Thermo Scientific, USA), with a heat removal capacity of 1250 Watts and temperature stability of ±0.1°C, for cooling the laser, AOM and beam dumps.

3.2.1 Computer controlled machining software

The control software of the machining system was developed by PowerPhotonic Ltd. on the LabView platform. Custom commands were created to instruct the movement of the translation stages to cut the required patterns. These commands were introduced through user input or text file. The use of custom instructions prevented us from directly converting design drawings into text files containing universal movement instructions, such as G-Code, recognized by any motion controller.

G-code is the widely used Computer Numerical Control (*CNC*) programming language, used mainly in automation. The advantage of G-code is that it can be translated directly from the Data eXchange File (*DXF*) generated from any Computer-Aided Design (*CAD*) drawing done in TurboCAD 2D, AutoCAD or other CAD design software. This gives the benefit of speed and ease of design.

In our case, every command for the movement of the translation stages was introduced manually in the input text file. As the complexity of the design was increased, the manual input became time-consuming and more prone to typing errors. For example, some of our text files required the input up to 1800 code lines.

To alleviate this, an interpreter on the LabView platform was created to translate a G-code file to a text file containing instructions recognized by the control software of the machining system. The flow process involved drawing the required pattern on TurboCad 2D (IMSI Design, USA) and saving it as DXF file. The DXF file was converted to a G-code file using the CAM Expert (RibbonSoft, Germany) software. Finally, the generated G-code file was converted to a text file with recognizable instructions using our translator software. This reduced the time of generating the text file from hours to less than 15 minutes. The translator software and examples are presented in Appendix 1.

3.3 Optimal Focal Position for Machining LTCC and Beam Size

The objective of the experiments described in this section was to determine the optimal focal position for machining LTCC and the size of the beam at this position. Because a circular spot was desired for machining and the laser beam had a slightly elliptical profile, it was necessary to find the position of the final lens in which the diameter in *X* and *Y* direction of the beam were almost equal. For this, craters were machined, moving the final lens in 25 µm steps around the focal region, on a 1 mm thickness fused silica substrate using pulses with a fluence of 108 J/cm^2. Figure 3.8 shows the evolution of the beam at different positions of the final lens.

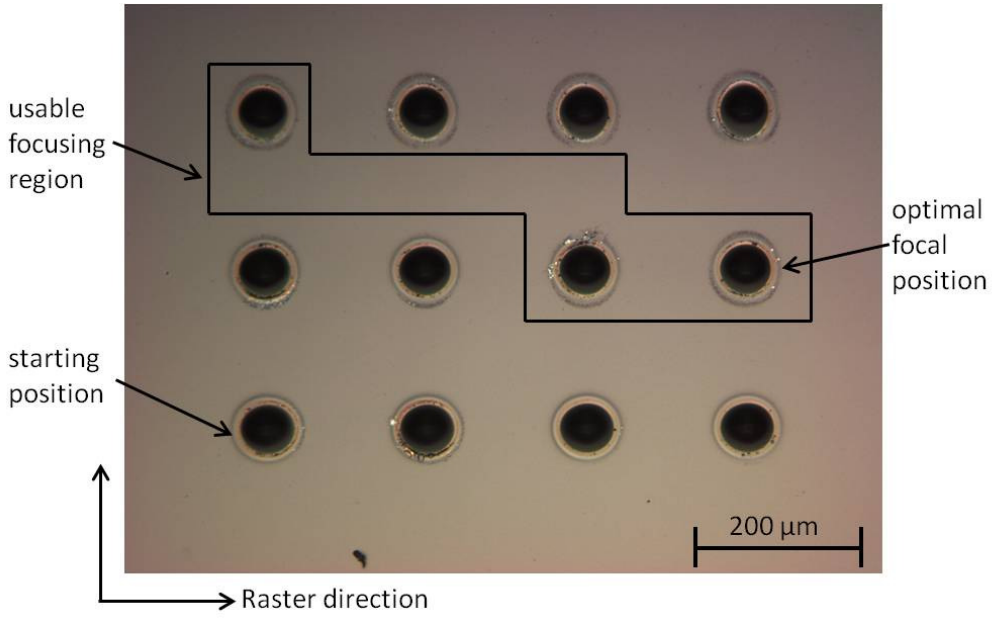

Figure 3.8 Matrix of machined craters spaced 25 µm along the focal region to determine the optimal position of the final lens

To determine the size of the machining beam at the optical focal position, diameters of machined craters on fused silica substrate using fluences from 27.5 J/cm^2 to 197 J/cm^2 were fitted to a Gaussian distribution. The resulting diameter of the machining spot was 98.4 µm ($1/e^2$ level).

3.4 Machining of LTCC and Nanocarbon Tapes

This section describes the experiments carried out to determine the conditions for machining LTCC tapes of different compositions and thicknesses such as HeraLock® and CeramTape. The calibration curve for material removal rate for nanocarbon tape, which will be used as sacrificial volume material during the lamination step, will be presented as well. It is worth mentioning, machining conditions for carbon tape have not been reported previously.

3.4.1 Machining of HeraLock® LTCC tape

The first experiment was carried on HeraLock® HL2000 to obtain the machining conditions. For this, matrixes at different irradiances and pulse durations were machined. To avoid potential handling damage of the tape and/or machining of the porous ceramic vacuum chuck, the machining was done with the tape on the Mylar carrier.

From now on, the fluences reported corresponded to the fluence deposited in the material by the peak of the Gaussian beam (beam axis) per a single laser shot. It was calculated using

$$F = \frac{2E_p}{\pi w^2} \tag{3.1}$$

where:
w is the radius of the beam at FW $1/e^2$
E_p is the energy of each pulse generated by the AOM and is defined as

$$E_p = t * P_{peak} \tag{3.2}$$

where:
t is the duration of the pulses
P_{peak} is the peak power.

As laser was operated in QCW mode, P_{peak} was considered approximately equal to the average power measured by a CW laser power meter placed after the final lens, when the AOM was driven by a control signal ≥ 60 sec (refer to Fig. 3.5).

Machining was done using raster mode in continuous pulsing, at a frequency of 200 Hz and fluences in the range of 0-50 J/cm^2. Speed of 10 mm/sec and 50 µm pitches in both *X* and *Y* directions were used. Pulses with duration of 100, 150 and 200 µs were used. The image in Fig. 3.9 shows four "stair-step" patterns machined using 150 µs pulse duration. Every "step" was machined in an area of 3.3 mm x 3.3 mm using different fluences. The dimensions of the step were chosen to have a macroscopic view of the machined area, making it easy to measure them. Four patterns were machined to investigate the repeatability of the process.

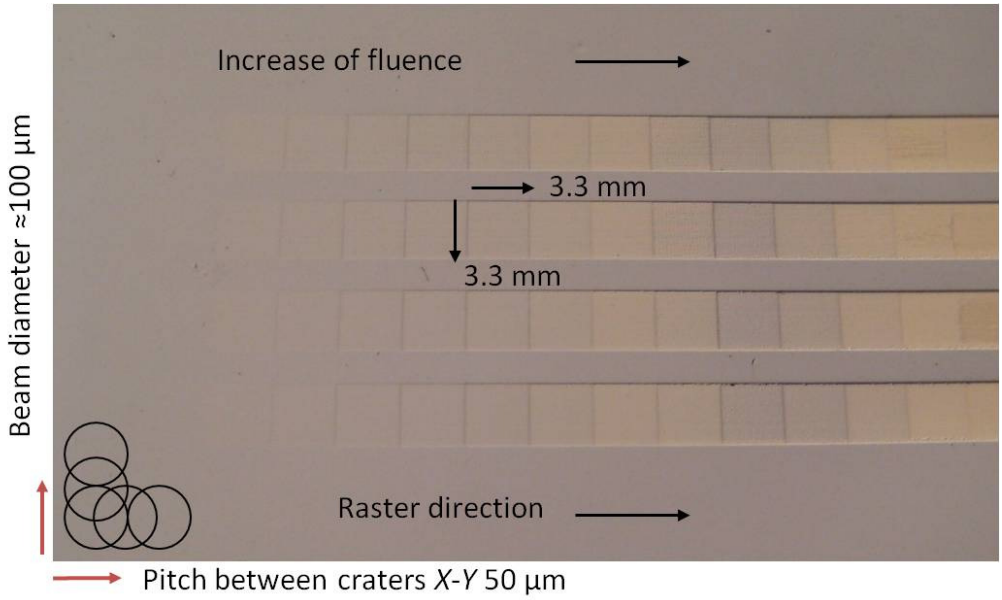

Figure 3.9 Machining pattern used to determine material removal rate

The measurement of the 3D patterns was done using a Proscan 1000, whose core is a non-contact chromatic white light confocal sensor consisting of a CHR-150 controller and OP300VM optical pen (STIL, France). The OP300VM has a working distance of 300 µm with an axial resolution and accuracy of 10 nm and 90 nm, respectively. At first, because of the granular nature of the tape which highly diffused the white light, the surface measurement was quite difficult. To overcome this, the equipment was sent to STIL for recalibration to allow it to be used with LTCC tapes.

Depth profiles along one scanning line of the machined patterns using 150 µs and 200 µm pulses at different fluences are shown in Fig. 3.10 and Fig. 3.11, respectively. The graph in Fig. 3.12 shows the machining depth for different fluences at different pulse widths.

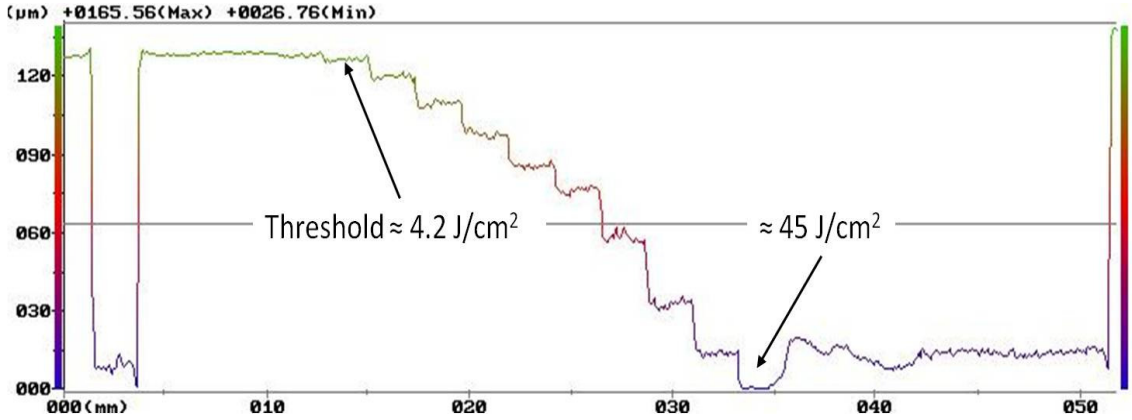

Figure 3.10 Central line depth profile of machined pattern using 150 µs pulses at different fluences

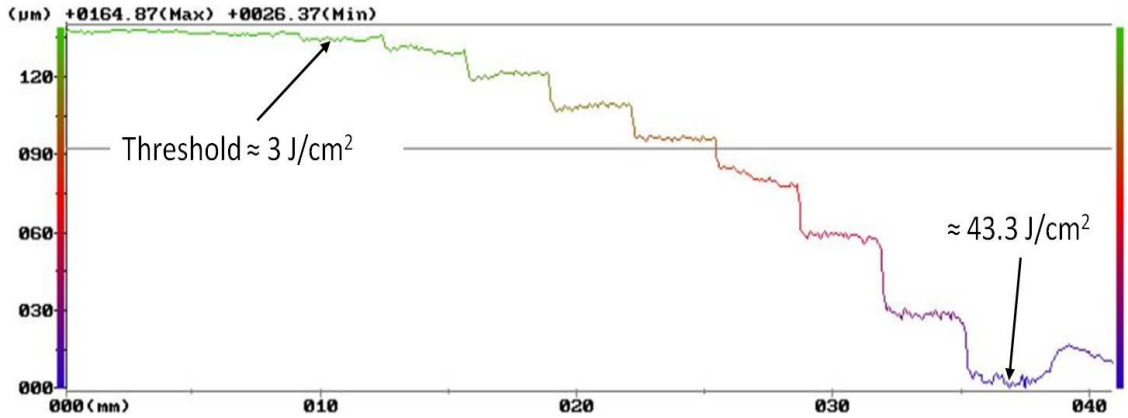

Figure 3.11 Central line depth profile of machined pattern using 200 µs pulses at different fluences

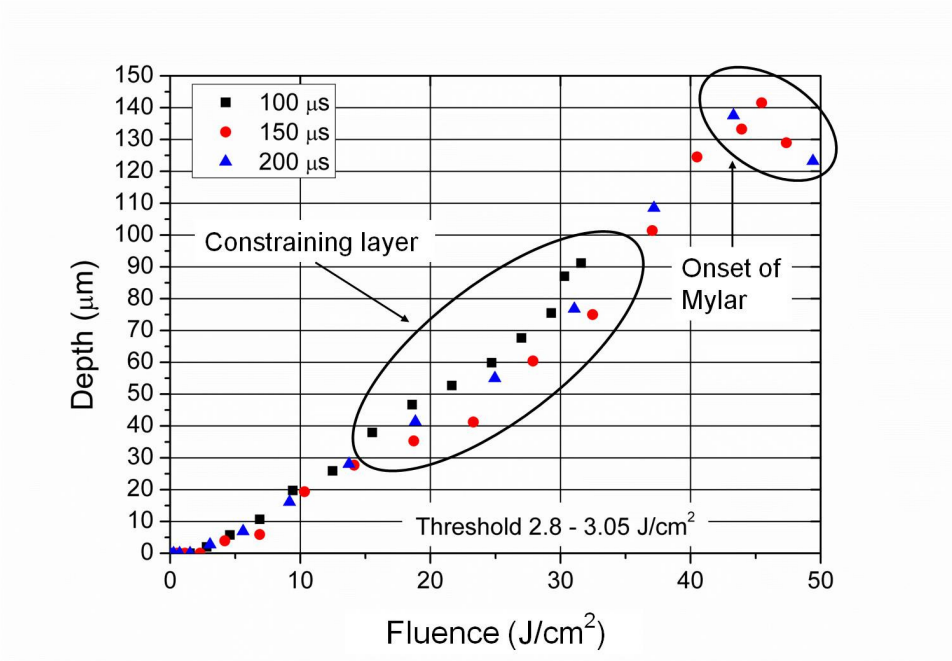

Figure 3.12 Machining depth in 130 µ HL2000 LTCC sheet for 100 µm beam diameter at different pulse widths

Results showed that the machining depth depends on the deposited energy in the material and not in the pulse length. In Fig. 3.12, decay in the etching rate is observed between 15 J/cm^2 and 34 J/cm^2. It is believed that the change was the effect of machining the middle or constraining layer, which has a different composition to the two layers in which is sandwiched, as explain in Sec. 2.3.7. A similar effect is observed in the results reported by Nowak [63] machining HL2000. The results indicate a threshold value close to 2.8 J/cm^2 and a maximum removal volume rate of 365 pico-litres per shot at fluence of 43.3 J/cm^2. The fluence to machine through the 130 µm tape was ≈ 43.9 J/cm^2.

3.4.2 Machining of CeramTape GC LTCC tape

The purpose of the experiment described in this section was to observe the machining performance in a tape of different composition and thickness to Heralock. The chosen tape was CeramTape GC (CeramTec, Germany) with a thickness of 330 µm. Unlike Heralock, Ceramtape is a standard tape which shrinks in *X-Y-Z* (20.5 %, 21.5 %, and 18 %) directions. The calibration curve for material removal rate was obtained with a similar method as the one for Heralock; raster mode using continuous pulsing at a speed of 10 mm/sec and 50 µm pitch in *X-Y* direction. As observed in Fig. 3.13 and Fig. 3.14, for fluences greater than a 45 J/cm^2 a re-deposition of the ejected particles over the machining area occurred.

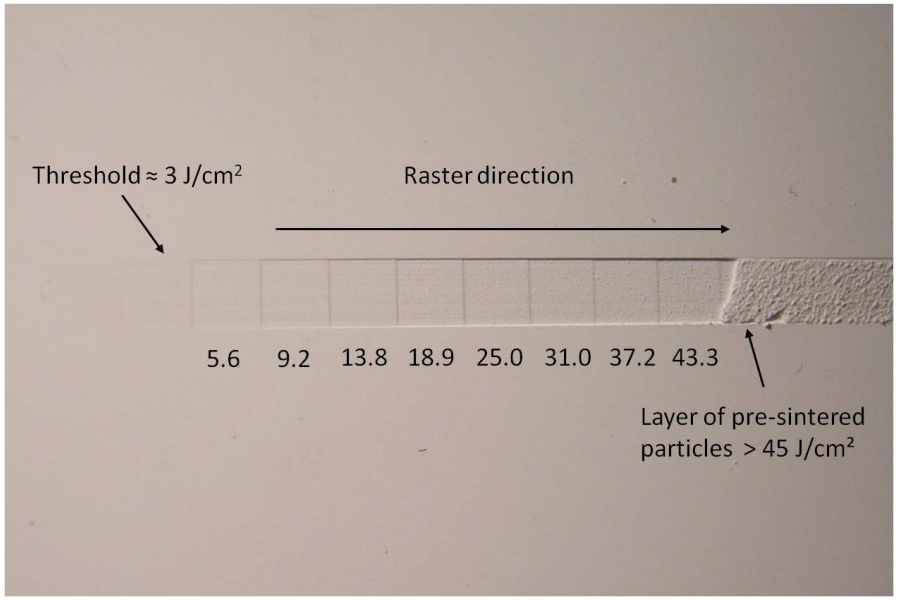

Figure 3.13 Picture of machined pattern on CeramTape GC showing a layer of pre-sintered particles formed using fluence greater than 45 J/cm^2

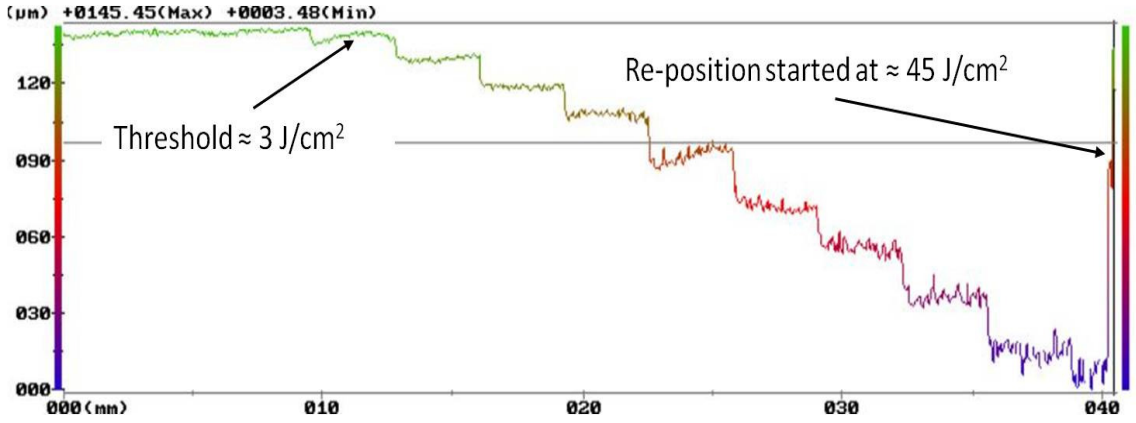

Figure 3.14 Central line of depth profile of machined pattern on CeramTape using 200 µs pulses

According to the experiment, it is believed that as the machining depth increases, the force of the expanding gases becomes insufficient to drag the ceramic particles far from the ablation site. Because of this, particles re-deposited over the same site. This limited the depth of machining to approximately 135 µm.

A similar machining performance was observed for the HeraLock® HL2000 and CeramTape GC tapes, as seen in Fig. 3.15. Results suggested that the "cold" machining was practically independent of the material composition of the two tapes.

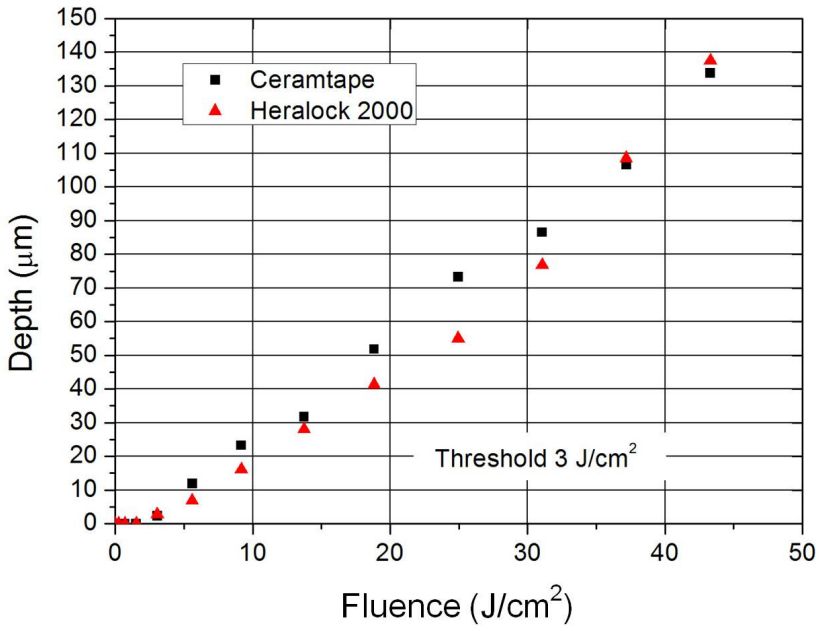

Figure 3.15 Machining depth rate in HL2000 and Ceramtape LTCC using 200 µs pulses

The capability of machining at different depths in one layer gives the ability of placing components at different levels on the same layer. In our case, it is important because it will allow the placing of Fast-Axis Collimation (*FAC*) lenses at the required height for the fast-axis beam correction.

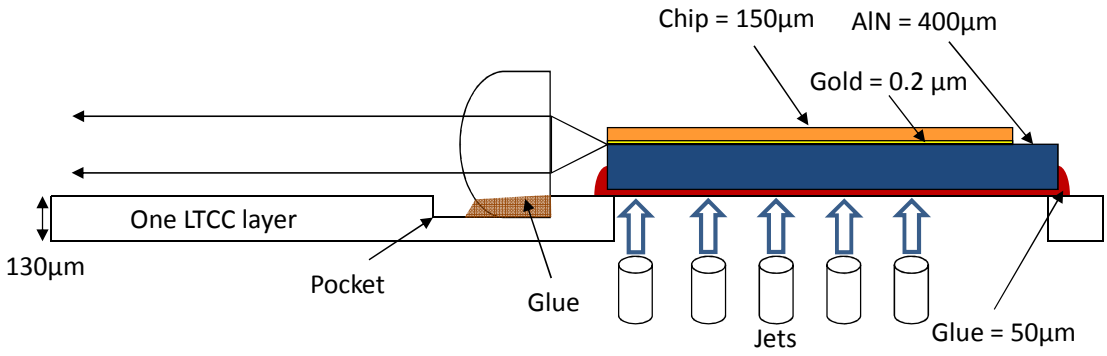

Figure 3.16 Machined pocket in one LTCC layer for the placing of a FAC lens at the optimal position

3.4.3 Machining of nanocarbon sacrificial volume material (SVM)

To avoid the collapsing or deformation of internal structures during lamination, nanocarbon tape was used as the sacrificial volume material. Tape from Thick Film Technologies (USA), designed to work with LTCC and HTCC tapes, was chosen. As carbon tape with thickness matching or close to the 130 µm ± 5 µm of HL2000 is not available, the use of 250 µm thickness carbon tape, which almost matches two HL2000 layers with a total thickness of 260 µm ± 10 µm, was decided upon.

Because a good fitting between carbon pieces and LTCC structure is needed to preserve the geometry of the inner structure, carbon pieces with cutting edges of high quality surface are required. This motivated us to investigate the possibility of laser machining of the carbon tape using our CO_2 system; little has been reported on laser machining of carbon tapes. In 2009, Malecha [70] reported using a Nd-YAG laser for cutting 150 µm carbon tapes, he found modification in the thickness of the tape in the vicinity of the ablation site, which led to a deformation in the geometry of the embedded channels during lamination [71]; in both publications, machining parameters were not provided. Malecha, also reported the deformation of channels due to the mismatch between widths and heights of channels and carbon pieces.

Although powder compositions are different in LTCC and nanocarbon tapes, the volumes of binder are similar in both cases; about 40 % in carbon tapes, 33 % in HeraLock HL2000 and 45 % in Ceramtape. Similar machining behaviour was expected for carbon tape, as binder is the vehicle for the particle ejection in the three-stage "cold" machining process.

The same experiments, as for HL2000 and Ceramtape, were carried out to obtain a calibration curve for material removal rate for nanocarbon tape; the results are shown in graph in Fig. 3.17. A concern during the experiments was the possible damage of the ceramic vacuum chuck because the carbon tape was machined without any carrier, even when the machining threshold for alumina is in the range of 750 J/cm^2 to 1000 J/cm^2. After experiments, indication of damage on the surface of the ceramic vacuum chuck was not found.

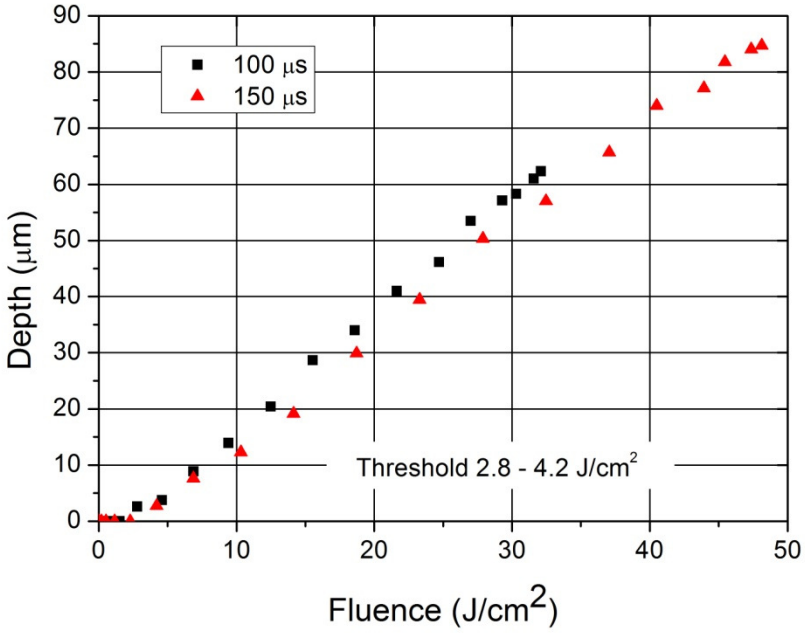

Figure 3.17 Machining depth rate in 250 µm nanocarbon for 100 µm beam diameter using 100 and 150 µs pulses

As seen in Fig. 3.17, the machining depth of nanocarbon tape was very similar to the one for green LTCC. Comparable threshold was observed for both materials, approximately 3 J/cm^2 but with a material removal rate for carbon 30% lower of that for LTCC tape. Modifications in the shape of the machined tape near of the ablation site, as reported by Malecha [70], were not observed.

It is believed, due to the low absoption of graphite at 10.6 µm as reported by Tuinstra and Friedel [72, 73], that the machining behaviour is caused by the CO_2 light deposited directly in the polymer binder. In the case of LTCC, light is highly absorbed by the ceramic particles and transferred as heat to the surrounding binder producing its decomposition. The decomposition of the binder creates gases at rates sufficient to drag the particles away from the machining site. Further investigation is needed to fully understand the machining mechanism of nanocarbon tapes.

The machining of nanocarbon tapes gives the possibility of fabricating internal structures of arbitrary height without any distortion. Designs are not limited to the thickness of the commercial carbon tapes.

3.5 Line and Trepanning Cutting of LTCC and Nanocarbon Tapes

In this section, the appropriate conditions for cutting LTCC and nanocarbon tapes are described. Materials were cut overlapping single laser shots, as seen in Fig. 3.18.

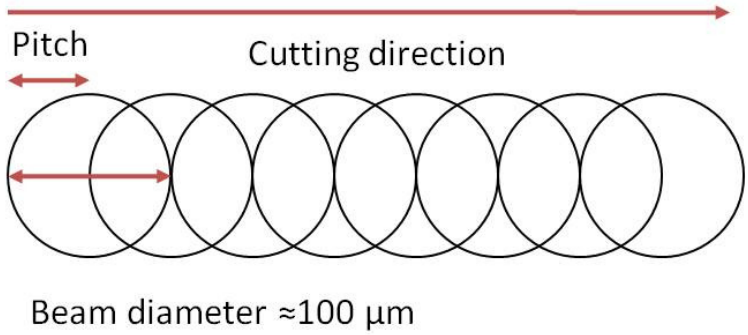

Figure 3.18 Overlapping of single shots to cut through LTCC tape

Parameters such as number of passes, pulse widths and pitch between shots were studied. All experiments were done with HL2000 on Mylar carrier. The optimal condition for cutting 130 µm HL2000 were double pass, 150 µs pulses with a fluence of 27.9 J/cm^2 and spaced by 25 µm. For fluences greater than 30 J/cm^2, carbonization of the binder and melting of the Mylar was observed. An example of the quality of cutting line on HL2000 is shown in the 5× micrograph in Fig. 3.19. A 20× micrograph of the cut is inserted in the same figure.

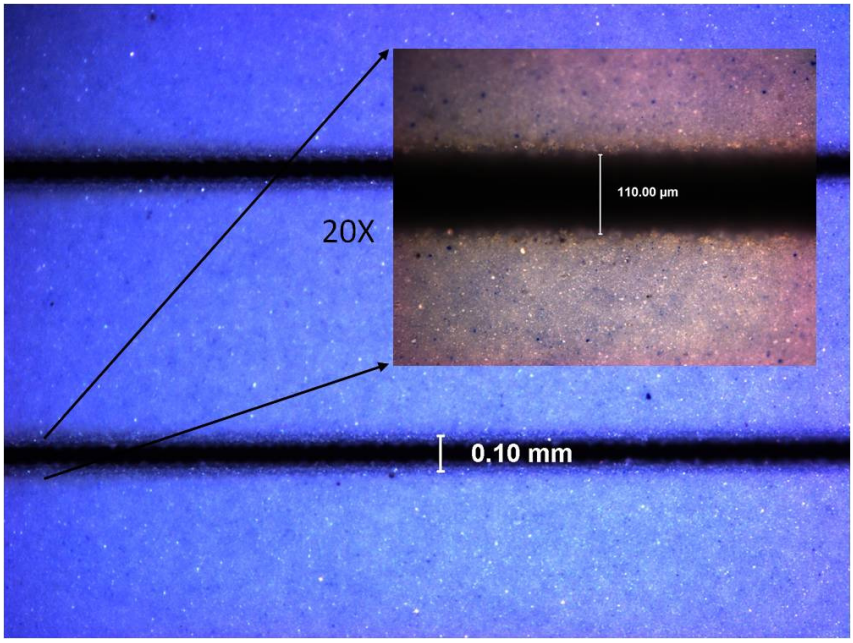

Figure 3.19 5× micrograph of cutting line on HL2000 using 27.9 J/cm^2 fluence. A 20× micrograph of the cut is inserted

In the case of machining holes of larger diameter than the beam size, trepanning cutting was used. In trepanning, the required hole is created by placing multiple laser drilled apertures next to each other in an overlapping circular path. The 5× micrograph in Fig. 3.20 shows an example of a 700 µm designed diameter via using trepanning cutting.

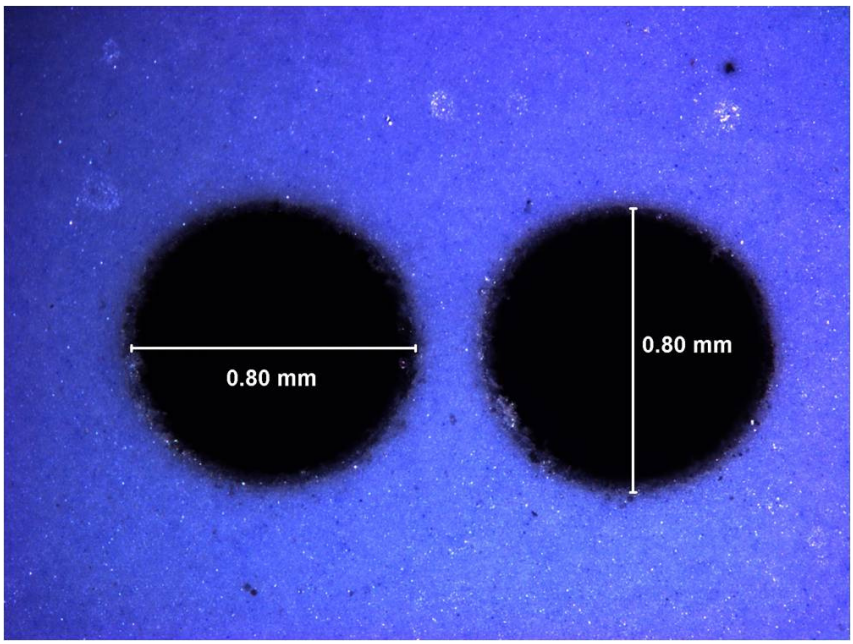

Figure 3.20 5× micrograph of a 700 µm designed diameter via using trepanning cutting

As the hole was designed to be cut using the centre of the 100 µm wide cutting line (Fig. 3.19), the diameter of the hole was increased from 700 to 800 µm. No evidence of heat affected zone (*HAZ*) is observed on the region cut. As well, the cut region is debris-free. However, the diameter of the trepanned holes was limited to no less than 300 µm because of the presence of HAZ in the cutting region. As the diameter of the hole is reduced and considering the size of the laser beam, the spacing between laser shots need to be smaller. As a result, a larger amount of energy is deposited in the same area producing the burning of the LTCC tape due to insufficient heat dissipation on the material. This led to irregular shaped holes.

Figure 3.21 shows the quality of 8 layers machined using line and trepanning cutting. Layers were stacked to form a water inlet and internal channels structures.

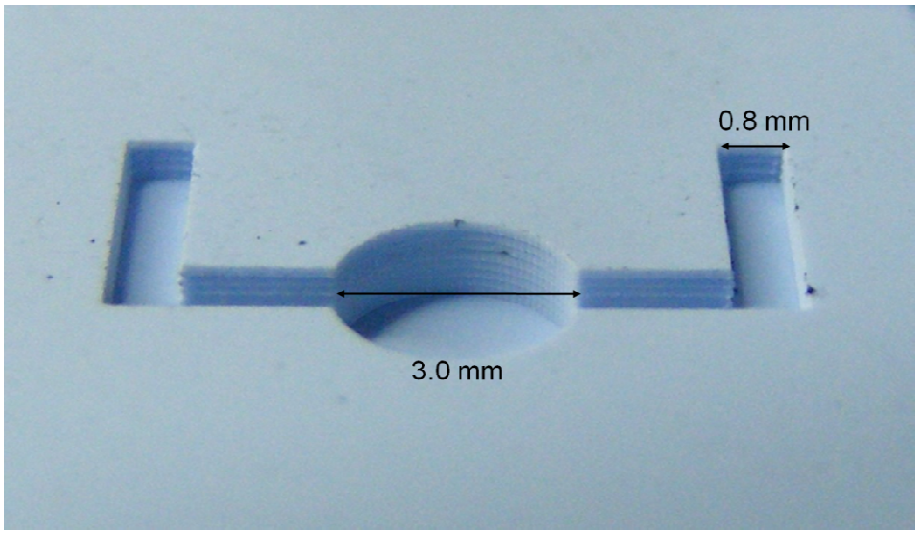

Figure 3.21 Layers stacked to form a 3000 × 780 µm^2 water inlet and 800 × 520 µm^2 water channels. Layers were cut using line and trepanning cutting

To obtain the optimal conditions for cutting the nanocarbon tape, similar experiments as for LTCC tape were carried out. Cutting conditions for nanocarbon were double pass, 350 µs pulses with a fluence of 65 J/cm^2 and laser drilling shots spaced by 25 µm. Image in Fig. 3.22 shows different cut carbon pieces of different dimensions.

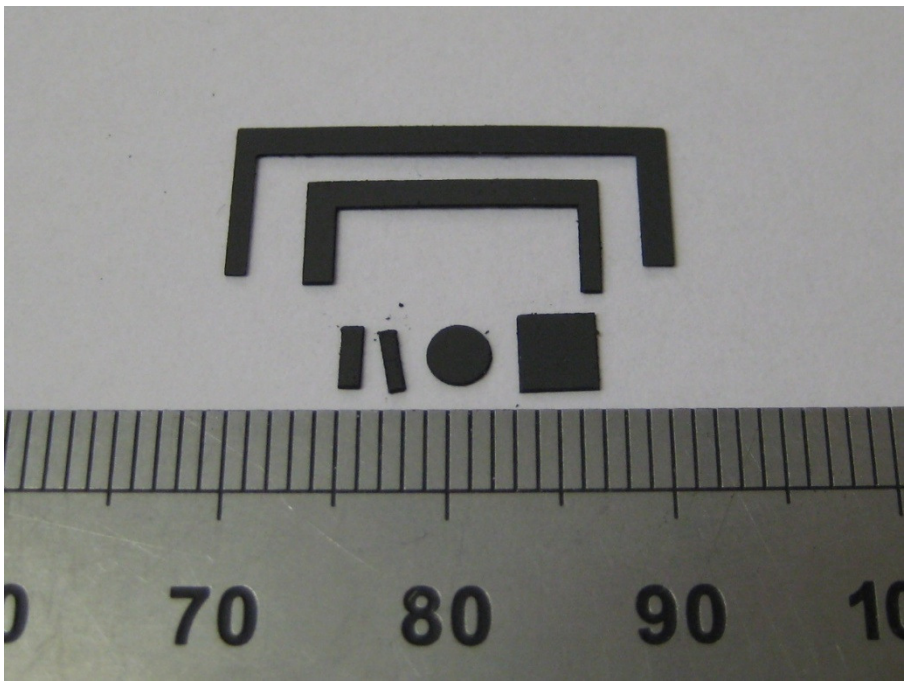

Figure 3.22 Nanocarbon pieces of different dimensions cut by line and trepanning cutting. Scale is in millimetres

3.6 Matching Between LTCC and Nanocarbon Tapes

As explained in Sec. 3.4.3, to obtain a defined inner structure, a good fit between the LTCC apertures and the carbon filler is needed. Due to the intensity profile of the laser beam, tapers always exist on laser machined components. At optimal conditions, the taper induced by the laser cutting on LTCC is approximately 13° while on nanocarbon it is approximately 10°. If same size cutting tracks are used for both pieces, consideration of both the taper and cut offsets results in a gap between the LTCC and nanocarbon is approximately 110 µm when there is no compensation. Picture in Fig. 3.23 shows an adequate fit between a nanocarbon disk and LTCC substrate, for both pieces with a designed cutting diameter of 3 mm. If the gap between the LTCC and nanocarbon pieces becomes larger, the internal structure can deform during the lamination process.

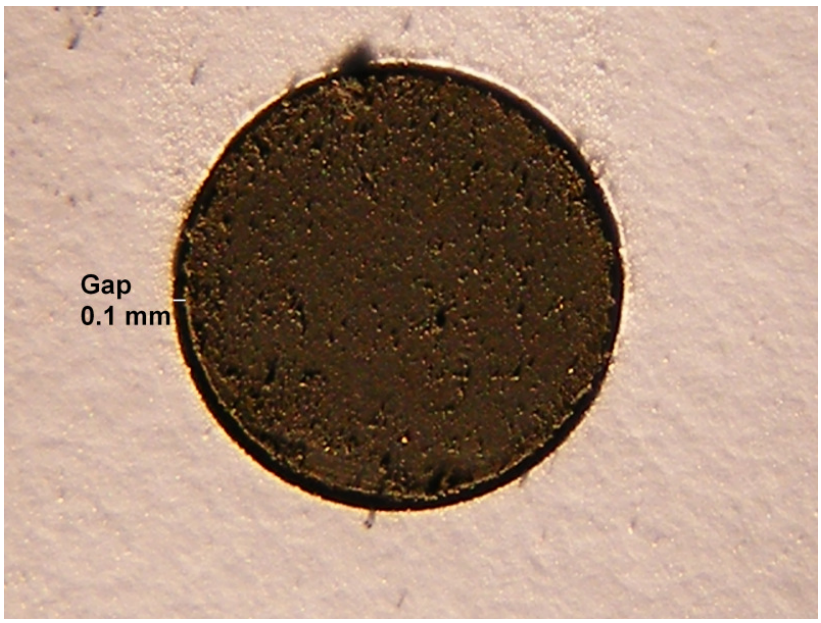

Figure 3.23 Water inlet filled with matching 3 mm nanonocarbon piece

The picture in Fig. 3.24 shows the insertion of a nanocarbon piece into two stacked LTCC layers forming a water channel.

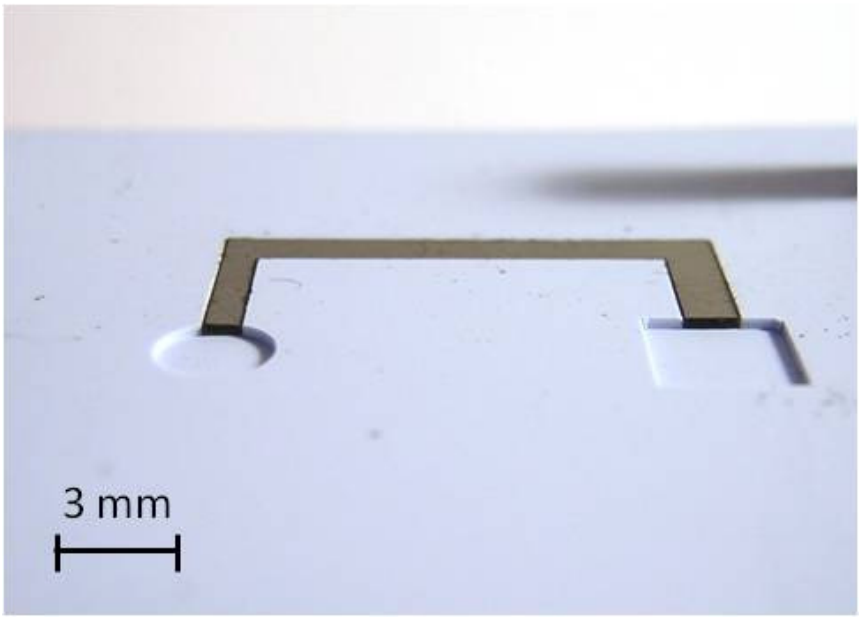

Figure 3.24 Embedded channel formed by two 130 µm LTCC layers and filled with a 250 µm carbon piece

3.7 Summary

We have presented a CO_2 machining laser system capable of machinning high-quality features in LTCC or nanocarbon tapes. We have demonstrated the immunity of the

“cold” process to the different compositions of LTCC commercial tapes. The machining conditions for carbon tape are reported for the first time. We have reported the conditions for line and trepanning cutting of LTCC and nanocarbon tapes, as well. Finally, we have demonstrated the good fitting between nanocarbon inserts and LTCC structures, which is necessary to avoid the distortion during the lamination process.

CHAPTER 4

FABRICATION AND TESTING OF A LAMINATED STRUCTURE IN LTCC FOR COOLING A HIGH POWER BROAD AREA SINGLE EMITTER DIODE LASER

4.1 Introduction

In this chapter we report the design and fabrication of a circular jet nozzle, capable of impinging water on the back surface of an AlN submount within a ceramic substrate using lamination of laser-cut LTCC and nanocarbon layers. The use of direct liquid jets offers the advantage that the thin liquid boundary layer just outside of the impingement region produces a higher heat removal rate [74]. This development addressed the thermal management of a high power broad area single emitter diode laser on an aluminium nitride (*AlN*) sub-mount through water jet impingement. The fabricated structure provided zero-distortion flatness allowing the accurate positioning of integrated optical elements, such as a fast-axis collimation lens, and the printing of silver tracks to supply high current on board. Key modifications to the manufacturing processes to obtain a structure with the quality required are reported. Performance parameters of the cooling structure, such as flow rate, pressure drop and thermal impedance are given. Two generations of coolers were developed, however just the fabrication process for the second generation and its performance parameters are reported in this thesis. A brief description of the first generation is given in Sec. 4.16. Finally, the correction of the high divergence in the fast-axis of the diode laser using a fast-axis collimation lens (*FAC*) placed on the LTCC structure is demonstrated. The knowledge gained during the development of this prototype will serve as the basis for the manufacture of structures capable of accommodating multiple single emitter diode lasers.

4.2 Cooling Structures for Diode Laser Bars Using LTCC Technology

The first successful use of LTCC material for the fabrication of coolers was done by Cutting Edge Optronics Northrop Grumman [22, 69]. LTCC was used to avoid the drawbacks of the copper microchannel coolers, such as erosion and corrosion caused by the use of deionised water. The design addressed the cooling of a 1 cm diode laser bar with a 1.2 mm cavity length and ≈ 54 % fill factor with an output power of 100 W mounted on the top of high thermal conductivity substrates. The back surface of the

substrate was cooled by 27 impingement jets with a diameter approximately of 200 µm using a water flow rate of ≈ 0.8 $lmin^{-1}$; with these parameters, jet velocity of 6.6 m/s and Reynolds number (*Re*) of 1900 were obtained. The predicted thermal resistant of the package using an AlN submount for the diode bar was 0.35 °C/W. Fabrication involved the use of a punching system for nibbling the LTCC tape, creating in this manner the channels and cavities of the structure. A key deviation from the standard LTCC process was used for the lamination of the device. It consisted in a progressive lamination using a reduced pressure of ≈ 7 MPa at 70 °C for 10 minutes. In this process, each layer was individually laminated with a uniaxial press to the previous layer to ensure a good bond between the individual layers. The Grumman design, which addressed the cooling of laser bars, served as guidance for the development of the cooling structures for single emitter diode lasers. However, different fabrication methods were used for the formation of channels and internal structures.

4.3 Design of a Cooling Structure for a Single Emitter Diode Laser

A LTCC water jet cooler using 24 layers of nominal thickness 130-µm Heraeus HL2000, shown in the diagram in Fig. 4.1, was designed.

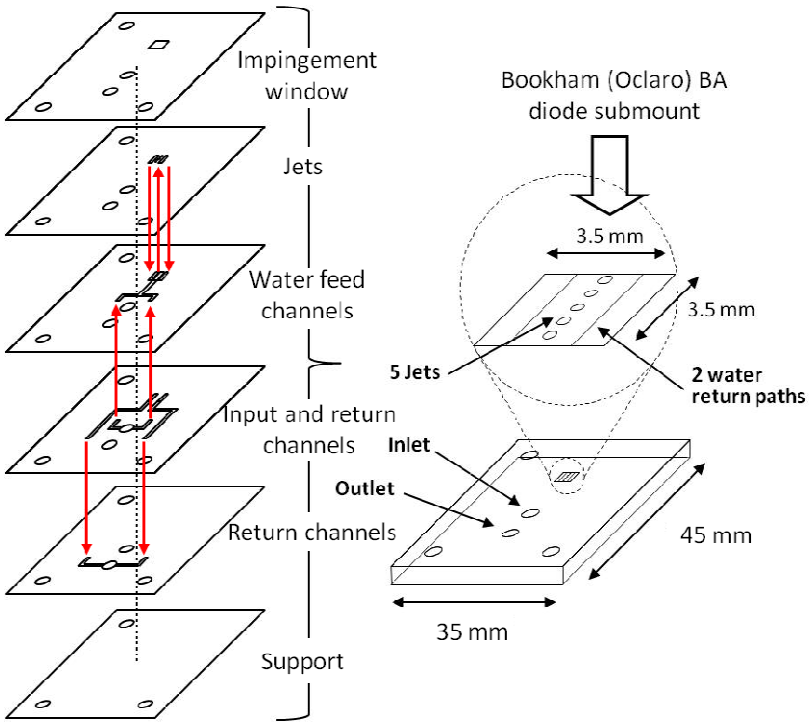

Figure 4.1 Design of LTCC water-jet cooler for a single-emitter BA laser diode. Every section consists of four 0.130 µm LTCC layers with red arrows indicating the water flow's direction

Twenty four layers were used to match, after firing, the thickness of commercial copper microchannel coolers (≈ 2mm). The first prototype was designed to obtain performance parameters, such as water jet velocity and Reynold's number, which define the cooling efficiency of the structure, similar to the LTCC coolers reported by Grumman. Reynold's number expresses the ratio of the inertial effects in the flow to viscous effects in the flow; it will be defined later by Equation 4.2. A high *Re* indicates a highly turbulent flow which thins the boundary layer. This produces a reduction of the thermal impedance. In this design, ideas for the distribution of internal water pathways were also obtained from the inner geometry of commercial copper MCC's. The designed structure consisted of five water jets, each with an internal diameter (*d*) of 300 μm, each one capable of impinging 5.0 ml/s of water with a velocity of 4.25 m/s and *Re* of 1632. As explained in Sec. 3.5, jets with smaller diameter than 300 μm cannot be machined. The jet layout was designed to impinge water across the centre of the back surface of a 3.90×4.05 mm^2 aluminium nitride submount, for intensively cooling. The AlN submount carries a Bookham SES7-975-01 0.4×3.6 mm^2 7 W single BA emitter laser diode chip (Oclaro, USA). The thermal simulation of the laser package reported in Section 4.17 showed that heat transfer from the laser chip to the bottom of the AlN submount occurred mainly through the central region of the AlN tile. Because of this, the geometrical centre of the jets was designed to coincide with the centre of the laser chip. Experimental results reported by Glynn [75] have shown than for submerged jets, the jet-to-target spacing (*H*) has a great influence on the average heat transfer, obtaining the higher values of heat transfer for $H/d < 4$. Because of this, the designed spacing *H* between the output of the jets and the back surface of the submount was 4 LTCC layers, which after sintering is ≈ 350 μm. Every one of the six sections forming the structure shown in Fig. 4.1, consisted of 4 layers. After lamination, the 24 layers formed a three-dimensional internal structure capable of receiving water from a cooling source and routing it toward the jets through internal channels and finally returning it to the source. The designed thickness of the structure in green state was 3.120 mm.

4.4 Stacking Processes of the Cooling Structure

The purpose of this section is to describe the assembly process of the LTCC and carbon layers to build the cooling structure. Also, the modifications made to the standard lamination process to minimize the deformation of the jet structures will be explained. Each of the 24 layers designated was cut with the required pattern using the in-house custom CO_2 system described in Chapter 3. Nanocarbon matching inserts, used as a

SVM to provide a mechanical support during the lamination process, were cut using the same CO_2 system. After cutting, each LTCC layer was stacked manually, to form the 3D structure, on the 45mm x 35mm x 15mm aluminium tooling plate, shown in Fig. 4.2. This has three 3.0 mm diameter alignment pins, which received corresponding holes in the LTCC layers. To prevent sticking of the LTCC structure to the aluminium plate during lamination, 80 µm Mylar sheets were place at the bottom and top of the stacked layers. The image in Fig 4.3 shows 12 layers stacked forming the water channels, the inlet/outlet and the inter-level water connectors.

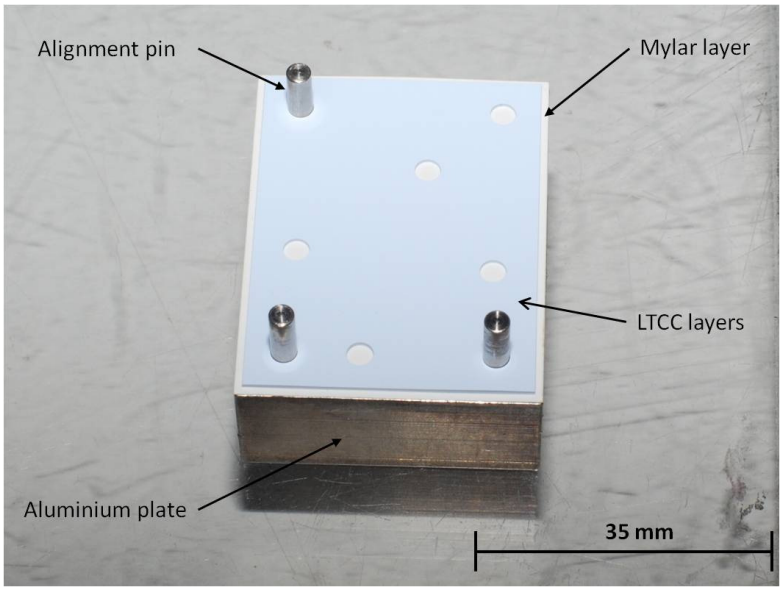

Figure 4.2 Stacking plate

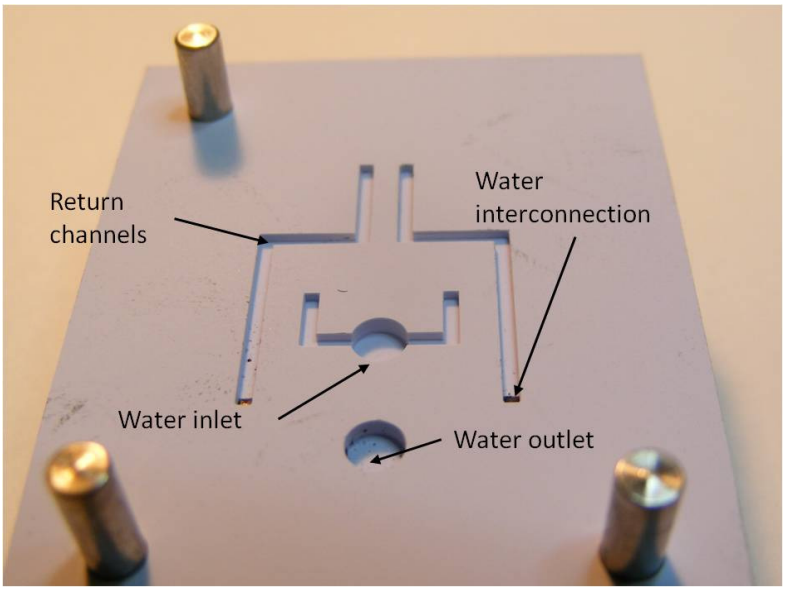

Figure 4.3 Twelve layers stacked forming internal water distribution paths

4.5 Lamination Process – Issues and Solutions

Because the lamination process determines the quality of the finished device, several techniques were investigated to fabricate precise water channels with well defined geometry and excellent bonding between layers. As explain in Sec. 4.2, to obtain precise channel and jet structures in its LTCC based coolers, Northrop Grumman reported the use of a progressive lamination process using a reduced pressure; however, the technique is time consuming and more prone to misalignments issues. Because of this, different bonding techniques are explored in this thesis.

Because an ILS-106 hot isostatic press (Keko Equipment Ltd, Slovenia) was available in the MIcroSystems Engineering Centre (*MISEC*) at HWU, the first approach for the bonding of the LTCC layers was performed using isostatic lamination. The stacked layers on the tooling plate were vacuum packaged in a Dri-Shield 2000 moisture bag (3M, USA) and pressed using typical parameters, 10 MPa pressure at 75 °C for 10 minutes. The great advantage of isostatic lamination is that the same uniform effect is applied to the whole structure, resulting in a better bonding between layers [76]. However, in the absence of a physical support inside the hollow structures during the lamination, the LTCC material extruded into the empty spaces, producing the closing of the hollow structures, as shown in Fig. 4.4. The image shows the centre part of a cooler, before and after applying isostatic pressure; jet structures and water inlet/outlet can be observed in the 2 pictures.

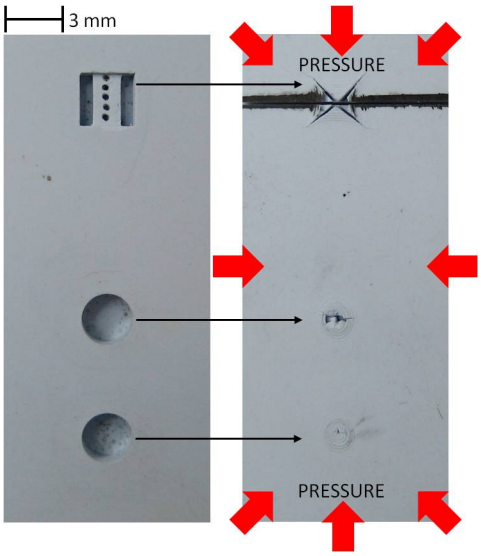

Figure 4.4 Centre part of a cooler, before and after lamination. The effect of the hot isostatic pressing in the hollow structures due to the lack of mechanical support is observed in the right image.

The effect was caused by the plastic deformation during the lamination, which occurs when the glass transition temperature of the binder in the tape is reached [77]. The binder in the HL2000 has a low transition temperature, which is in the range of 35 to 40 °C [78].

To avoid the deformation, a sacrificial volume material (*SVM*) was placed into the hollow spaces to provide mechanical support during lamination. As explained in Sec. 2.3.6, different materials, such as wax, polymers or graphite based layers have been proposed as SVM. Nanocarbon tape from Thick Film Technologies (USA) was chosen as SVM. Because a good fitting between the carbon pieces and the LTCC structure was needed to preserve the geometry of the inner structures, carbon pieces were cut with high quality using our in-house CO_2 machining system, as described in Sec. 3.4.3. The image in Fig. 4.5 shows twelve layers stacked forming internal water distribution paths filled with carbon inserts.

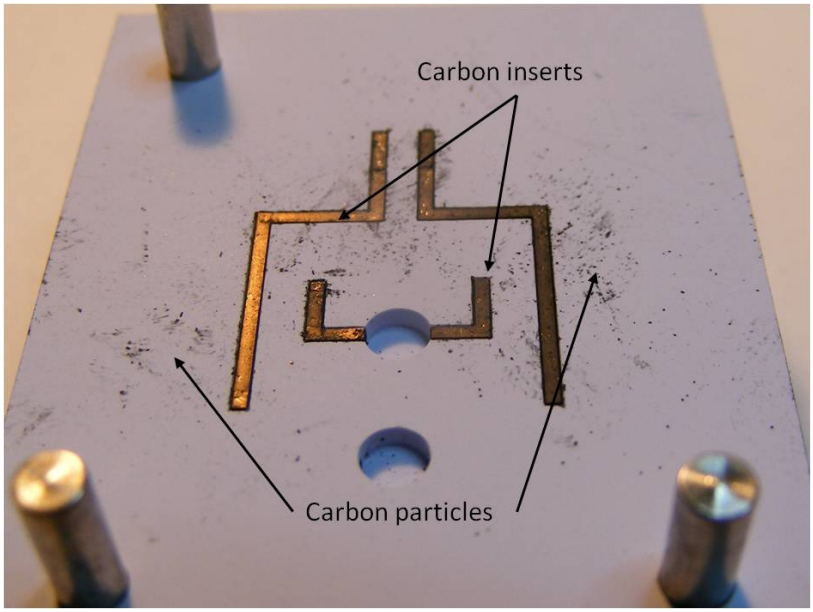

Figure 4.5 Laser cut nanocarbon pieces inserted in the hollow structures to avoid its deformation during lamination

Carbon contamination, produced whilst placing the carbon parts into position, can be observed on the surface of the LTCC layer. The concern with this was the possible decrease in the bonding between layers during pressing which could lead to delamination of them after firing. This could produce water leaking in the cooling

structure during operation. However, as it will be demonstrated later no defects were produced by the carbon contamination.

Every internal structure, except for the jets due to their dimensions, was filled with nanocarbon. Although, the internal structures preserved their geometry, due to the lack of carbon support, the jets were closed and/or deformed. The 5x micrograph in Fig. 4.6 is for 3 distorted jets in a sintered sample. The blocking of the jets due to displacement of the layers below the top one is visible.

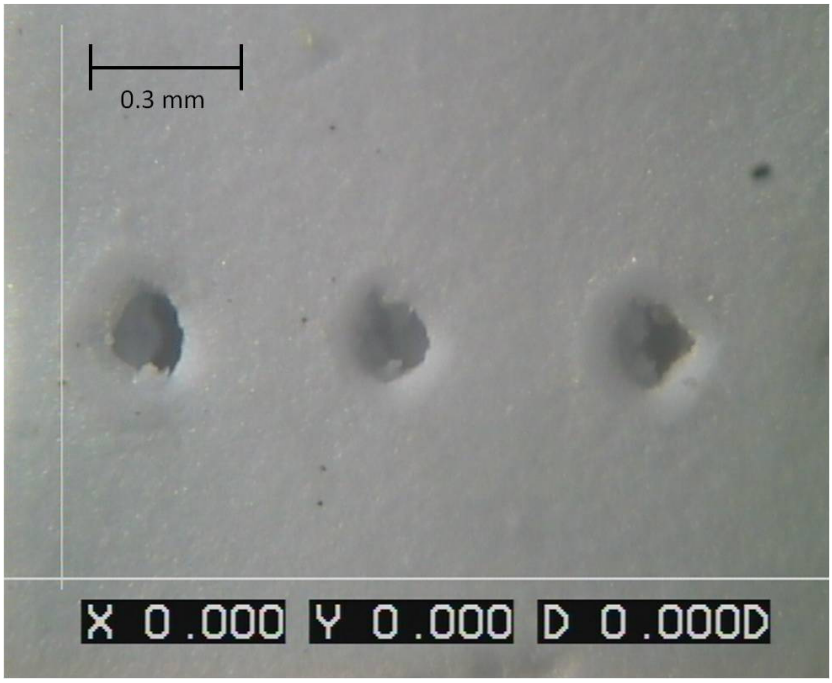

Figure 4.6 5× micrograph of collapsed jets due to the lack of mechanical support during isostatic lamination

4.5.1 Uniaxial lamination

Because jets of better quality were required, lamination using a uniaxial pressing was explored. For this, a C-30 manual 30 Ton hydraulic lab press (Research & Industrial Instruments Company, UK) was modified to allow the thermo-compression of the structure. Two aluminium plates containing cartridge heaters were adapted to provide the heat necessary to bond the LTCC layers. The temperature control was a simple variable transformer, which supplied a constant voltage to the heaters. Temperature was monitored attaching thermocouples to the heater plates and LTCC holder. Layers of FR4 material were used as insulator material to avoid the heat dissipation through the press. A schematic of the press is shown in Fig. 4.7.

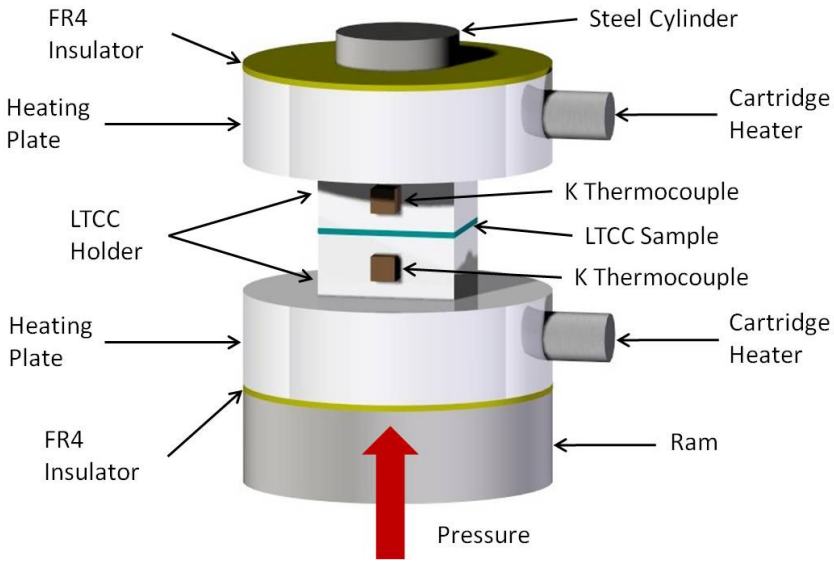

Figure 4.7 Schematic of the modifications done to the uniaxial press to allow thermo-compression

The first trials using uniaxial pressing were done using typical parameters, 10 MPa pressure at 75 °C for 10 minutes without the placing of nanocarbon inserts into the hollow spaces. However, as observed in Fig. 4.8, nanocarbon inserts are still needed using uniaxial lamination to avoid the collapsing and distortion of internal structures.

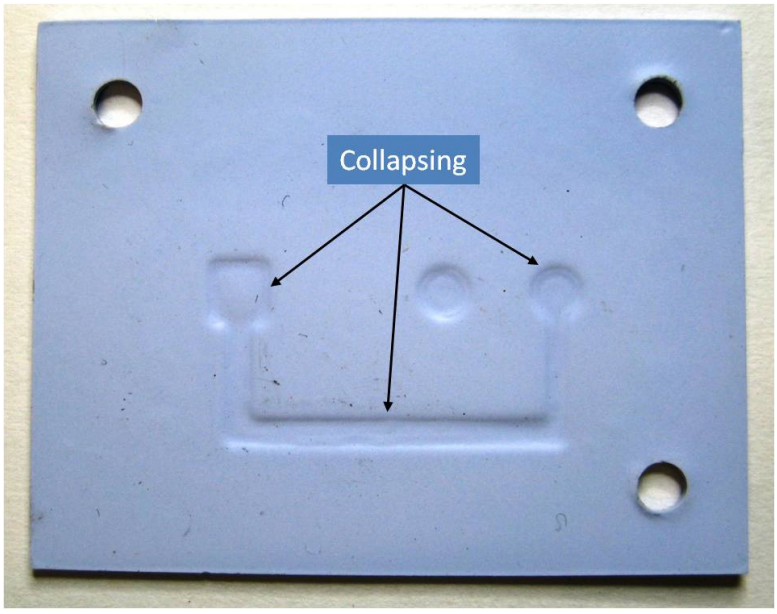

Figure 4.8 Collapsing of internal structures due to the lack of mechanical support during uniaxial lamination

Although the collapsing of internal structures was avoided using the nanocarbon inserts, owing the lack of lateral support, samples were extruded in the perpendicular directions to the pressing direction. An example of a deformed structure is shown in Fig. 4.9.

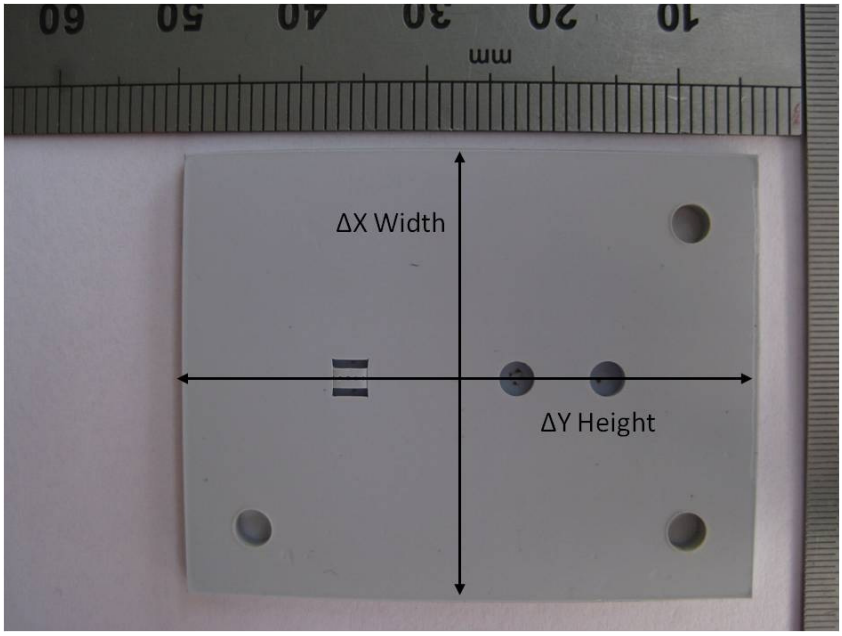

Figure 4.9 Sample showing deformation in both directions due to lack of lateral support during uniaxial pressing

Some of the deformation observed in the structure is due to the barrel distortion introduced by the camera lens. Rulers were used to observe the real distortion of the structure in the picture. Graph in Fig. 4.10 shows the percentage of extrusion in both directions for different lamination pressures.

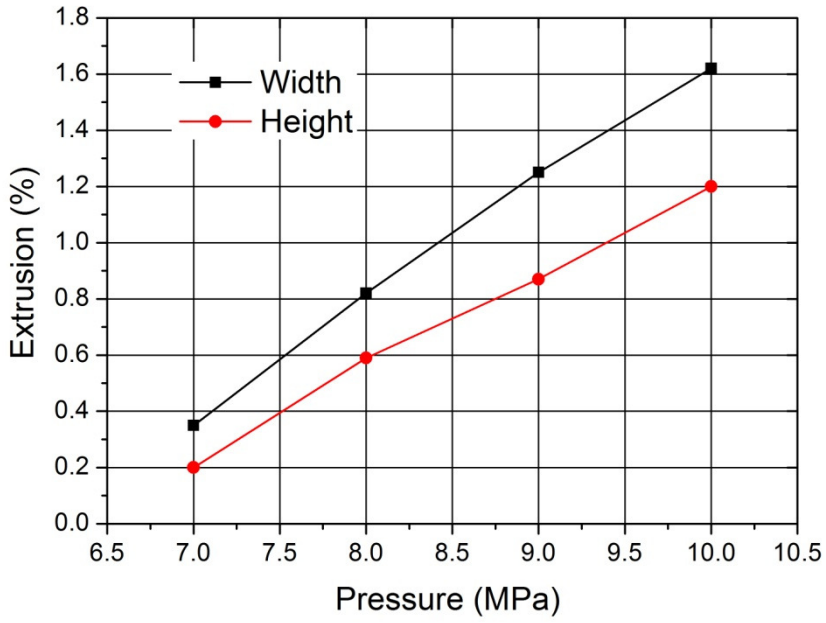

Figure 4.10 Percentage of extrusion in both directions as function of the applied pressure

The extrusion of the material during lamination removes the advantage of near zero X-Y shrinkage or distortion during firing of the HL2000 tape. Because of this, extrusion was reduced using a lamination pressure of 7 MPa, obtaining an extrusion comparable to the 0.2 % shrinkage of the HL2000 tape. To avoid poor bonding between layers, which could cause delamination during firing, the pressure was limited to not less than 7 MPa.

As seen in the graph, all the samples tested showed a larger extrusion in the width direction, which coincides with the transverse direction of the tape casting; further investigation is needed to determine the mechanism which caused the differential X-Y extrusion.

4.6 Issues During the Firing Process

This section addresses the deformation and destruction of the laminated structures, as a result of the co-firing of carbon and LTCC using a standard firing profile. A modified version of the firing profile which prevents the deformation of the structure during firing is reported.

Following lamination, the next process was the sintering of the laminated body. Initially, the sintering of the laminated body was done using the firing profile recommended by Heraeus for HL2000 tapes; it is depicted in Fig. 4.11. For the sintering, a programmable StableTemp® (Cole-Parmer, USA) high-temperature box furnace was used. The structures were placed, during the firing, between two porous fired zirconia (ZrO_2) plates with a thickness of 1.0 mm, nominal porosity of 40 % and flatness of 0.5mm/100 mm, to ensure the permeability of generated gases and the adequate flatness of the fired structure. According to the manufacturer of the nanocarbon tape, the binder burns out during the stage B of the profile, at approximately 325-450 °C, and should not interfere with the binder burn out of the LTCC tape. Sublimation of the carbon will then occur later during the stage C, at temperatures approaching 600 ºC.

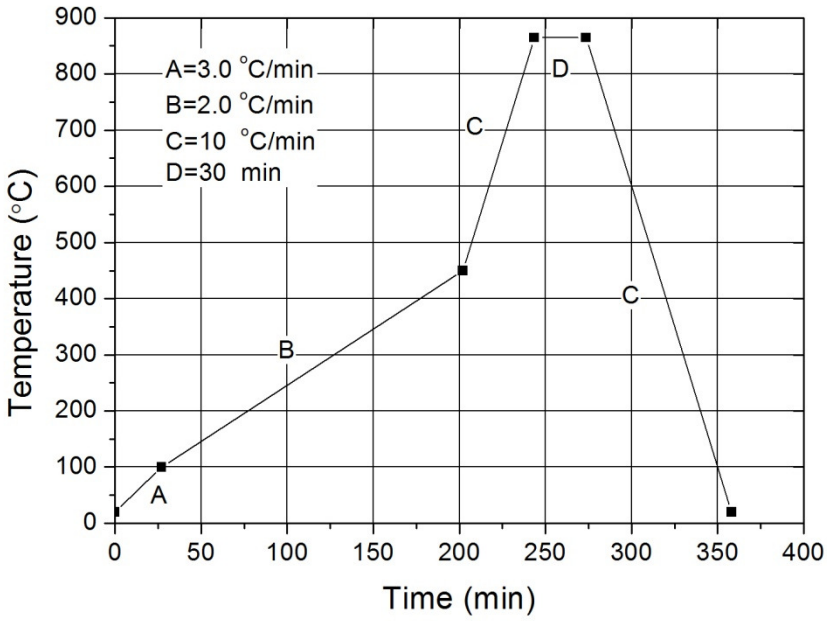

Figure 4.11 Firing Profile Recommended by Heraeus for HL2000

Nevertheless, after firing, the structures showed swelling on the top and bottom surfaces as observed in Fig. 4.12. Also, delamination and broken layers in the sections below and above the nanocarbon-filled cavities were observed as seen in micrograph shown in Fig. 4.13. The image shows the cross section of the LTCC structure after sectioning with a 25 µm diamond saw.

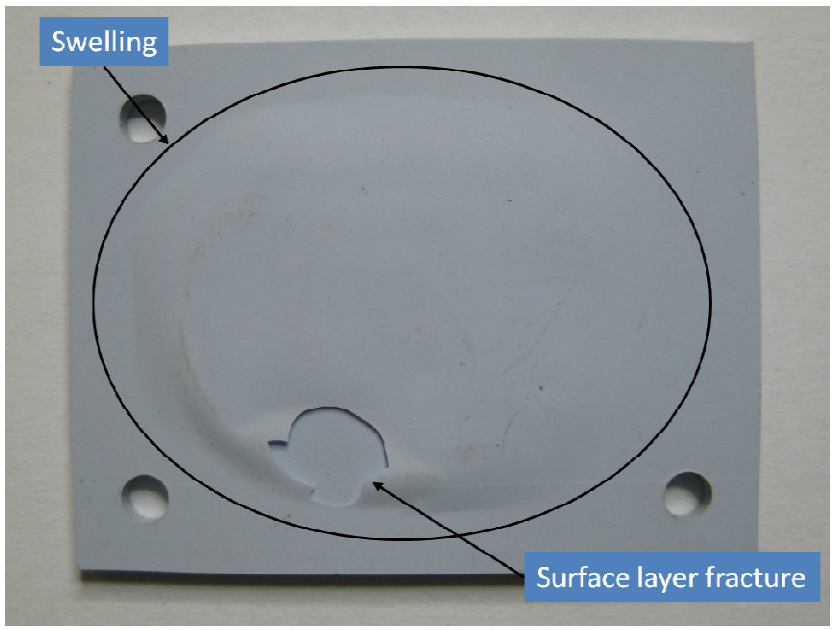

Figure 4.12 Swelling and fracture of the bottom surface due to gas trapped during the sintering

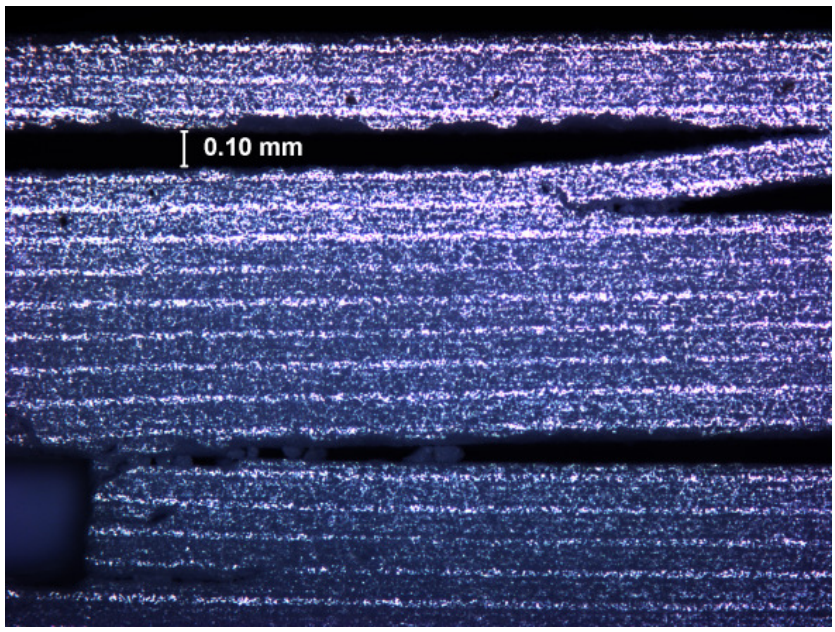

Figure 4.13 5× micrograph of the LTCC cooler cross section showing delamination and broken layers caused by gas trapped during the sintering of the structure

Deformation and delamination of layers resulted from internal gas pressurization and gas trapped during the firing process. In two stages, gases are generated by the nanocarbon filler. At 350 °C the organic binder of the nanocarbon tape decomposes and subsequently, starting at 600 °C, the remaining carbon sublimes. Swelling was attributed to the pressurization caused by the large amount of gases generated during the burning of organic binders, while cracking and delamination were attributed to the gas produced by the sublimation of carbon trapped during the densification of the structure. This was attributed to the large number of layers used. As the number of layers increase, the open pore volume is reduced, as demonstrated by Khoong [79], making it more difficult for the gas to escape through the structure. He attributed the reduction to the increased frequency of overlapping open pores with glass ceramic composite material as the thickness of the structure is increased.

For a complete burn out of the carbon materials before the closing of the pores, different options have been reported. Birol [49] reported the completed burn out before sintering, modifying the ratios and the size of the carbon particles. Khoong [80] proposed a modified profile with a slower heating ramp-up rate and two holding temperatures at 700 °C and 750 °C. The first holding was to suppress the carbon burn out before the initial crystallization of the glass component and the second to ensure the complete burn out. However, the quality of the embedded cavity was not optimal since it still presented

a reduced swelling in the centre and deformation in the edges. Our first approach was to follow the firing profile used by Khoong with heating ramp of 1 °C/min from 100 °C to 450 °C. From 450 °C to 875 °C the structured was heated at rate of 8 °C/min, with holdings temperatures at 700 °C for 30 minutes and 750 °C for 15 minutes. After applying the heating profile, the structure still showed swelling and broken layers as seen in Fig. 4.14.

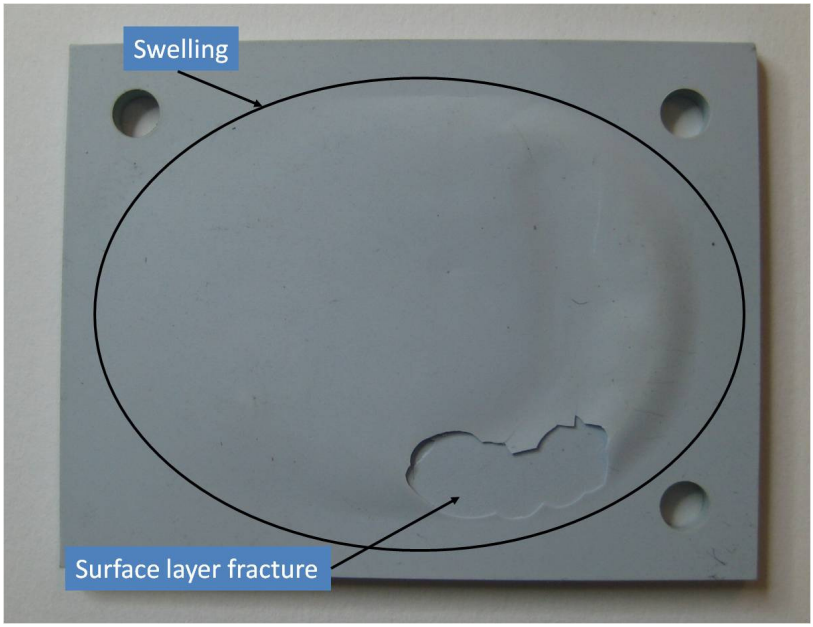

Figure 4.14 Deformation and fracture of the surface during firing using Khoong heating profile

As deformation occurred due to the pressure build-up during the burning of the organic binders, a holding of 120 minutes at 450 °C was introduced in the profile to ensure a complete binder burn out of the LTCC tape [56]. Additionally, the holding temperatures at 700 °C and 750 °C were extended to ensure the complete removal of carbon before the pores in the LTCC structure were closed, avoiding in this way the fracture of the deformed layers. Although swelling was reduced and fracture did not appear, still there was a slight swelling as seen in Fig. 4.15.

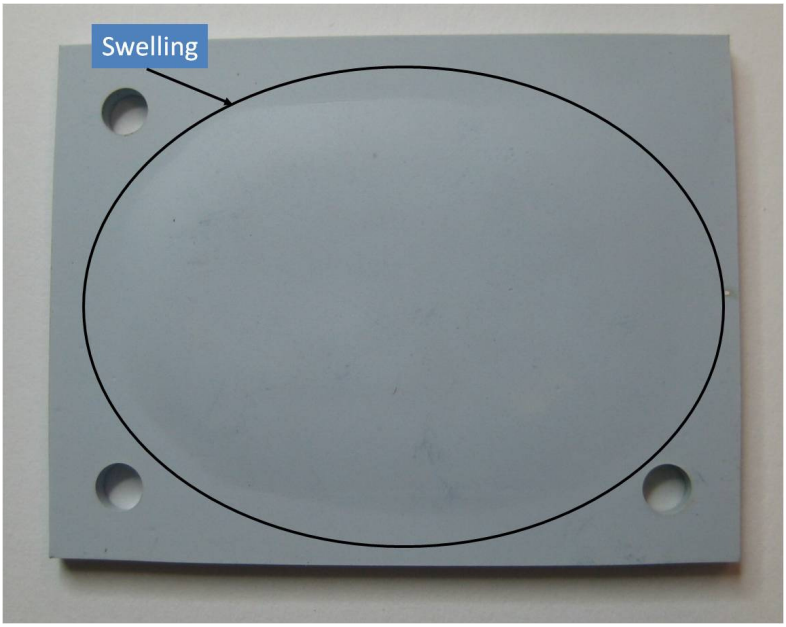

Figure 4.15 Deformation of the surface during sintering using extended firing profile

To alleviate this, a slower heating ramp-up of 0.5 °C/min between 100 °C and 450 °C was used. Additionally another holding at 350 °C for 45 minutes was introduced, as binder burn out of the carbon tape occurs at approximately 325-450 °C (stated by the manufacturer). The modified profile is shown in Fig. 4.16.

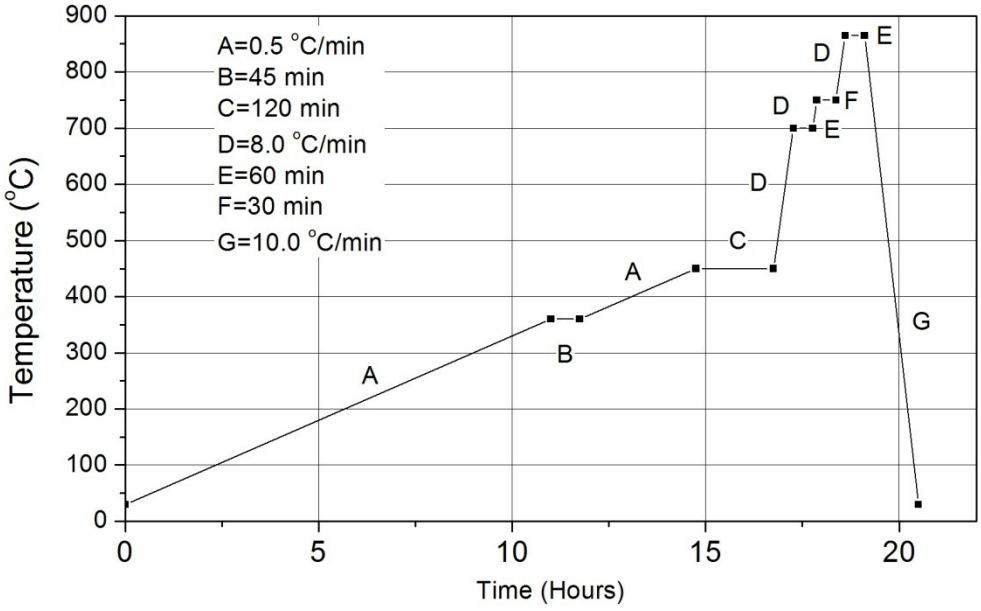

Figure 4.16 Modified co-firing profile for LTCC structure filled with nanocarbon tape

The micrograph in Fig. 4.17 shows an embedded water channel in a 24 layer structure successfully sintered using the modified firing profile showed in Fig. 4.14. The cross-section is a water interconnection, without delamination or cracking above or below the buried cavity.

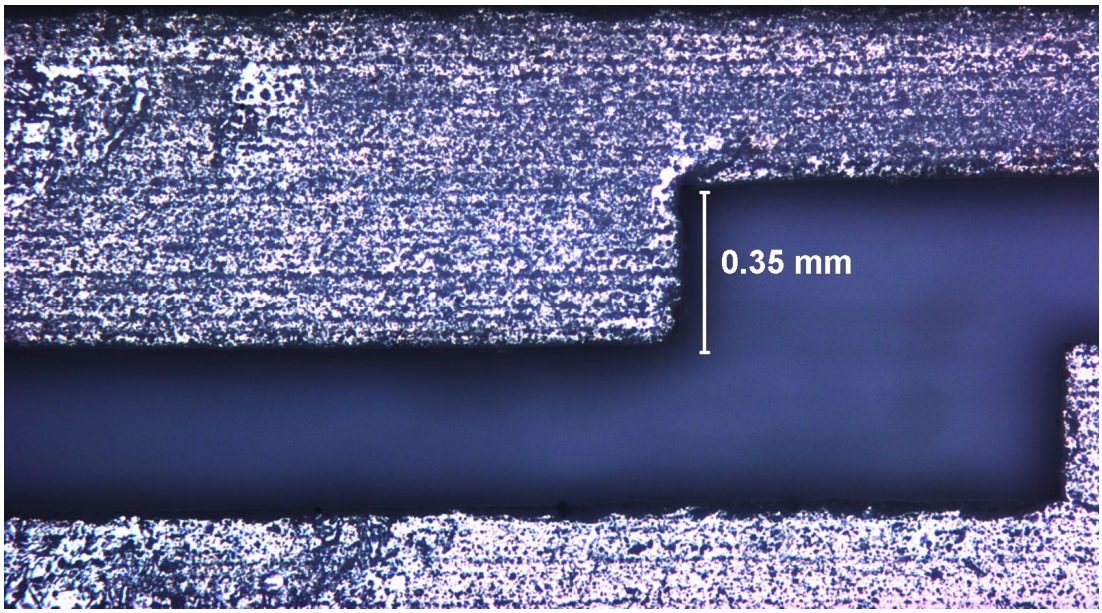

Figure 4.17 Successful embedded water channel created using the modified firing profile. No delamination or cracking is visible

After firing, the top surface of the cooler showed a maximum variation from flatness of 50 µm in a length of 35 mm. The surface was measured using the non-contact chromatic white light confocal sensor described in Sec. 3.4.1.

4.7 Electrical Connections for the Diode Laser

One of the requirements for the cooling structure was to supply high current on board. At full output power, the Bookham laser requires an operating current of 8 A. Because of this, LTCC coolers were provided with gold plated silver electrical tracks, which allowed the distribution of high current on board and the placement of gold wire bonds.

Conductive silver tracks on LTCC are easily fabricated using conventional screen printing, as describe in Sec. 2.3.5. However, as the fabrication of screens is time consuming and every change in the design would require the use of a new one, a different approach was used. Instead of using a highly tensioned mesh structure woven from fine stainless steel or polyester wire over a frame, a 23 µm thickness Mylar film

was used as a printing mask. Conductive paste was transferred to the LTCC surface in green state, through patterns cut previously in the Mylar film using the micromachining CO_2 system. To ensure an excellent transfer of the paste without bleeding paste under the mask, the Mylar layer was stuck to the LTCC surface by thermo-compression. For this, a second uniaxial lamination was performed at 3.45 MPa for two minutes at the temperature of 75 °C. No deformation of the structure was caused by the second lamination.

The TC0307 paste from Heraeus was used as conductor. It is a pure Ag conductor with a content of solids of 80%, resistivity lower than 3.0 milliohms per square at 20 µm dried film thickness. Ohms per square is the unit of surface resistivity across any given square area of a material. Paste was carefully spread over the mask using a flexible metal blade to obtain a layer with equal thickness to that of the Mylar layer on the top of the LTCC structure. After the paste was spread, the mask was peeled away, leaving the desired pattern. Later, the structure was dried in a conventional oven at 80 °C for 20 minutes to remove the organic solvents of the silver paste. Finally, the paste was successfully co-fired with both LTCC and nanocarbon using the profile described in Sec. 4.6.

While silver metal has the highest room-temperature electrical conductivity of any substance, the major disadvantage of silver metallizations is the corrosion of it in the presence of moisture and applied bias which leads to electrical failures [81]. To prevent corrosion and oxide formation on the fired silver tracks, a layer of soft pure gold Type III, Grade A (99.9 % gold minimum) was deposited on them by electroless plating.

Soft gold allowed high reliability gold wire bonding between them and the gold plated AlN submount containing the BA single emitter diode laser. Gold wire bonded to gold plating is extremely reliable because the bond is not subject to interface corrosion, intermetallic formation, or other bond-degrading conditions. The optimal thickness for gold plating is between 1.25 – 5 µm, however, as our design involved wire bonding and soldering operations on the tracks the thickness was limited to 3 µm to avoid formation of weak, brittle gold-tin intermetallic compounds and other effects which can result in a decrease in the reliability of the solder joint [82]. Gold metallization was done by L.E.W. Techniques Ltd.

4.8 Summary of the Fabrication Processes

Lamination of high quality laser-cut LTCC layers, with minimum lateral distortion and no collapsing of internal features was achieved using a modified uniaxial press and nanocarbon inserts as mechanical support. Also, a modified co-firing profile which allowed the complete removal of the nanocarbon inserts during sintering of the cooler has been reported. These modifications to key processes allowed the fabrication of precise water channels and jets needed to cool the 7W Bookham single BA emitter laser diode. In addition, printing of high quality silver tracks to allow the distribution of high current on board was achieved using laser-cut Mylar masks. Finally, the flatness of the surface will allow the collocation of optical elements without the need of post-grinding.

4.9 Process for Mounting and Bonding of Diode Lasers onto LTCC Substrates

The AlN submount needed to be accurately bonded on the top of the window containing the jets in order to allow adequate cooling. A displacement of the laser chip, especially the front part, with respect to the position of the jets could cause an increase in the thermal resistance, producing reduction in the conversion efficiency and thermal overload of the diode laser. On the other hand, an incorrect placement of the submount, also, might produce water leakage which can contaminate the front facet or produce electrical shorts, leading to irreversible damage and failure of the laser.

In order to manipulate and place the laser on submount in the optimal position, a manual assembly station was set up, as shown in Fig. 4.18. It was fitted with a 3-axis grip with a 10 µm resolution in each direction, two cameras, a heating plate and a He-Ne laser to measure the tilt of the laser diode by reflection.

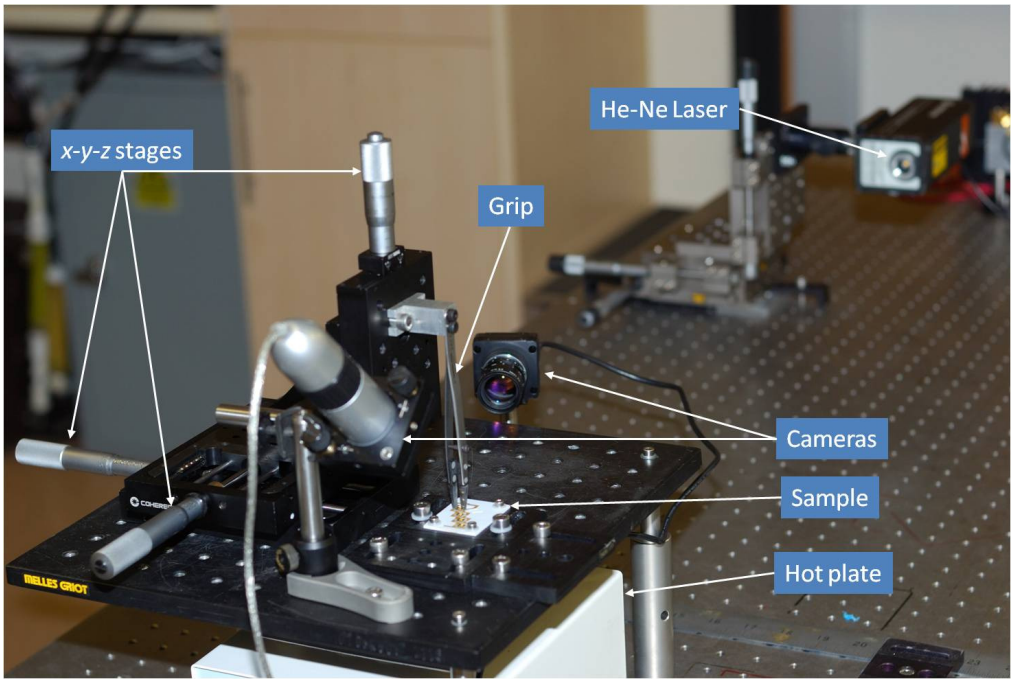

Figure 4.18 Manual assembly station used for mounting the diode laser on submount on the LTCC cooler

The AlN submount was bonded to the LTCC substrate using the two-part epoxy 302-3M (Epotek, USA). The 302-3M has good adhesion to ceramics and it is resistant to water. Moreover, the 302-3M is a space qualified low-outgassing epoxy, meaning there is a lower risk of contamination of the laser facet. It has a minimum bond line cure schedule of 24 hours at room temperature.

Adhesive was dispensed using a precise fluid dispensing system TS9150 (Techcon Systems, Inc., USA). To obtain a continuous and uniform pattern of epoxy on the LTCC substrate, the substrate was moved under the air powered syringe containing the adhesive using the linear *XY* motor stages of the CO_2 laser system. The air powered syringe was held perpendicular to the LTCC surface using an aluminium frame attached to the translation stage configured as *Z*, as shown in Fig. 4.19.

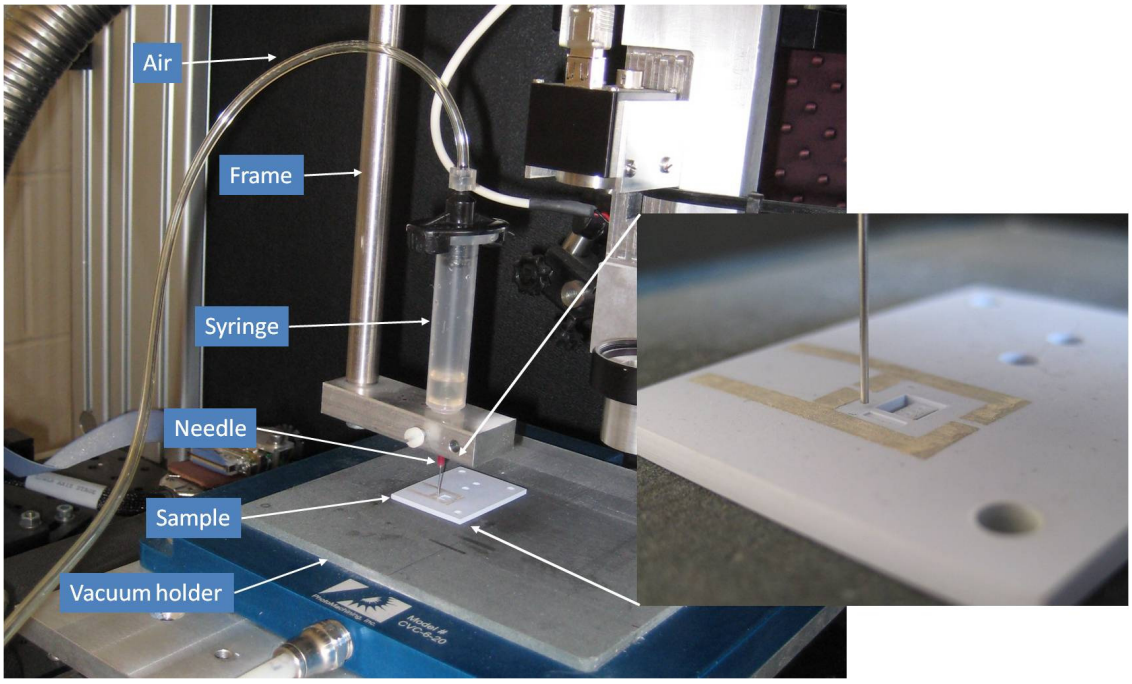

Figure 4.19 Fluid dispensing station attached to the CO_2 laser system

Due to the low viscosity (800-160 cPs) of the 302-3M, it tended to flow away from the bonding region before placing the submount. To alleviate this problem, the adhesive was precured to get a harder consistency before dispensing it. The optimal precuring conditions were heating the adhesive for 30 minutes at 30 °C.

According to Kondo [83] the parameters which should be adjusted to obtain the optimal dispensing conditions are needle size, air pressure and dispensing time. For our application, the optimized conditions were to use a syringe with a 25 gauge needle (inner diameter 254 µm), air pressure of 25 psi and dispensing time of 9 seconds. These conditions resulted in the dispensing of adhesive frames of 15.9 mm perimeter, width of 500 µm and 250 µm thick. If a thicker track of adhesive is dispensed, there is the risk to contaminate the facet of the laser. As well, there is the risk to spread adhesive over the impingement area on the AlN submount or over the jet holes, therefore reducing the cooling effect.

The left image in Fig. 4.20 shows the designed clear space for mounting the AlN submount, while the right image, used for illustrative purposes, shows the adhesive dispensed over it. The adhesive shown in the picture is a silver-loaded epoxy which was utilized as a first option for the bonding of the Bookham laser.

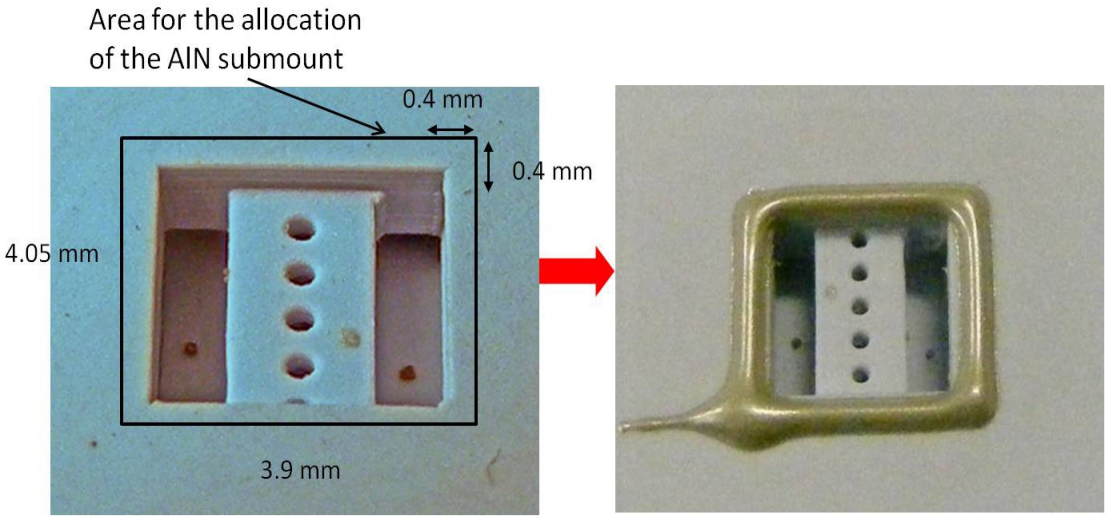

Figure 4.20 The left image shows the clearance space for mounting the AlN submount, while the right shows adhesive dispensed over it

The Bookham laser was positioned using the placing station shown in Fig. 4.16 leaving a bondline with thickness of 50 µm. After curing, the bondline thickness was confirmed using the profilemeter described in Sec. 3.4.1.

4.10 Wire Bonding Process

As reported in Sec. 4.7, a thin layer of soft gold was electrodeposited over the printed silver tracks to allow reliable gold wire bonding between them and the AlN submount on which the single emitter laser diode is p-side mounted.

Gold wires were bonded to both surfaces by thermosonic ball bonding using a Palomar 8000 (Palomar Technologies, USA) equipment. The Palomar 8000 has a placement accuracy of ±2.5 µm with an effectiveness of 99.73% (3σ). For further information about thermosonic bonding, consult excellent reviews on the matter, detailing the foundations, operating principles and issues [84-86].

For the interconnection, ninety-eight gold wires with 33 µm diameter and 4 mm length were used. Half of the wires were connected to the anode connection, and the other half to the cathode. Wires were split in four sections to have a thermal balance in the submount. Figure 4.21 shows the wire bonding between the gold plated silver tracks and the submount carrying the diode laser.

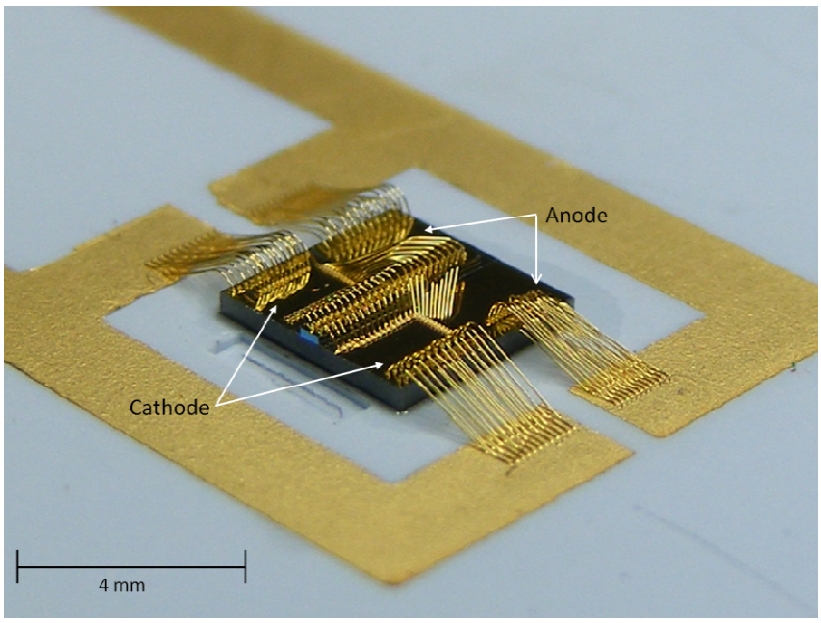

Figure 4.21 Wire bonding between the gold plated silver tracks and the gold plated AlN submount

The wire resistance was calculated using the Equation 4.1.

$$R = \frac{\rho l}{A} \tag{4.1}$$

where:

ρ is the resistivity of the gold (Ω*m)

l is the length of the wire (m)

A is cross-section of the wire (m²)

The calculated resistance per wire was 144 mΩ with a total parallel resistance for the forty-nine wires of 2.34 mΩ. The theoretical power dissipated by the wires, considering an electrical input power in the laser of 16 W, was 0.3 W.

4.11 Performance of Jet Coolers and Leak Testing

In this section, key performance parameters of the jet coolers, such as water flow, pressure drop, Reynolds Number and jet velocity are given. In addition, results from the leak testing are presented.

The first test of the cooling structure was done without mounting the Bookham laser. The cooler was connected to a water supply pipe, using a custom made manifold made

of Poly(methyl methacrylate). A photograph of the jets in action without the spreader is pictured in Fig. 4.22. The manifold is shown on the left of the image. Five jets of water with approximately equal flow and near equal directionality are shown towards the right of the image. Excess water from splash back is also shown on the LTCC substrate at the bottom of the photograph.

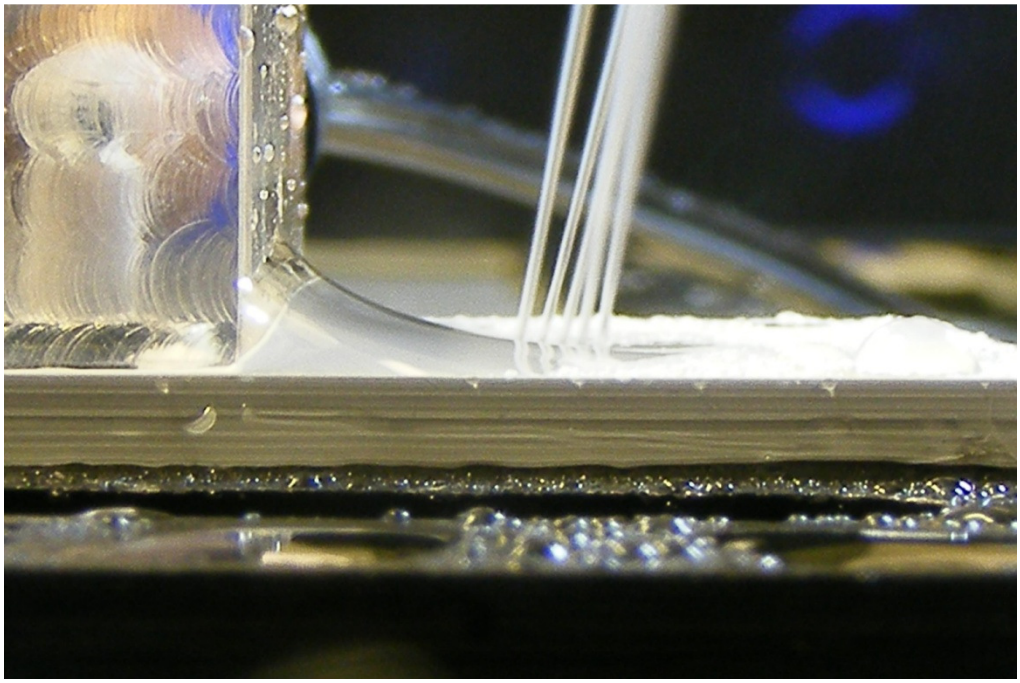

Figure 4.22 Jets in action with approximately equal flow and near equal directionality, demonstrating the quality of the laser drilled jets

For a closed circuit test of the cooler, water at different flow rates was passed through the jets. The structure was connected to a CR8U20 (Thermal Exchange, UK) recirculating chiller unit. Flow rate was controlled using a stainless steel integral bonnet needle valve and measured using a digital fluid flow sensor. The cavity containing the water jets was sealed using an AlN submount with the same dimensions as the Bookham one.

Considering the jets' diameter and water flow rates, jet velocity and Reynolds number were calculated using Equation 4.2 for a flow in a circular pipe. Results, considering a jet diameter of 380 µm, are shown in Table 4.1.

$$Re = \frac{QD_H}{\nu A} \tag{4.2}$$

where:

D_H is the hydraulic diameter of the jet

Q is the volumetric flow rate (m^3/s)

A is the jet *cross-sectional* area (m^2)

ν is the kinematic viscosity of the water

Table 4-1 Reynolds Number and Velocity for Different Flow Rates

Flow Rate ($lmin^{-1}$)	Reynolds Number	Velocity (m/s)
0.06	644	1.76
0.08	859	2.35
0.1	1073	2.94
0.115	1235	3.38
.13	1396	3.82
.145	1557	4.26
.160	1718	4.7

As reported in several papers [87-89], it has been demonstrated that for a constant jet diameter, the heat transfer increases with the increasing of the Reynolds number. This was attributed to the increment of the turbulence caused by the higher jet velocities. Therefore, according to the data shown in Table 4.1, a reduction of the thermal impedance of the cooling structure is expected as the flow rate increases. The flow rate was limited by the pressure drop across the cooling structure due to the pumping capacity of the chiller. The pressure drop across the cooler at different flow rates is shown in graph in Fig. 4.23.

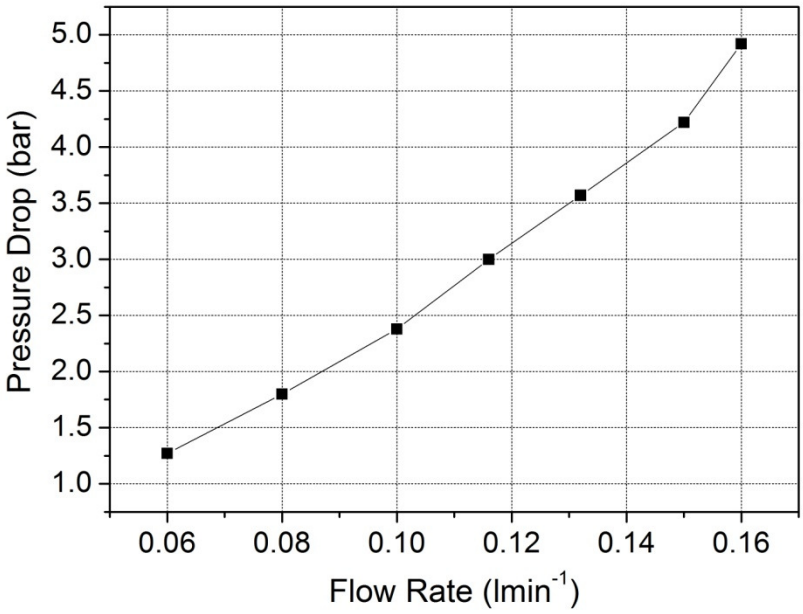

Figure 4.23 Pressure drop across the LTCC cooler as function of the water flow

For a longer testing of the cooler with the Bookham laser attached, the structure was placed in a sealed container and water with a flow rate of 0.160 $lmin^{-1}$ was passed through it for 500 hours. No evidence of leakage in the structure or the laser bonding area was observed.

4.12 Bookham High Power Single Emitter Laser Diode Specifications

As mentioned in Sec. 4.3, the cooling structure was designed to address the thermal management of the high power single emitter laser diodes on submount SES7-975-01 from Oclaro Inc. (formerly Bookham Inc.). The SES-975-01was designed to provide the output power, coupling efficiency and reliability for pumping next generation fiber lasers. It has a typical CW output power of 7 W with a central wavelength of 975 ±10 nm at 25 °C. The nominal operating current is 8 A with voltage across the laser diode of 1.9 V. It has a threshold of 400 mA with a slope efficiency of 1 W/A. The beam divergence at full-width at half-maximum (*FWHM*) of the fast-axis is 29° while the slow-axis is 8°. The laser has a footprint of 3.60 mm by 0.4 mm and a height of 0.15 mm. The laser chip has been mounted on a 4.05 mm by 3.9 mm AlN tile with 0.4 mm thickness.

4.13 Method for Measuring the Thermal Impedance of the Cooling Structures

This section explains the method used to determine the thermal efficiency of the LTCC cooling structures. It was obtained by calculating the temperature rise at the junction of the lasers as function of the power dissipated using the wavelength shift technique.

As a measure of the thermal performance of diode laser packages, commonly the total thermal resistance R_{th} is used. Thermal resistance is defined as

$$R_{th} = \frac{\Delta T}{P_{therm}}, \tag{4.3}$$

where:

P_{therm} is the thermal power dissipated by the laser (W)

ΔT is the temperature difference between the hottest point of the laser and a reference temperature measured at the bottom of the heat sink ($°C$)

In a laser diode, heat is mainly generated in the active region, with the hottest point located in the waveguide at the front facet of the laser diode. For water cooling, the water temperature at the inlet is considered as the reference temperature. The power dissipated by the laser as a function of the laser driving current I is obtained from

$$P_{therm}(I) = V \times I - P_{opt}(I), \tag{4.4}$$

where:

$P_{opt}(I)$ is the optical output power (W)

V is the operating voltage of the diode laser (V)

As the wavelength of the laser diode depends on the temperature of the junction, the thermal impedance can be calculated introducing the term $\Delta\lambda/\Delta T$. The thermal shift $\Delta\lambda/\Delta T$ is a parameter characteristic for each type of laser and represents how the centre emission wavelength shifts as the temperature of the junction increases around its operating value. Typically, for diode lasers it is about 0.3 nm/°C [90] and it is provided by the lasers manufactures. Therefore,

$$R_{th}(I) = \frac{\Delta T}{P_{therm}} = \left(\frac{\Delta\lambda}{\Delta T}\right)^{-1} \times \frac{\Delta\lambda}{V \times I - P_{opt}(I)}. \quad (4.5)$$

4.14 Optical and Electrical Characteristics of the Diode Laser Mounted on the Cooler

This section describes the experiments conducted to determine the thermal efficiency of the LTCC structure cooling a 7 W broad area single emitter diode laser. Experimental data, such as typical output power vs. current curves and emission spectrums for different flow rate conditions at different operating currents are reported.

The first experiment was carried out to obtain a complete characterization of the diode laser. This involved a series of voltage (V), current (I) and output power (P_{opt}) measurements at various water flow rates. Figure 4.24 shows a schematic of the overall experiment setup.

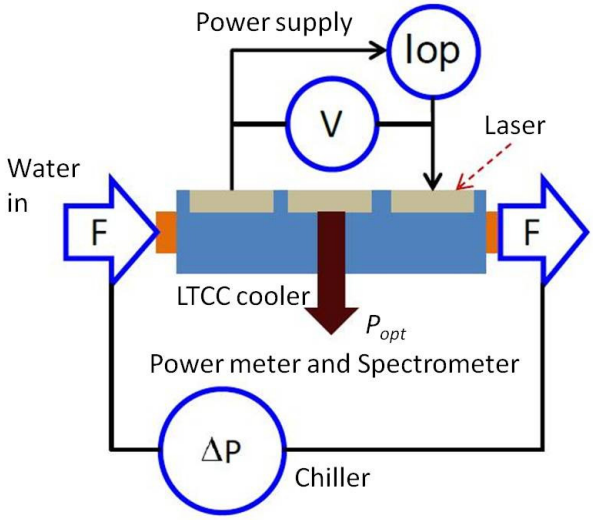

Figure 4.24 Set-up used for the completed characterization of the SES7-975-01diode laser mounted on LTCC cooler

Simultaneously, output light was sensed by a high-resolution HR4000 (Ocean Optics, USA) fibre optic spectrum analyzer to determine the laser center wavelength. Light was collected and transmitted to the spectrum analyzer using a SMA air-spaced doublet collimator connected to a single mode FC/PC patch cable. At each point the diode laser was allowed to reach thermal equilibrium before recording each set of data. Equilibrium was easily verified with the emission wavelength stability. With the collected data,

typical output powers versus operating current curves were constructed. Figure 4.25 illustrates the curves for different flow rates. The results showed that the output power is independent of the laser diode temperature.

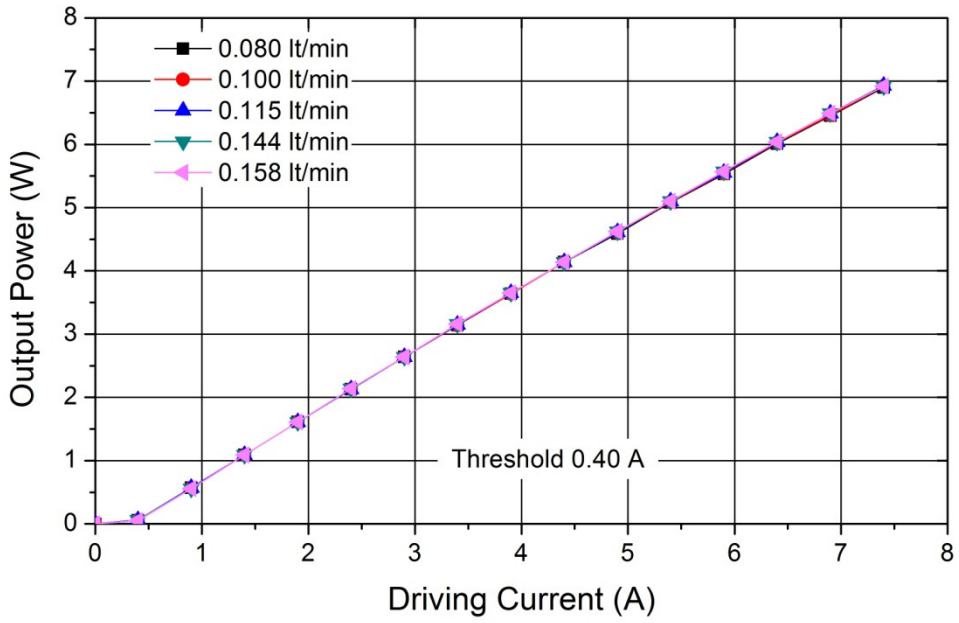

Figure 4.25 Output power vs. operating current for different flow rates

The emission spectra of the laser diode as a function of the drive current for three different flow rate are shown from Figs. 4.26 to 4.28. In the graphs, the red shift of the emission wavelength as the operation current increases is depicted. The shift, which is common in semiconductor lasers, is caused by the increment of the operation temperature in the junction which leads to a reduction of the band gap energy of the active region material; for a detailed explanation of the phenomenon, review [91-93]. Typically, the thermally induced wavelength shift for GaInAs QW broad area diode lasers is about 0.25 - 0.35 nm/°C.

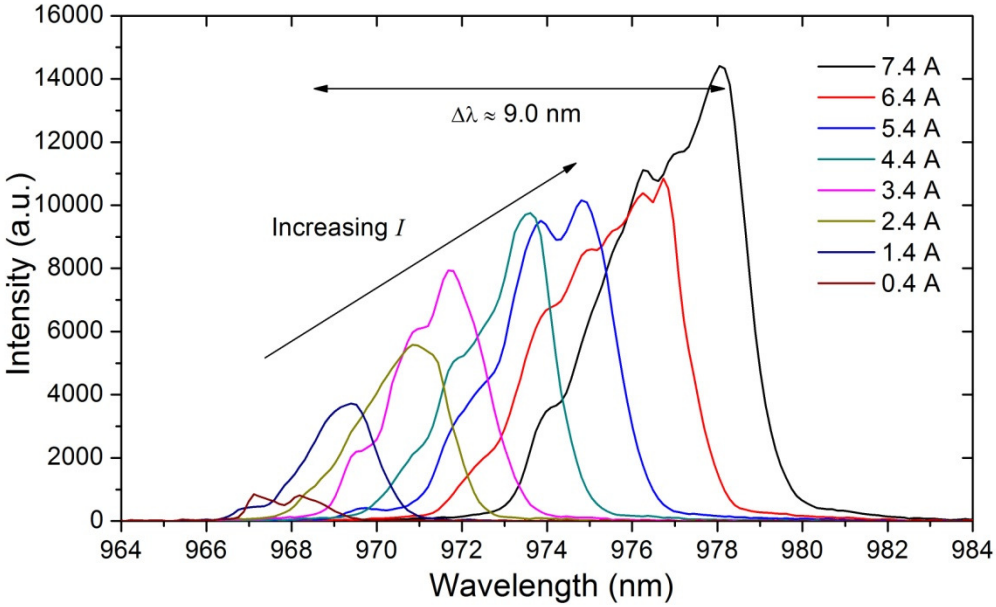

Figure 4.26 Wavelength shift as function of the operating current for a flow rate of 0.060 lmin^{-1}

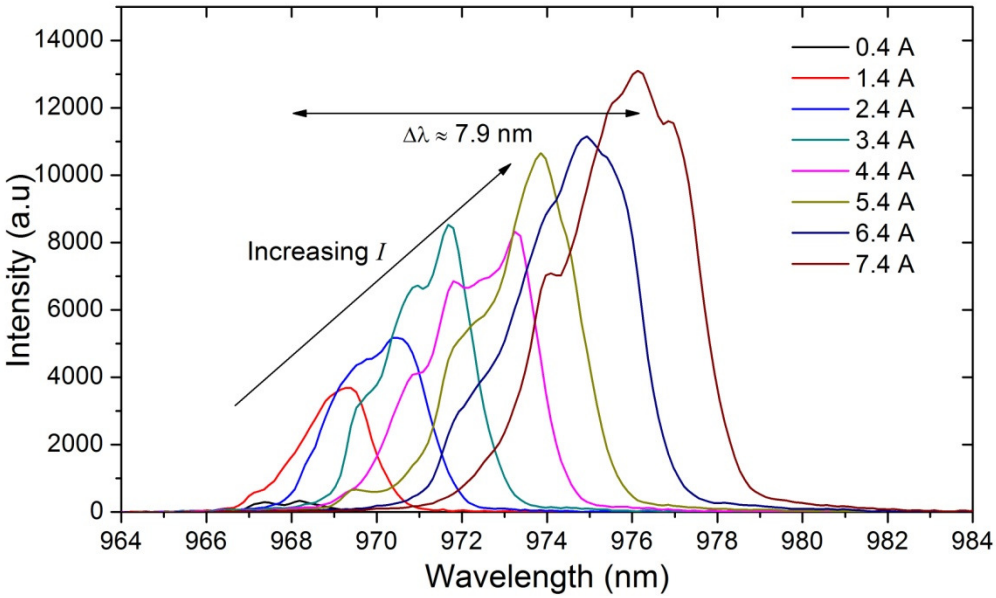

Figure 4.27 Wavelength shift as function of the operating current for a flow rate of 0.115 lmin^{-1}

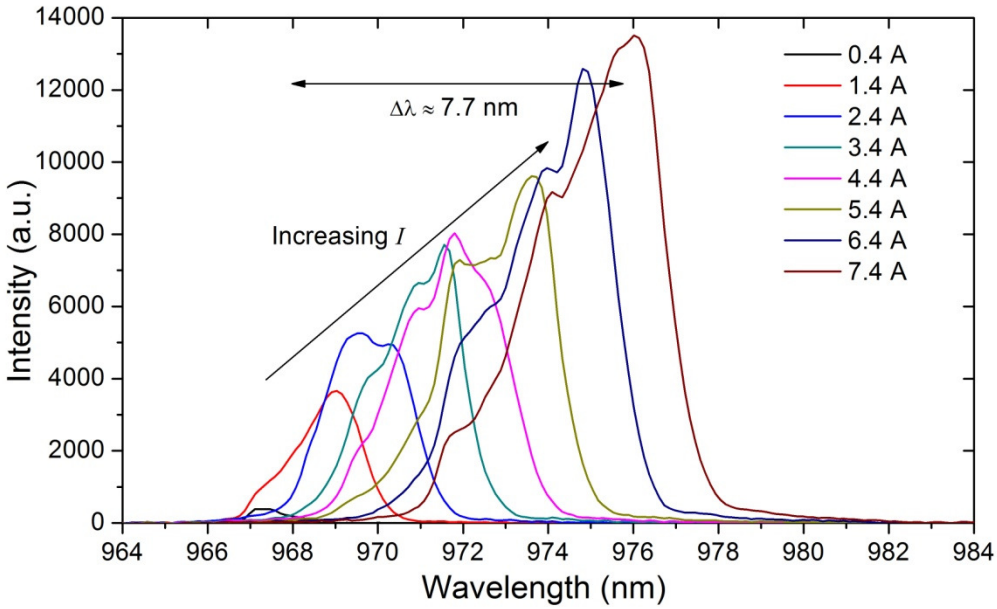

Figure 4.28 Wavelength shift as function of the operating current for a flow rate of 0.158 lmin^{-1}

A reduction in the thermal shifting Δλ with increasing flow rate is observed in the previous spectrums. The effect was caused by the increment in jet velocity of the water impinging on the back surface of the AlN submount. As expected, the increment in the velocity led to a reduction in the thermal impedance of the package producing a lower temperature of the junction.

By looking at the spectrums, the non symmetrical shape of the spectral distribution which is typical in diode lasers is clear. Despite the fact that the asymmetry is not fully understood, different mechanisms such as intracavity defects, the shape of the gain profile, time-dependent mode-competition or frequency-dependent diffraction losses have been proposed as the possible causes [94].

Because of this asymmetry, the peak of the spectrum does not correspond to the center of mass of the spectral distribution. Therefore, the central wavelength, which is required for the calculation of the thermal resistance according to Equation 4.5, was defined by the centroid of the spectrum. Utilizing the experimental data and the calculated centroid wavelengths, the wavelength versus power dissipated curves for the different flow rates were constructed, as presented in Fig. 4.29.

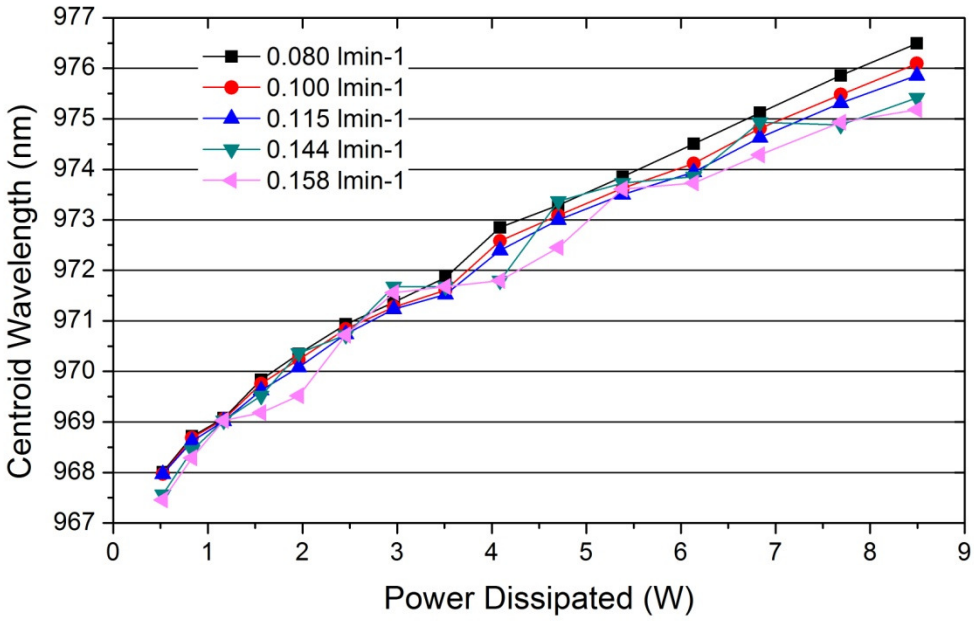

Figure 4.29 Wavelength vs. power dissipated curves for the different flow rates

A linear fit was then calculated for each data set. The interception of the regression line with the wavelength axis corresponded to the centroid wavelength at zero power output; at zero power output, the power dissipated by the laser is zero. At zero power, the laser junction temperature is equal to the water temperature at the inlet of the cooler. With this value is possible to calculate the total thermal shifting $\Delta\lambda$. Fitting, as shown in Fig. 4.30, was done considering a minimum operating current of 0.5 A above the threshold current of the diode laser.

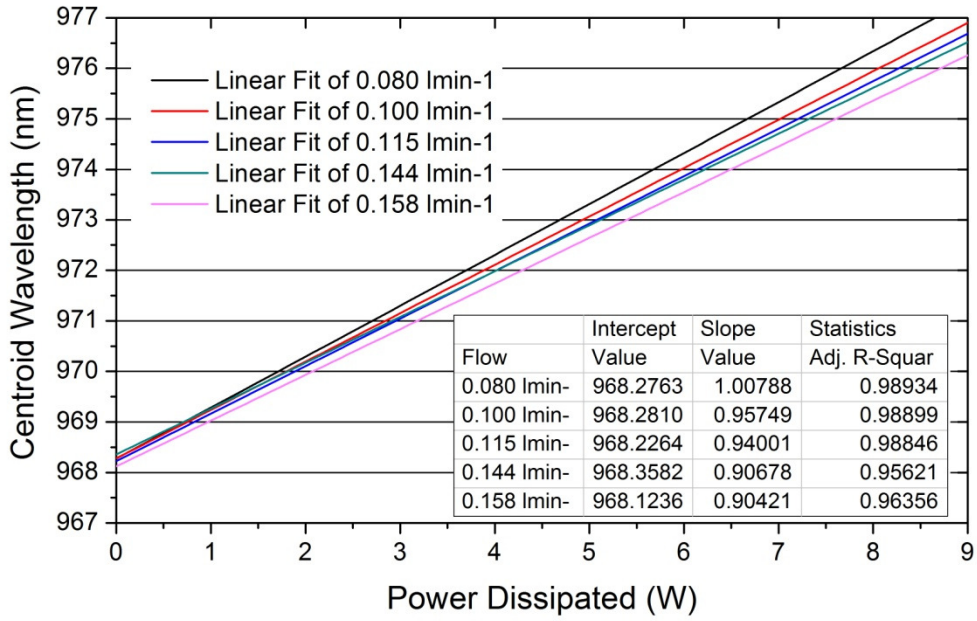

Figure 4.30 Linear fit to wavelength vs. power dissipated curves to determine the laser wavelength at room temperature

As observed in the table inserted in the Fig. 4.30, there is a slight difference in the intercept value of each linear fit. This difference has been attributed to the variations of the water temperature crossing the cooler. These variations correspond to the ±1 °C temperature stability of the CR8U20 recirculating chiller. Because of this, the mean of the intercept values was used as the wavelength associated to the no output power. The zero power wavelength and the data plotted in Fig 4.30 were utilized to calculate the $\Delta\lambda$ value for every flow rate.

4.15 Calculation of the Thermal impedance

The values of $\Delta\lambda$ and $P_{\_therm}$ were substituted in the Equation 4.5 to calculate the thermal resistance of the cooler. A thermal shift ($\Delta\lambda/\Delta T$) of 0.3 nm/°C was used. This thermal shift value was obtained from the data sheet of the Bookham laser. Figure 4.31 shows the thermal resistances obtained for different flow rates.

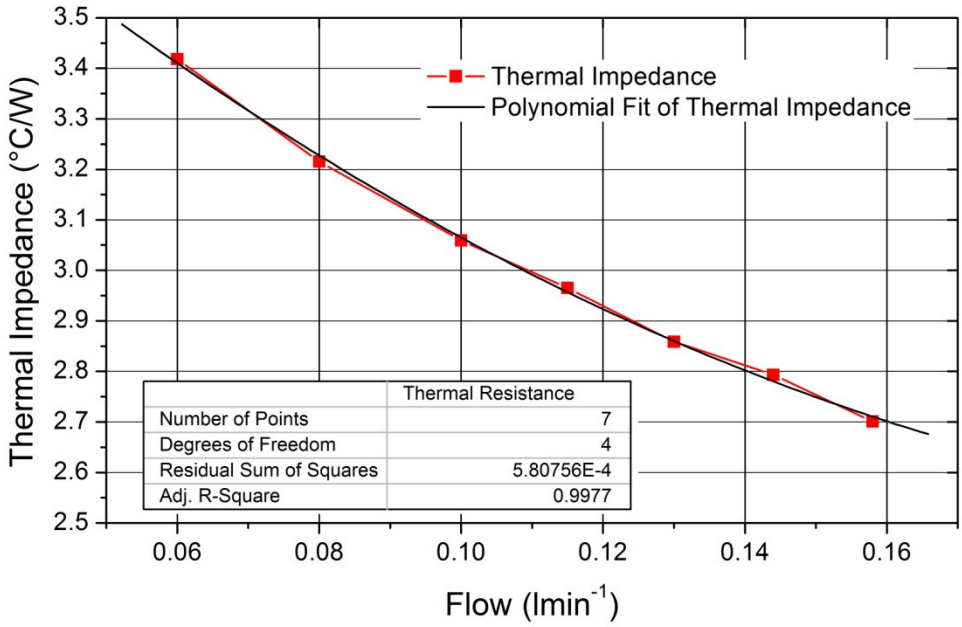

Figure 4.31 Thermal resistance of the LTCC cooler for different flow rates

A thermal impedance as low as 2.7°C/W at 0.158 $lmin^{-1}$ was obtained. Published experimental data for thermal impedances of broad area single emitters are between 2.8-9 C°/W depending on the emitter width, resonator length and mounting scheme [95-97]. With a thermal impedance of 2.7°C/W, the LTCC cooler could dissipate up to 18.5 W at 70°C junction temperature with a reference temperature of 20 °C. This value is adequate for the latest commercial broad area single emitter diode lasers which deliver up to 13 W of optical power.

Because the difference in the geometry and power dissipated between the laser simulated by Grumman and the Bookham laser, the way to compare the efficiency of the two cooling structures was through the power removed by the jets. While the Grumman laser dissipated 83 W (691 W/cm^2), the Bookham generated 8.5 W (590 W/cm^2) operating at full power. Considering the number of jets in every structure, the Grumman cooler removed 3 W while our design removed 1.7 W per jet.

4.16 Comparison between the two generations of LTCC Cooling Structures

The second generation of coolers showed a reduction of 16 % in the thermal impedance compared with the first generation. Reduction was attributed to improvements in the cooling device, such as the incorporation of gold plated silver tracks, wire bonding and

attachment of the Bookham laser using an adhesive more suitable for the application. In addition, the thermal impedance of the first prototype was calculated using the theoretical output power of the laser. First and second generations of coolers were developed with the support of Dr. Aaron M. McKay, currently working at the Macquarie University in Sydney Australia.

In the first generation of coolers, electric current was provided to the laser soldering enamelled copper wires (magnet wire) onto the gold plated surface of the AlN submount. Because the maximum temperature recommended by Bookham for soldering the laser diode was 250 °C, a solder with a low melting point was chosen. The soldering was done using a Pb-free fluxless Indalloy® 281 with a melting point of 138 °C and TACflux 020, both from Indium Corporation. A picture of the electrical connections is shown in Fig. 4.32. At the top of the picture a block of Poly(methyl metacrylate) can be observed, it served as a manifold for the cooling water which flowed in and out of the LTCC structure.

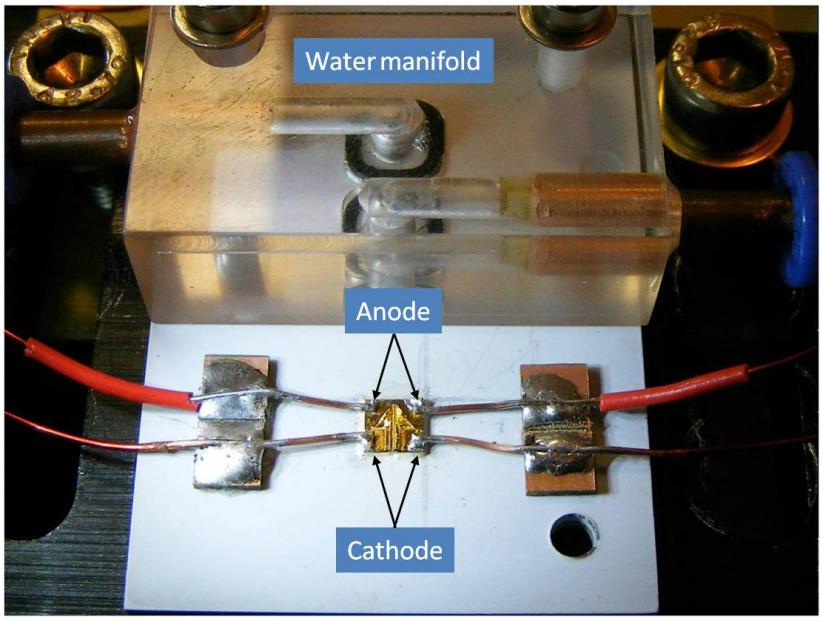

Figure 4.32 Electrical connections using enamelled copper wires soldered directly onto the AlN tile using low melting point solder

Although successful soldering was achieved, the diode laser was prone to damage. The main causes of damage were contamination of the diode facet due to the fumes generated by the flux, solder bridges between anode and cathode and breaking of the wire bonds. Because of this, the second generation of coolers was provided with gold

plated silver electrical tracks to allow the distribution of high current on board and the placement of wire bonds. Another upgrading from the first prototype was the change in the adhesive used to attach the Bookham laser to the LTCC structure. It was initially bonded using a DM6030Hk-PT/H579 (Diemat, Inc., USA) silver-loaded epoxy adhesive with high thermal conductivity. However, due to its high curing temperature, 150 °C for 4 hours, it was necessary to place the structure in a nitrogen-rich environment to avoid facet oxidation at mirror surfaces. Oxidation could quickly lead to degradation of the laser performance and eventual failure. In addition, the DM6030 showed water leakage after a few hours of operation.

Results obtained from the first prototype were presented in the 42nd International Symposium on Microelectronics IMAPS 2009. Paper presented in IMAPS 2009 was awarded as the "Best Paper" of the Thermal Management Materials session and the "Outstanding Student Paper" of the conference [98].

4.17 COMSOL Simulation of the Heat Transfer of the Diode on Sub-mount Attached to an "Infinite Heat Sink"

In this section, the contribution of the LTCC structure to the overall thermal impedance was calculated. To obtain this value, the thermal impedance of the laser diode chip mounted on the AlN submount was calculated simulating the thermal transfer through it using Finite Element Analysis (FEA) software.

As the thermal impedance of the SES7-975-01 on the AlN submount was not provided by the manufacturer, the heat transfer in the structure was simulated using COMSOL (COMSOL Group, Sweden) to calculate the thermal impedance. COMSOL is a commercially available FEA software package. Heat transfer simulation was done for the diode laser on submount on an ideal "infinite heat sink". Simulations were done in Convection and Conduction application mode, solving the partial differential equation for heat transfer by conduction and convection

$$\nabla \cdot (-\kappa \nabla \mathrm{T}) = Q - \rho \mathrm{C}_p \mathbf{u} \cdot \nabla \mathrm{T} \tag{4.6}$$

where:

ρ is the density of the material

C_p is the heat capacity

κ is the thermal conductivity

Q is the heat source

∇T is the temperature gradient

Given the boundary conditions and material parameters, COMSOL generated temperature distribution maps. For the thermal modelling of the package, the boundary conditions were constant temperature at the bottom of the device, thermally insulated side walls and thermally insulated upper surface of the laser chip [99]. In addition, the joule heat generated on the 2 µm thickness gold layer deposited over the upper surface of the AlN submount was considered in the model. The underside temperature was fixed to 25°C in the model. Threshold current of 0.5 A, operating voltage of 2.2 V and series resistance of 0.03 Ω were considered in the model. As heat is generated in the active region of the laser, the heat source was represented by a GaAs heating stripe with a volume of 1.62×10^{-12} m^3 generating the power dissipated by the laser using 50 % electrical to optical efficiency. The material library of COMSOL was utilized to provide temperature-dependent material properties for the model. Figure 4.33 shows a simulated temperature distribution of the diode laser on submount for an operating current (I) of 9.5 A and voltage (V) of 2.2 V.

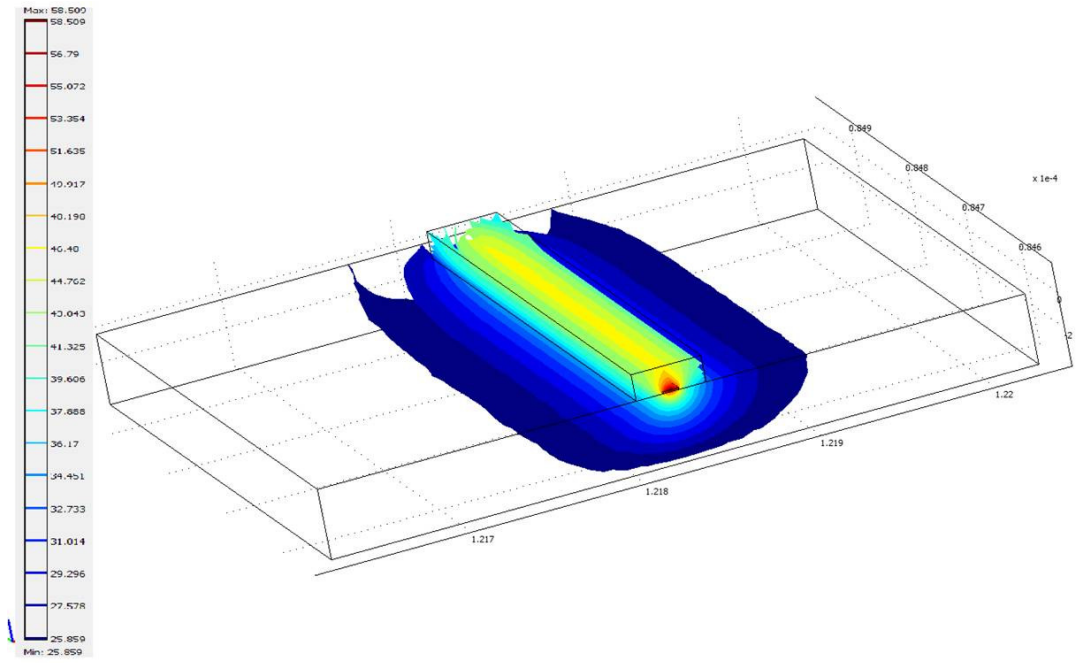

Figure 4.33 Temperature distribution of the diode laser on submount for an operating current (I) of 9.5 A and voltage (V) of 2.2 V

According to Equation 4.3, to calculate the thermal impedance of the package it is necessary to obtain the temperature difference between the hottest point of the laser and the reference temperature at the bottom of the AlN submount. In Fig. 4.33, an in-homogeneous temperature distribution in the laser chip is observed, with the front facet the hottest point. Because of this, in order to calculate the thermal impedance the average temperature of the laser chip between the front and rear facets was used. Figures 4.34 and 4.35 show the temperature profiles from the top of the laser chip to the bottom of the AlN submount for different operating currents at the front and rear facets, respectively.

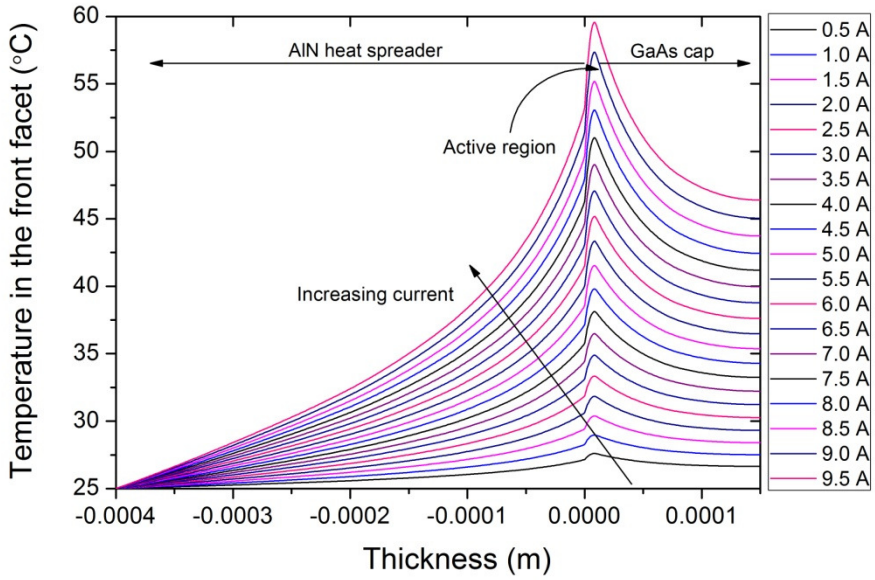

Figure 4.34 Temperature profile from the top of the laser chip to the bottom of the AlN submount for different operating currents in the front facet of the laser chip

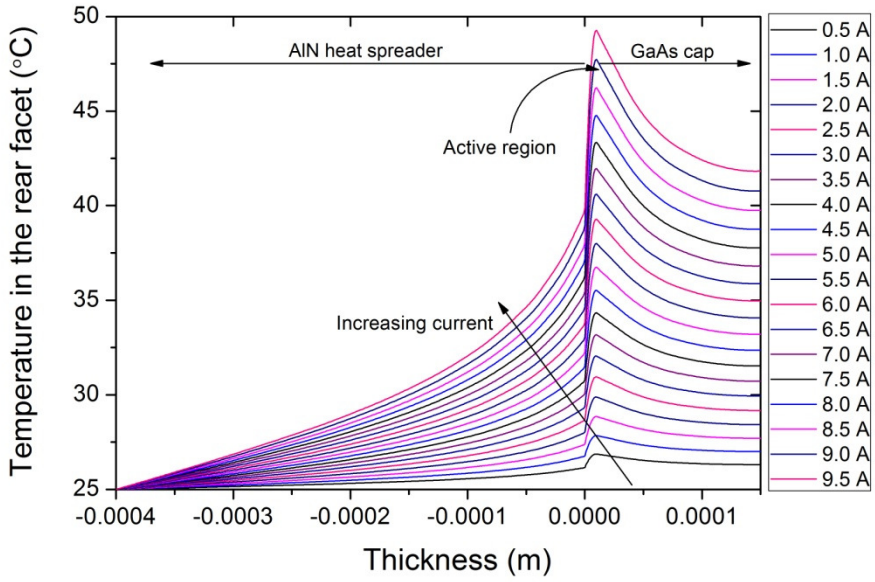

Figure 4.35 Temperature profile from the top of the laser chip to the bottom of the AlN submount for different operating currents in the rear facet of the laser chip

The average maximum temperatures obtained in the package for different operating currents are shown in Fig. 4.36.

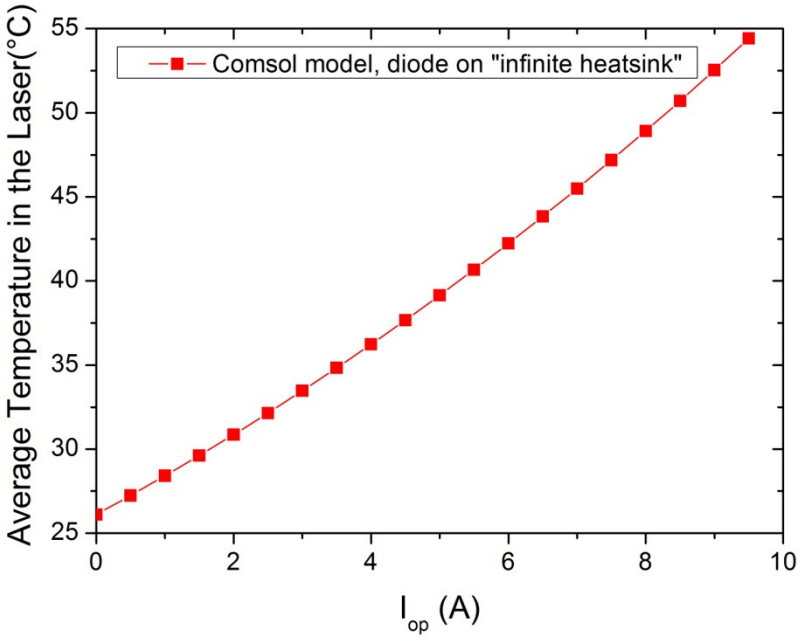

Figure 4.36 Maximum temperature in the Bookham laser as function of the operating current

Figure 4.37 shows the temperature difference (ΔT) vs. the thermal power dissipated by the laser (P_{therm}) curve. The thermal impedance for the package was obtained by a linear fitting of the data, yielding a value of 2.15 °C/W.

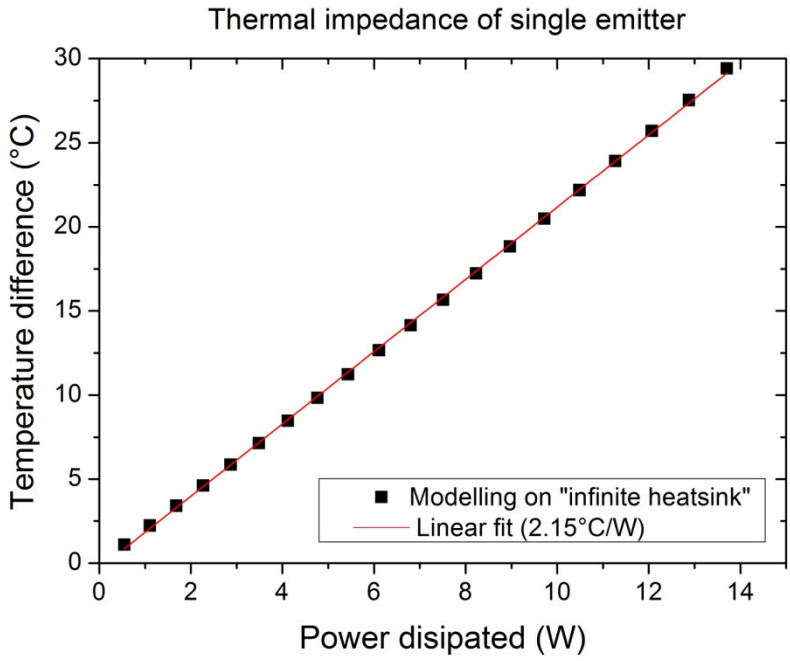

Figure 4.37 Temperature difference (ΔT) between the hottest point and the bottom of submount as function of the thermal power dissipated by the laser (Ptherm)

The thermal impedance of the SES7-975-01 obtained after simulations was 2.15 C°/W, meaning this, that the larger fraction of the overall thermal impedance in the LTCC cooling structure corresponded to the Bookham laser in the AlN submount.

4.18 Conclusions

We have demonstrated the fabrication of a water-tight jet LTCC cooling structure using a successful modified firing profile, which allow the co-firing of LTCC, nanocarbon and silver paste, resulting in a structure with no distortions, able to manage high current on board and with the required flatness to allow the placement of optical elements without the need of post-grinding. The bonding of 24 layers stacked to form a 3D structure with internal cavities was achieved using nanocarbon inserts and a single uniaxial lamination. Also, the printing of high quality silver tracks using inexpensive laser-cut Mylar masks was reported. The resulting thermal impedance of 2.7°C/W, will allow the LTCC structure to cool the latest commercial broad area single emitter diode lasers which deliver up to 13 W of optical power.

CHAPTER 5

PLACEMENT OF OPTICAL ELEMENTS ONTO LTCC STRUCTURES

5.1 Introduction

In recent years, the need for fibre coupled lasers with higher power and brightness for direct applications and fibre laser pumping has increased. Traditionally, pumping sources consisted of several BA single emitters, each one mounted in a pigtailed telecom grade package, multiplexed into a single fibre using single or multi stage fused-tapered fibre combiners. However, the use of multiple fibres combiners to reach high powers reduces the quality of the beam. To solve this, the new approach is to combine in free space multiple BA emitters placed in the same module and couple them into a fibre. Because of this, the possibility of mounting optical elements onto the LTCC cooler, needed for the correction and steering of the beam was studied.

In this chapter we report the procedure for the placement of a fast-axis collimation (*FAC*) lens onto the LTCC cooler for the correction of the high divergence of the Bookham laser. The divergence and pointing stability of the corrected beam as function of the power dissipated through the cooling structure is reported.

5.2 Optical Correction

As introduced in Sec. 1.4, because of their geometry, single emitter broad area diode lasers suffer from a highly divergent emission in the direction perpendicular to the junction. To correct this, commonly a cylindrical lens with high numerical aperture is placed close to the emitting region.

To correct the 29° full width at half maximum (*FWHM*) divergence of the SES7-975-01 diode laser, fast-axis collimation lenses from two companies were considered. The XB FAC-08-600 (Ingeneric Gmbh, Germany) with a 0.6 mm effective focal length (EFL) and the D141-362 (Doric Lenses Inc., Canada) with EFL of 0.590 mm were tested. A better beam correction was obtained using the Doric lenses. Only the results obtained using the Doric lenses are reported in this Chapter. The dimensions of the D141 were 1.05 mm height and 3.00 mm width. The working distance of the lens was 0.150 mm with a focal length tolerance of ±3%.

To obtain the correction of the beam, it was necessary to match the centre of the lens with the height of the laser emitter; the position of the emitter was 450 µm over the top surface. Because of this, it was necessary to machine a pocket in the surface to allow the optimal position of the lens. The top 2 layers were machined in green state and filled with nanocarbon tape to create, 0.5 mm away of the laser emitter, a 4 mm (L) × 1 mm (W) × 0.180 mm (D) pocket.

The accuracy of the alignment and positioning of the FAC lenses needs to be in the submicron and mrad regime in order to avoid degradation of the beam. According with Brauch [100], the most sensitive processes leading to beam degradation due to misalignment, are axial defocusing and lateral beam twist. For example, an axial defocusing of 0.5 µm of a FAC lens with focal length of 200 µm results in an excess loss of 50% in the main spot [101]. For an excellent explanation of the effects on the beam caused by the misalignment of a FAC lens with similar focal length to the D141-362 see reference [102].

To avoid these problems, a precise manipulation and positioning of the lens was done manually using an aluminium frame fixed to a 6-axis alignment (x, y, z, β_x, β_y, β_z) system (Elliot Scientific Ltd., UK) with a resolution of 20 nm for the three spatial axes and 0.1 arcsec resolution in the three rotational axes. The lenses ware attached to the aluminium frame using double-sided adhesive tape. It was done manually under a stereo microscope using a 3× magnification.

Alignment of the lens was done measuring the profile of the collimated beam in the far-field. The beam was projected on a rotating disk and measured using a LBA-710PC (Spiricon Inc., USA) frame grabber beam profiler. The experimental set-up used is shown in Fig. 5.1.

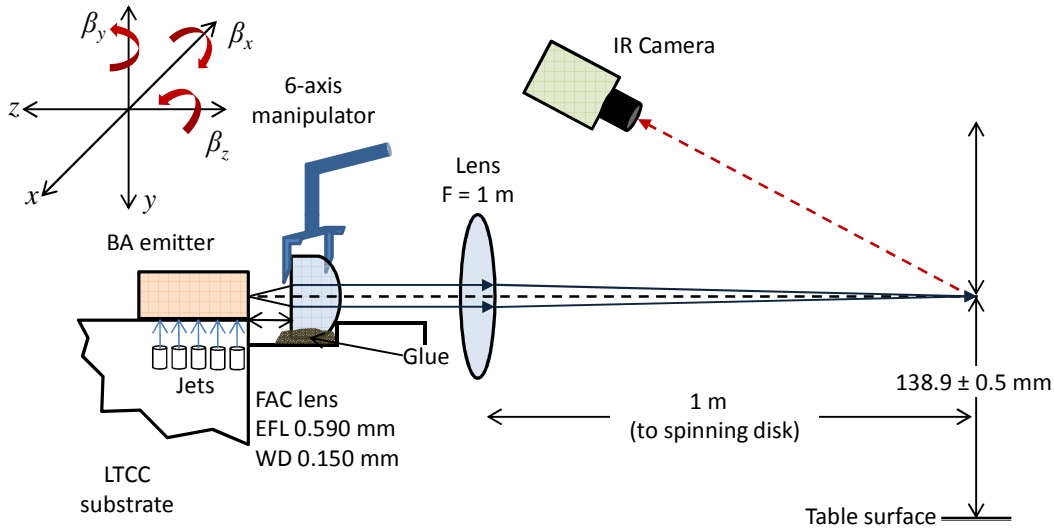

Figure 5.1 Set-up used for the placement of the FAC lens

Profiles were acquired using a monochrome CCD CS8630HC (Toshiba Teli Corportaion, Japan) with a 6.5 × 4.85 mm CCD chip, which covered the near infrared spectral range. The size of the images captured was 512 × 480 pixels with a resolution limited to 52 µm per pixel.

Profiles were taken with the diode laser running with an output power of 4.5 W at 0.138 lmin^{-1} flow rate. Figure 5.2 shows the image of the far-field beam profile at the focal plane of a lens with an effective focal length of 1m, at the optimal position of the FAC lens. Graph in Fig. 5.3 shows the normalized intensity beam profile after processing the acquired image.

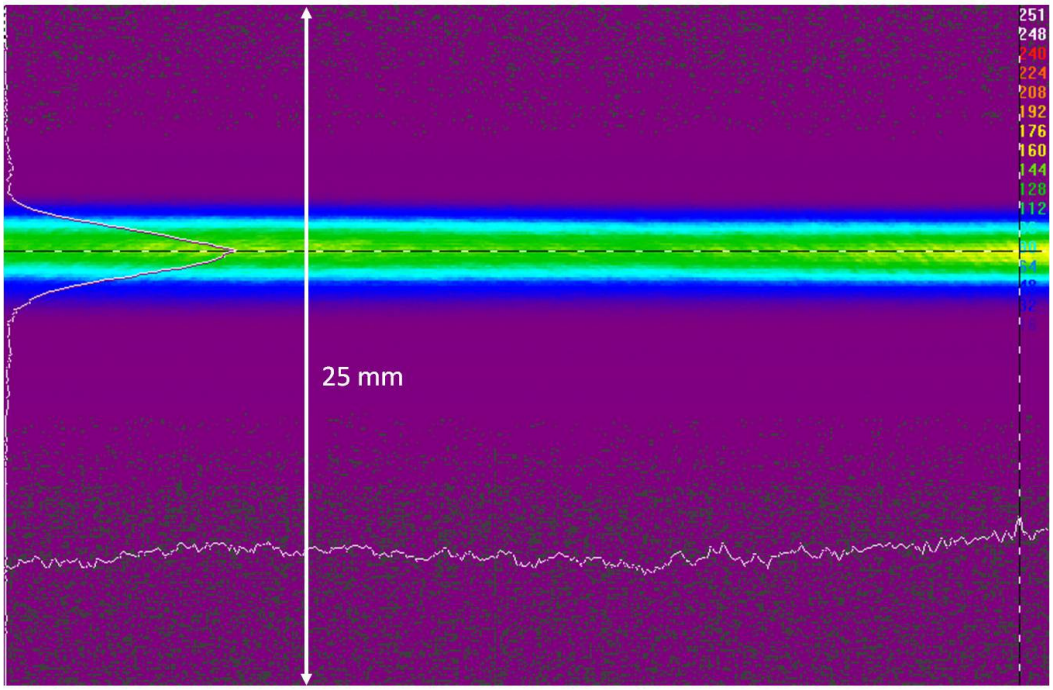

Figure 5.2 Image of the far-field beam profile after collimation at the focal plane of a lens with an EFL of 1m

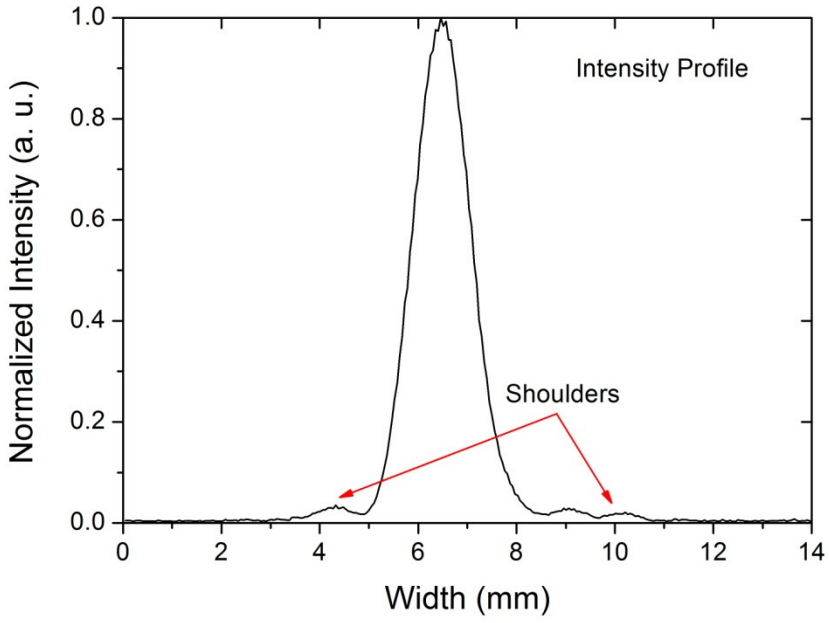

Figure 5.3 Fast-axis normalized intensity beam profile

Next to the main lobe of the intensity profile, shown in Fig. 5.3, “shoulders” can be observed. Shoulders are usually attributed to imperfections in the fabrication of the FAC

lens or poor aberration correction in the lens design [103]. Moreover, they can be produced by a slight misalignment of the FAC lens.

The quality of the collimated beam was measured using a one dimensional power-in-the-bucket (*PIB*) curve, which is the integrated power of the normalized intensity beam profile versus the far-field beam angle as shown in Fig. 5.4. The beam divergence of the corrected beam was defined as the angle containing the 90 % of the beam power.

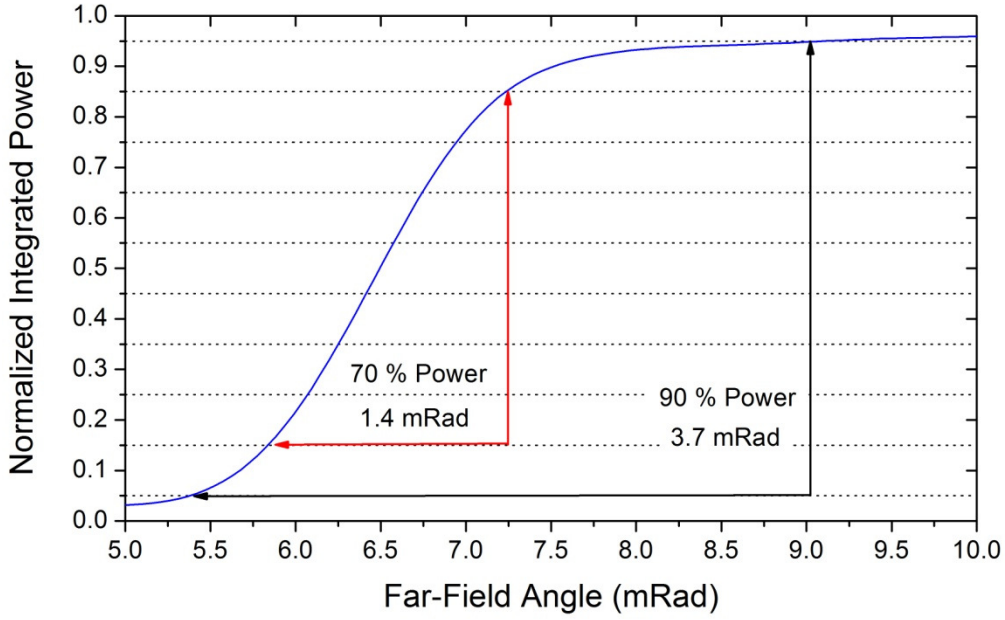

Figure 5.4 Fast-axis cumulative power profile (PIB)

The beam divergence considering a 90% enclosed power beam was 3.7 mRad, as depicted in Fig. 5.4. As a result of the fast-axis collimation, the divergence was reduced by a factor of ≈ 233, from 49.2 ° to 0.211 °.

Once the FAC lens was placed in the optimal position, it was bonded to the LTCC structure using a UV adhesive NOA 68 (Norland Products, USA). The curing time was approximately 12 minutes in periods of 30 seconds. Simultaneously, beam profile was monitored to correct any misalignment caused during the shrinkage of the adhesive. After curing, lens was detached from aluminum frame. Figure 5.5 shows the diode laser on submount attached to the LTCC cooler and completed with the FAC lens.

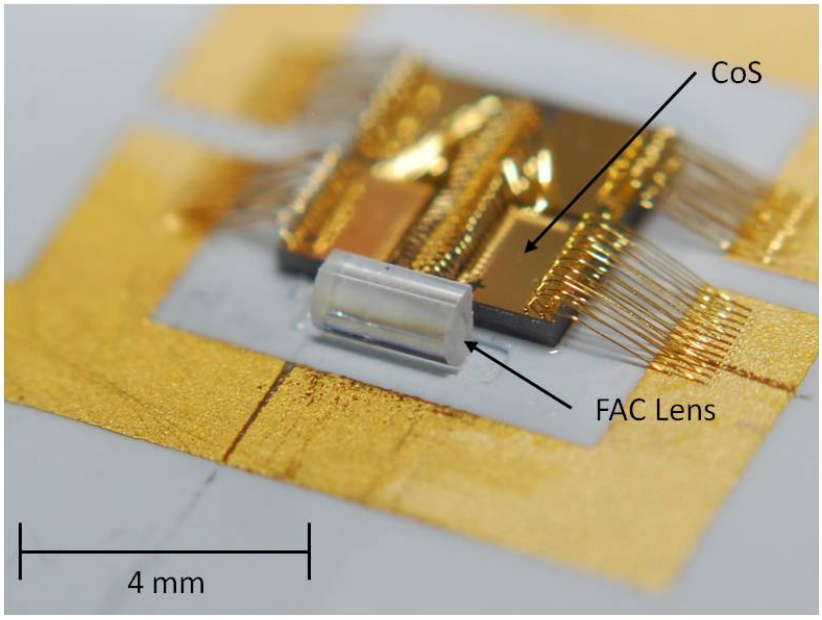

Figure 5.5 FAC lens bonded to the LTCC cooler using a UV adhesive

Figure 5.6 shows the far-field profile of the corrected beam with laser running at full power and flow rate of 0.158 $lmin^{-1}$. In Figure 5.7, the normalized intensity beam profile after processing the acquired image is shown.

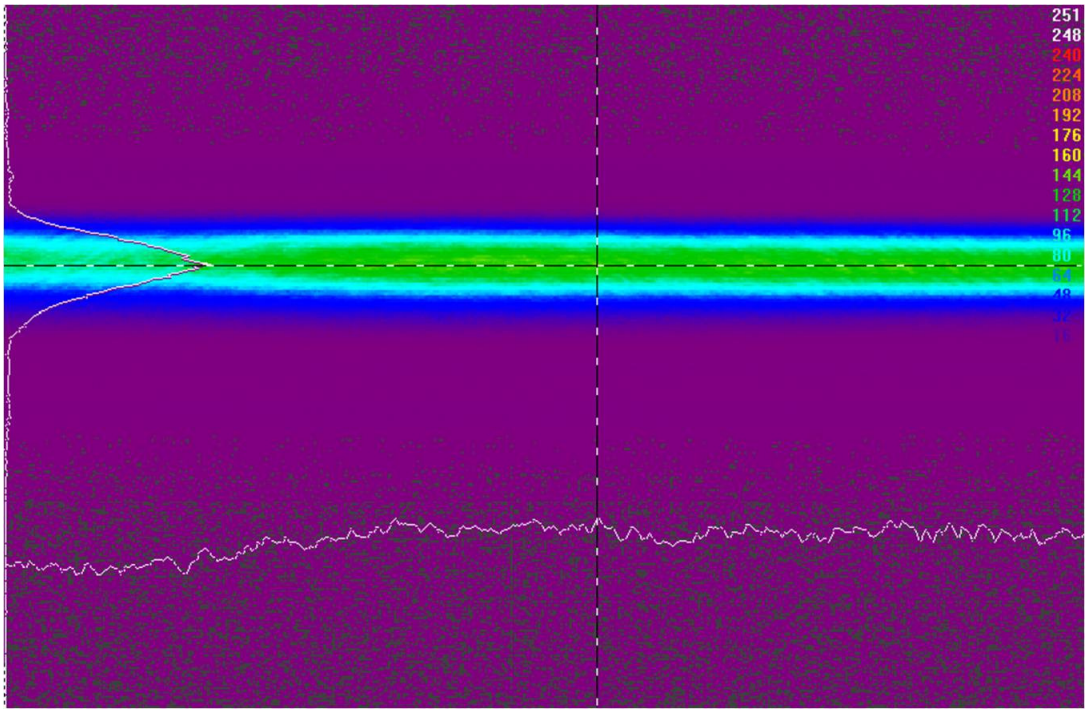

Figure 5.6 Far-field profile of the corrected beam with laser running at 7 W with flow rate of 0.158 $lmin^{-1}$

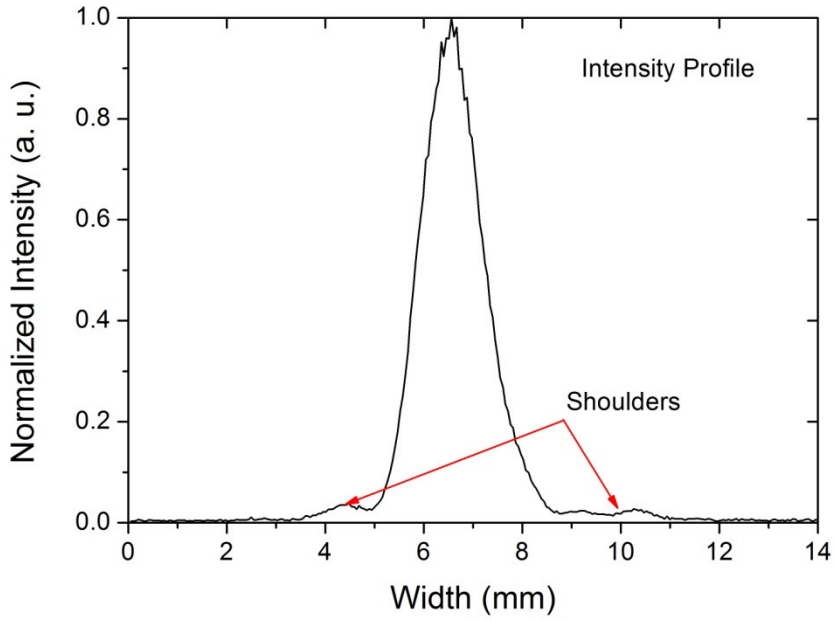

Figure 5.7 Normalized intensity beam profile with laser running at 7 W with flow rate of 0.158 lmin^{-1}

At full power, the beam position moved around of 0.1 mRad with respect to the position obtained during the aligning and attaching of the lens. Also, the beam divergence for a 90 % enclosed power was increased from 3.7 to 4.2 mRad, as shown in Fig. 5.8.

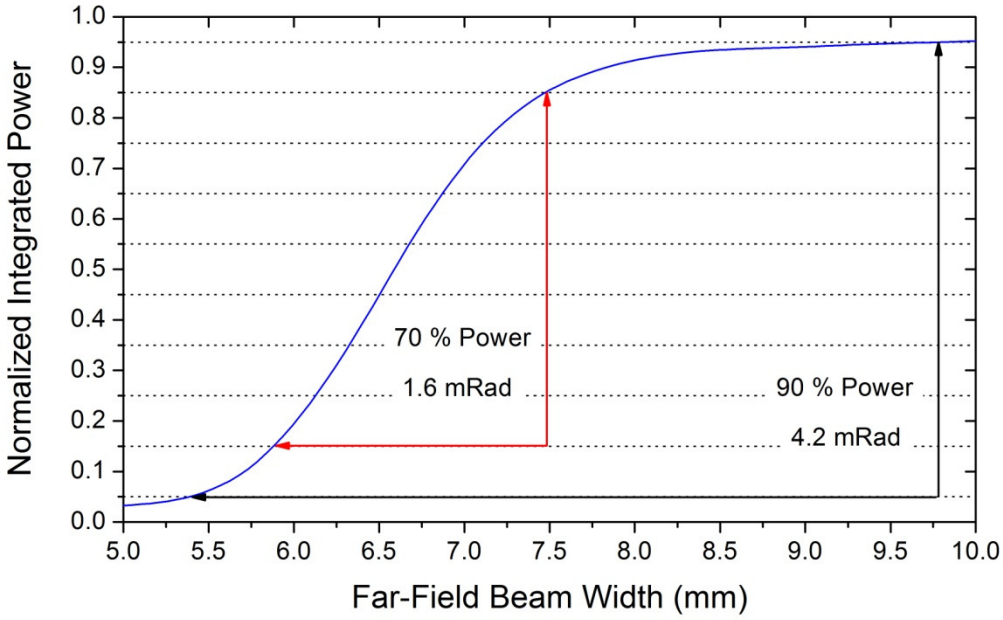

Figure 5.8 Cumulative power profile (PIB)

Although there was a pointing error, it is lower than the 0.5 mrad in the fast-axis reported by Karlsen [104] using a precise aligning and attaching technique developed by nLight for single emitters diode lasers.

5.3 Pointing Error and Beam Divergence Variations

The final objective of our research was to fabricate a fiber coupled module containing multiple single emitter lasers spatially multiplexed and fiber coupled. Because of this, it was necessary to know the variations in the pointing and divergence of the beam which could affect the efficiency of the coupling into the fiber.

Variation in the pointing direction and increment of the beam divergence was attributed to errors, such as defocus, transverse offset or twist of the lens, during the curing of the UV adhesive. In addition to the lens misalignment, another factor which introduced variations of the beam position from the centre of the lens was the increment of temperature in the structure as the operating current was increased, leading this to variations in the pointing and divergence. For example, lens aligning and attaching was done with the Bookham laser dissipating 80 % less power compared with the laser running at full power, which caused a lower change in the dimensions of the structure due to thermal expansion. This produced changes in the position and divergence of the beam as observed in Figs. 5.3 and 5.7. Bonding was done at low laser output power to reduce the risk of burning the UV adhesive. Fumes generated during burning could contaminate the front facet of the laser leading to a permanent damage.

The variation in the position and divergence of the beam due to the power dissipated were determined measuring the far-field beam profiles, with the laser running over a broad current range. Pointing and divergence deviations are shown in Fig. 5.9 and Fig 5.10, respectively.

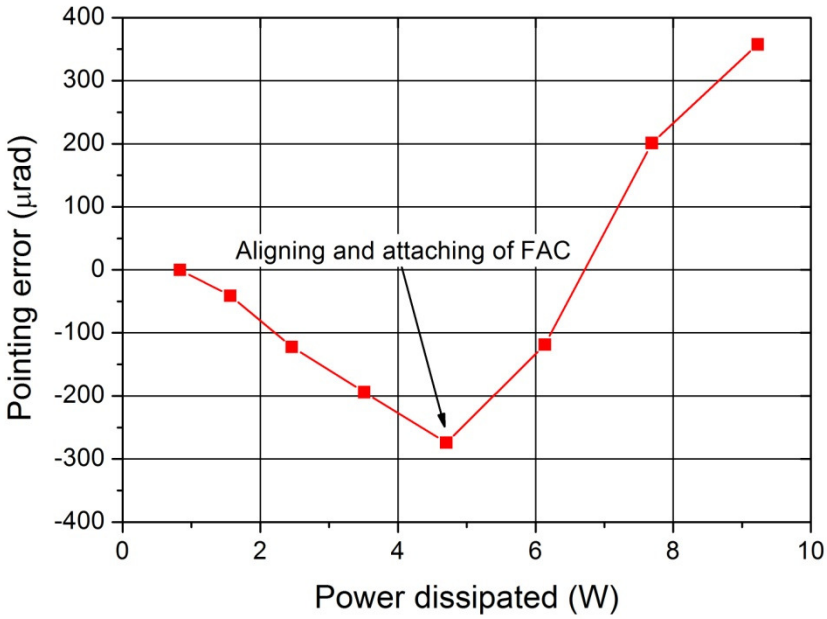

Figure 5.9 Pointing error in the far-field as function of the power dissipated by the laser with the height of the emitter at room temperature as reference

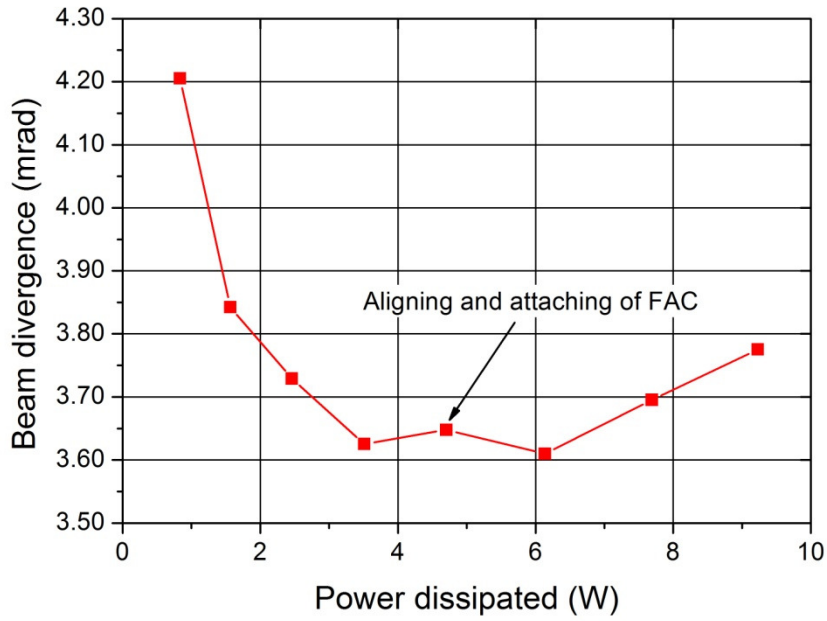

Figure 5.10 Variations in the beam divergence as function of the power dissipated by the laser

Because the transverse offset from the center of the lens is the most critical error [100], the vertical beam displacement due to the thermal expansion of the structure was calculated. For this, the thermal expansion of every material constituting the laser

package and the bonding adhesive, shown in Fig. 5.11, was calculated for the maximum power dissipated using the equation

$$\Delta L = \alpha_L L \Delta T, \tag{5.1}$$

where:

ΔL is the change in length (m)

α_L is the linear expansion coefficient (10^{-6}/°C)

L is initial length (m)

ΔT is the temperature change in the structure (°C).

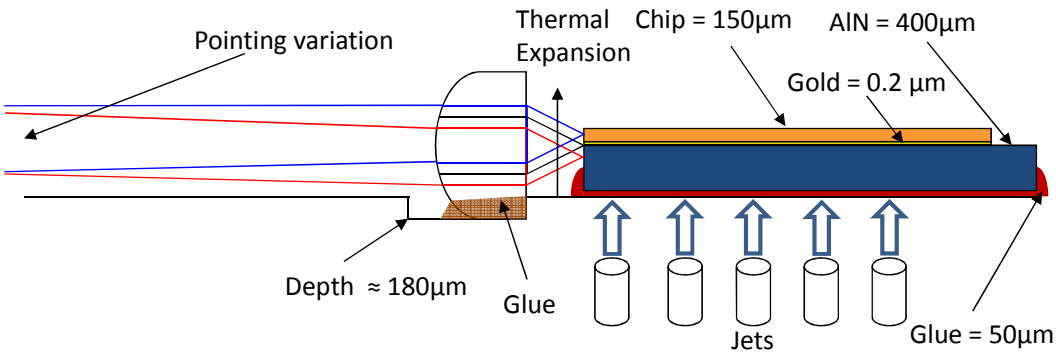

Figure 5.11 Thickness of the materials constituting the laser package

Expansion coefficients of 4.5, 6.9, 14.2 and 56.6 for AlN, GaAs, Gold and adhesive were used, respectively. The ΔT was calculated from the thermal simulation of the laser on submount reported in Sec. 4.17. The calculated vertical displacement of the structure was ≈ 0.1 µm, which contributed to an increase in the beam divergence of 0.04 mrad. This corresponded to less than 10 % of the maximum variation of the beam divergence, shown in Fig. 5.10. Total variation was attributed to multiple contributions such as horizontal and/or uneven expansion of the laser structure and misalignment of the FAC lens during curing of the adhesive. To know the exact contribution of every factor to the divergence and pointing, a more complex analysis is required. Although the pointing error was noticeable, it was enclosed within of an acceptable 10 % of the far field divergence.

Because it is not possible, considering the actual design, to compensate the thermally induced changes in the position of the beam with respect to the center of the lens, the option to minimize the variations in pointing and divergence is to reduce the lens misalignment during the adhesive curing. This is possible using a UV-curing adhesive with minimal linear shrinkage (about 1-2 %) and well defined drop volumes as well as symmetric placement of the drops with respect to the FAC lens. To minimize the misalignment, it will be necessary to incorporate to the process a microdrop dosage system capable of dispensing adhesive with high reproducibility and positioning accuracy.

Finally, the solder attachment of the AlN submount to the LTCC structure is considered to avoid the use of the 302-3M epoxy, which has the higher coefficient of thermal expansion. Thereby, the thermal displacement of the beam from the centre of the FAC lens will be reduced. To allow this, the metallization of the area designed for placement of the submount, shown in Fig. 4.18, will be required.

5.4 Conclusions

In this chapter we have reported the successful fabrication of pockets on the top surface of the cooler to allow the placement of optical elements required for the correction and steering of the laser beam. The accurate positioning of a FAC lens using a 6-axis manipulator to correct the high divergence in the fast-axis of the Bookham laser has been achieved. The FAC lens was attached to the LTCC structure using an UV curing adhesive. The variations in the pointing direction and beam divergence as a function of the power dissipated by the laser have been reported. The pointing error was enclosed within of an acceptable 10 % of the far field divergence.

CHAPTER 6

BEAM COMBINING OF 4 SINGLE EMITTER DIODE LASERS PLACED ON A LTCC STRUCTURE

6.1 Introduction

A recent trend in industry is to combine multiple BA single emitter laser diodes in a common package to reach the beam brightness and power required for pumping fibre lasers and for direct-diode industrial applications, such as welding, cutting, and etching. Packages based on multiple single emitters offer advantages over those derived from monolithic diode bars. Compared to laser bars, discrete diodes provide higher brightness, negligible thermal crosstalk between neighbouring emitters and protection against cascading failed emitters. In addition, insulated sub-mounted BA laser diodes based on telecommunication standards are preferred to diode bars and stacks because of the degree of assembly automation, and improved lifetime [105].

Although many commercial systems are still based on single emitter pumps, advances in single-emitter beam-combination methods have raised the state-of-the-art performance level to 100 W output power from a 105/100 μm core fibre [106-108]. These methods include wavelength, polarization, and spatial beam multiplexing or a mixture of them [109]. One of the more reliable and efficient devices are the Pearl™ modules, developed by nLIGHT Corporation (USA). In these modules, the emitters are stacked in a "staircase" formation to provide an excellent thermal path from the diode to the cooling plate and conveniently stack the emitters in the fast-axis, maintaining the brightness of the diode lasers. In a "staircase" configuration, lasers are offset vertically by machining the heat sink structure with a staircase-shaped face. Each diode is collimated individually in the fast and slow-axis and free space coupled into a fibre [104]. The present generation of such modules use single emitters rated at 9 W, allowing the use of passive cooling. However, the number of chips per module increase and recent advances in the development of single emitters now allows up to 20 W in the 9xx nm spectral range [110] and 25 W in the 780-820 nm range [111], therefore the use of active cooling methods to removed the higher heat load will become necessary. For this reason, the feasibility of accommodating multiple BA single emitter diode lasers on a water-jet cooled LTCC structure was studied.

In this chapter we present a LTTC structure capable of accommodating four 7W BA single emitter diode lasers, providing high power and active cooling on board. Because the technical difficulties for the fabrication of a "staircase" on LTCC, we proposed a novel in plane optical layout on board for the spatial stacking of the 4 laser beams.

6.2 Design and Fabrication of a LTCC Structure Containing 4 BA Single Emitter Diode Lasers

To allow the location of multiple lasers in the same structure, it should satisfy several requirements such as equal cooling of the 4 diodes, low pressure drop across the flow path, provision of high current connections on board and the placement of optics for the spatial beam multiplexing. Due to the difficulty of fabrication of a staircase shaped LTCC structure, a different arrangement of the optics was needed. Several optical configurations were considered [112, 113]. However, as these designs lacked compactness, a novel optical layout was designed to obtain an elegant and compact free space combination of the laser beams. The lenses, mirrors and diodes arrangement was designed considering the slow and fast-axis divergences, so the minimum dead space on the stacked beams could be obtained. The internal water and electrical layout was determined by the optical components and lasers arrangement.

6.2.1 Optical layout

As an alternative to the "staircase" formation of the diodes, as in the nLIGHT modules, the placement of the 4 single emitters on the same plane was considered. Using the coplanar arrangement, the challenge was to stack the 4 beams on top of one another in the fast-axis direction using a compact optical layout. To achieve this, each beam after being corrected using FAC lenses, was folded back and elevated by means of individually tilted and aligned dielectric folding mirrors. As the tilting of the mirrors introduced a slight rotation on the beam, a fifth compensating mirror was introduced to correct the rotation. All the surface details can be observed in Fig. 6.1. The schematic shows 4 diode lasers electrically connected in series through gold plated silver tracks and gold wire bonds. In front of each laser a FAC lens for correction and a tilted "edge mirror" for elevation and folding are depicted. Finally, a compensation mirror and a cylindrical lens for "slow" axis collimation are represented.

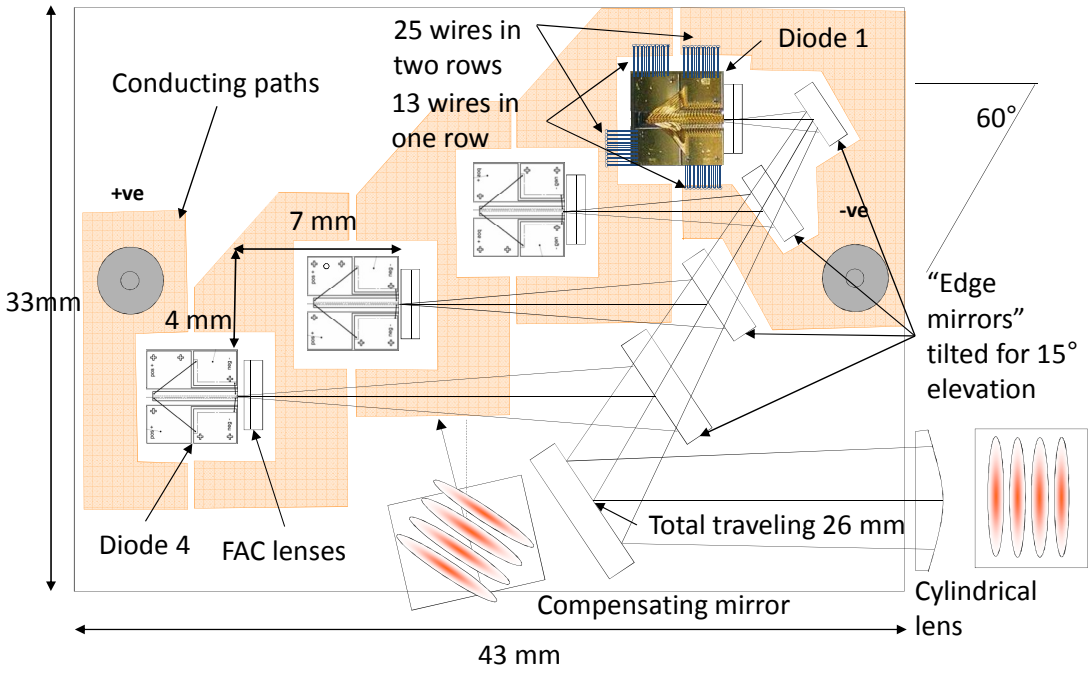

Figure 6.1 Surface details of the LTCC structure for cooling 4 Bookham lasers

The diodes and optics layout was determined by the beam divergence ($1/e^2$) in both directions and the need to have the minimum centre-to-centre spacing of adjacent stacked beams reducing the dead space with a low clipping loss produced by the mirrors. To avoid the blocking of the laser beams by the FAC lenses, wire bonds or electrical paths, several diode configurations were studied. Finally, each Bookham laser was separated by 7 mm and staggered by a further 4.05 mm, as seen in Fig. 6.1. The correction of the fast-axis was done using the D141-362 FAC lenses, described in Sec. 5.2.

Because a compact device was preferred, a folding mirror arrangement was used. In this configuration, the laser outputs are individually folded by 60 ° horizontally, viewed from the top, with an elevation angle of 15 ° from the plane parallel to the top surface of the LTCC structure using 2 mm height HR @ 980 nm dielectric coated mirrors. By reflecting from the mirrors, the beams were brought together as a closely spaced array of parallel beams. However, the vertical bend introduced a rotation of the beams, which was compensated by a vertical deflection of -15 ° using a fifth mirror. The planned optical path length between the diode lasers and the correction mirror was 26 mm. The designed dimensions for the 4 parallel beams after the correction mirror considering the slow and fast-axis divergence provide by the manufacturer, are depicted in Fig. 6.2.

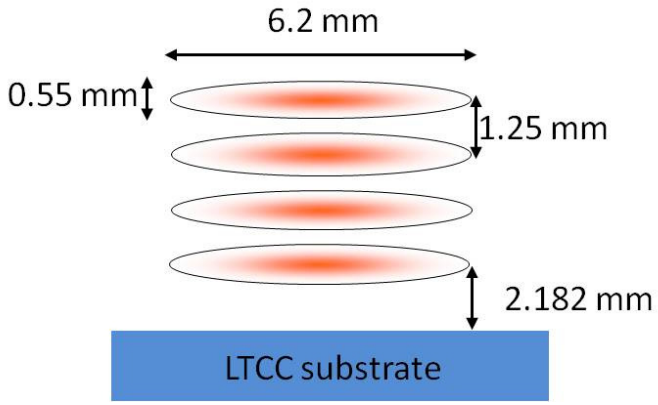

Figure 6.2 Dimensions of the designed stack, 26 mm away from each laser after the correction mirror

6.2.2 Internal water cooling and electrical layout

The design of the internal structures was determined by the optical requirements. Water paths were designed to obtain the same performance parameters such as water jet velocity and Reynold's number for all the coolers. The design was done to match the cooling parameters of the LTCC structure for one BA single emitter reported in Sec 4.11. To minimize the pressure on the soft bonded lasers and keep the same temperature of the water impinging on all lasers, ensuring in this way similar emission wavelengths, parallel internal water distribution was chosen. Because of geometrical limitations, the flow balance was obtained by distributing the water in two manifolds of the same dimensions as seen in the x-ray shown in Fig. 6.3.

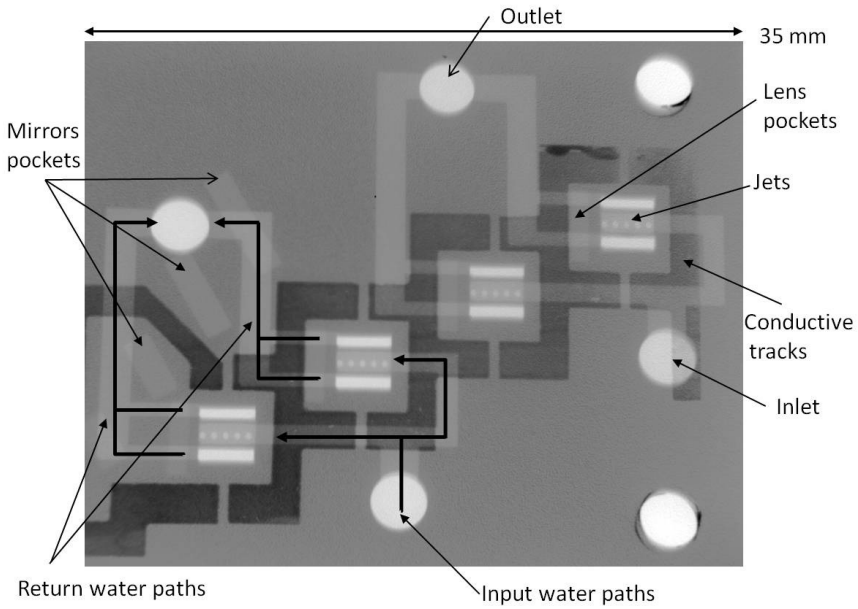

Figure 6.3 Internal water cooling layout

The two internal manifolds were fed externally by two parallel pipes connected to the recirculating chiller, as seen in Fig. 6.4.

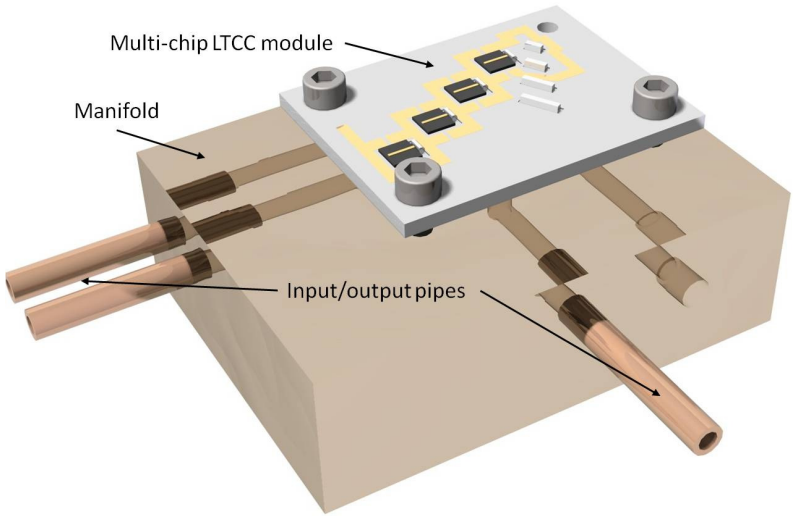

Figure 6.4 Water feeding using two pipes in parallel

Using the fabrication processes described in Chapter 4, 22 layers of nominal thickness 130-µm HL2000 were laminated and sintered to obtain a structure without internal deformations and the flatness required to place 4 diodes. The dimensions of the water pipes were modified from the original design for cooling one diode laser, to get an impingement water flow of 0.15 $lmin^{-1}$ per diode. This should give the same thermal impedance as for a single laser structure, reported in Sec. 4.15. Different levels of the structure could be observed in the x-ray image shown in Fig. 6.3. The jets, pockets for FAC lenses and electrical paths are identified in the left arm, while the water paths and pockets for micro mirrors can be observed in the right arm.

The structure was co-fired with silver paste, to obtain electric tracks for the distribution of high current on board. Series electrical connection of the 4 diodes was utilized to have the same current flowing across each laser, ensuring a similar output power. In addition, series connection is more efficient and reduces the total current required from the PSU, enabling rapid power adjustment while preserving the reliability of the laser [25]. Electrical layout was designed to allow the placement of optics and gold wire bonds without blocking the laser beams. Silver tracks were plated with a thin layer of soft gold by electrodeposition to allow a reliable gold wire bonding. This process was done by L.E.W. Techniques Ltd.

6.3 Process for Mounting and Wire Bonding of Lasers onto the LTCC Substrates

For mounting the 4 Bookham lasers onto the LTCC, the adhesive dispensing and placing procedures, described in Sec. 4.9, were utilized. The precise placement of a Bookham laser using the manual assembly station can be observed in Fig. 6.5.

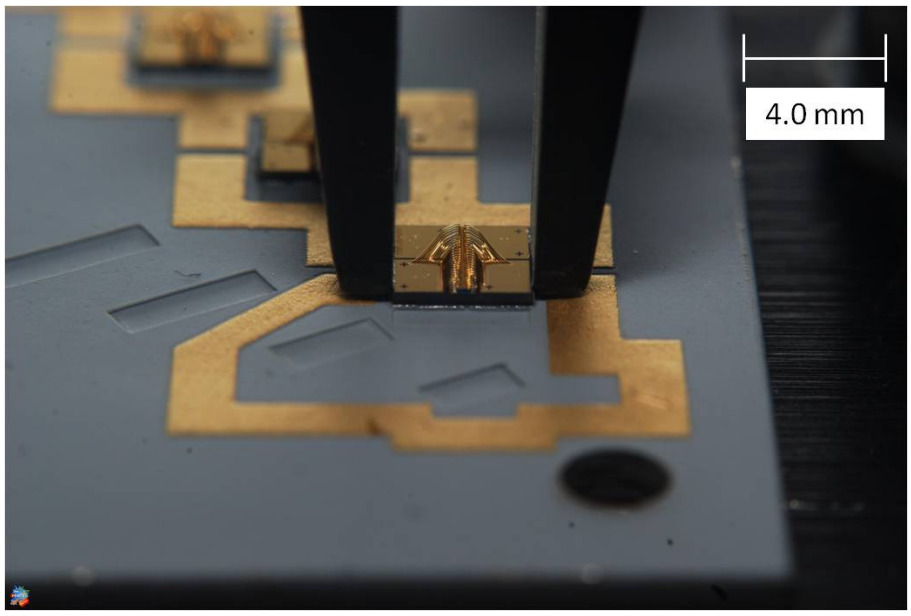

Figure 6.5 Precise positioning of a Bookham laser over the impingement window

After successfully bonding of lasers, they were connected to the gold plated tracks using the wire arrangement shown in Fig. 6.1, by means of 76 gold wires of 33 µm diameter and ≈ 4 mm length. Wire bonding was realized by Optocap Ltd. Two complete modules were assembled, but only results of the second are reported as during the electrical testing of the first module, 3 of the diode lasers suffered of catastrophic failure. At the beginning it was thought the fault was caused by inefficient cooling on the two diodes, but as observed on the spectrums shown in Fig. 6.8, the four diodes were running almost at the same temperature. The 4 spectra were taken before the failure of the 3 lasers. Failures were attributed to laser facet contamination. As lasers were open heatsink and there was no protection for the chip, dust particle could accumulate on the laser front facet leading to a permanent damage. Also, contamination of the facet could be generated during the gluing of the FAC lenses or by the fumes generated during the soldering of the electrical wiring, shown in Fig. 6.11. Because of this, the assembly of the modules must be realized in a cleaner environment and the use of solder for electrical connections must be avoided in the future.

6.4 Placement of FAC Lenses

FAC lenses were placed on the designed pockets using the alignment technique reported in Sec. 5.2. Bonding to the LTCC structure was done using the UV curing adhesive NOA 68. Fig. 6.6 shows the positioning of a FAC lenses using an aluminum arm attached to a 6-axis manipulator. Alignment and bonding of lenses were done projecting the far-field patterns on a rotating disk and measuring them with a LBA-710PC frame grabber beam profiler. After each FAC lens was placed in the optimal position, the corrected beam was deviated away from the spinning disk to avoid interfering with the correction of the next diode using a HR @ 980 nm dielectric coated mirror.

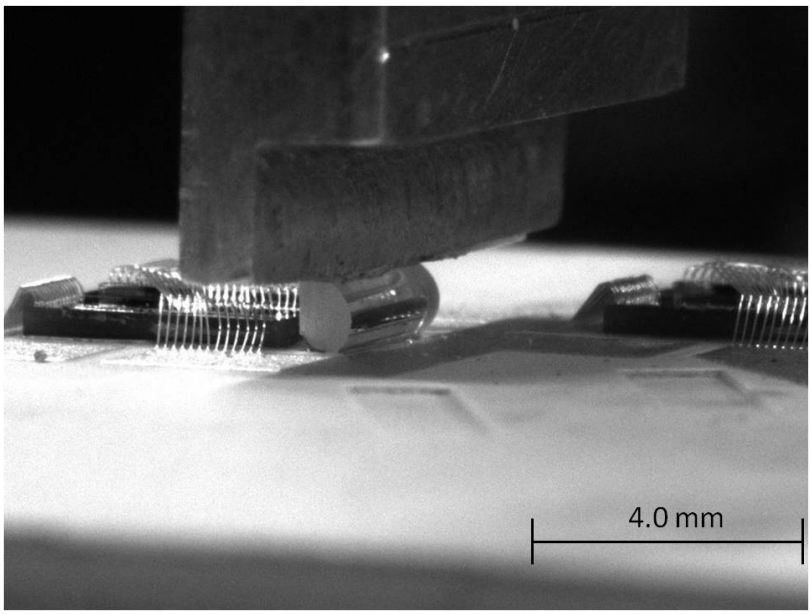

Figure 6.6 Placement of a FAC lens using an aluminium arm attached to a six axis manipulator

The group of far field profiles in Fig. 6.7 shows the 4 beams before and after bonding the FAC lenses to the LTCC substrate. As happened with the single laser modules, reported in Sec. 6.3, the ideal position of the lens could not be maintained during the curing of the UV adhesive, producing an increase in the divergence of the beam and error in the pointing as observed in Fig. 6.7. As we stated in Chapter 5, for the bonding of lenses in future designs, it will necessary to incorporate to the process a microdrop dosage system capable to dispense adhesive with high reproducibility and positioning accuracy to minimize the displacement of the lens during the curing. Additionally, the use of double sided tape to attach the FAC lenses to the aluminium arm made manipulation of the lens difficult when the adhesive began to harden. Because of this, in future the use of a grip to hold the lens is recommended. It is important to mention that

lens alignment and attachment processes in commercial products are performed using automated systems.

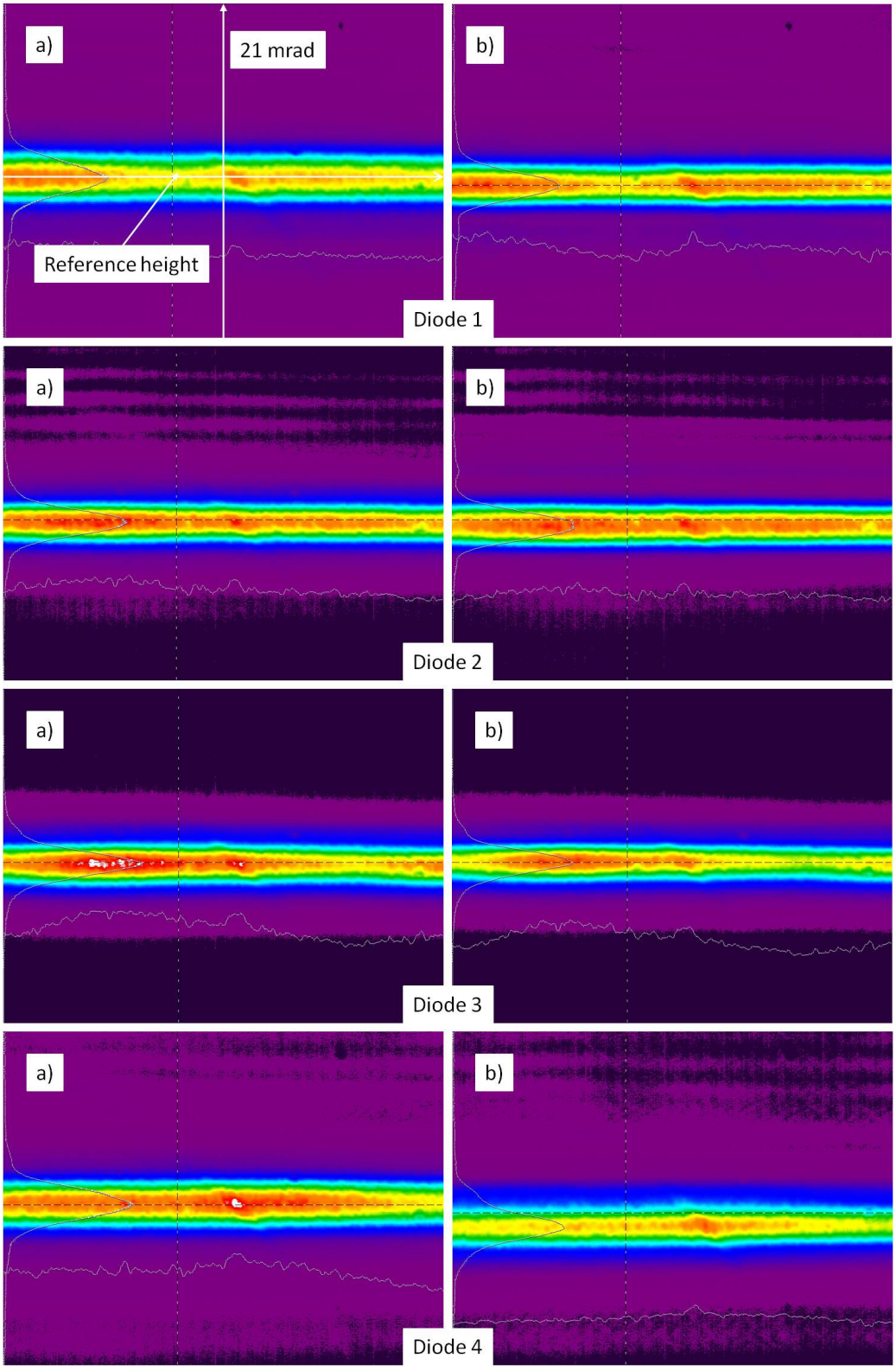

Figure 6.7 Far field profiles of the 4 laser beams a) Before and b) After the gluing of the FAC lenses

6.5 Internal Structures Testing

A 100 hours test of the cooler with the Bookham lasers attached was done passing 0.6 $lmin^{-1}$ through it with a pressure drop of 5.5 bar. No evidence of leakage in the structure or the laser bonding area was observed.

The internal water manifold previously described in Sec. 6.2.2, was fabricated to obtain the same water flow rate impinging at the back surface of each laser and similar operating temperature. As operating temperature determines the emission wavelength of the laser, the optical spectrums of the 4 lasers were taken to confirm similar running temperature on the 4 lasers. Figure 6.8 shows the 4 spectra of the lasers running at operating current of 5.9 A. This spectrum correspond to the first module, it was taken before the failure of two of the laser diodes due to contamination on the output facets.

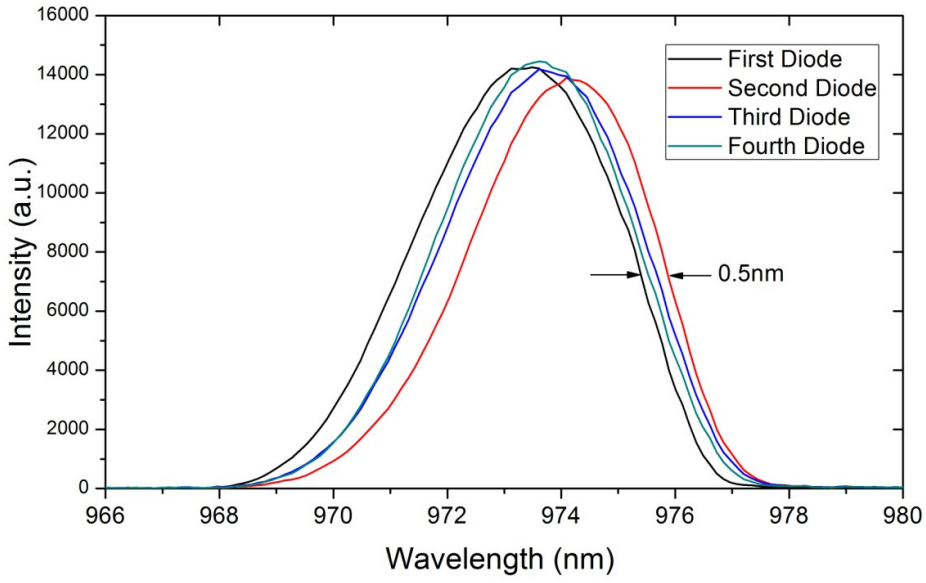

Figure 6.8 Spectra of the 4 lasers running at 5.9 A using a water flow rate of 0.150 $lmin^{-1}$ per chip

Using the wavelength shift with temperature of 0.3 nm/°C, the maximum difference in operating temperature calculated between the lasers was 1.7°C. The difference in the operating temperature was the result of some but not serious imbalance in the water distribution. In addition to the imbalance, small differences in the natural emission wavelength of each laser could contribute to the resulting spectra shown in Fig. 6.8.

6.6 Out of Plane Beam Combining

To achieve the stacking of 4 beams, they were combined out of plane, after being corrected by the FAC lenses, using individually tilted aligned dielectric folding mirrors. Initially, it was planned to obtain the elevation angle by tilting the mirror and placing adhesive under it to keep the desired position. However, after observing the pointing error introduced during the curing of the adhesive, tilting was avoided by cutting the base of the mirrors at angle of 7.5° resulting in a substrate with a flat surface easier to place and minimizing the required adhesive, as shown in Fig. 6.9. Pockets for mirrors were fabricated using the same process as for the FAC lenses, described in Sec. 5.2. In future designs, the LTCC substrate could be machined at the required angle to place the mirrors using the grey scale machining described in Sec. 3.4.1.

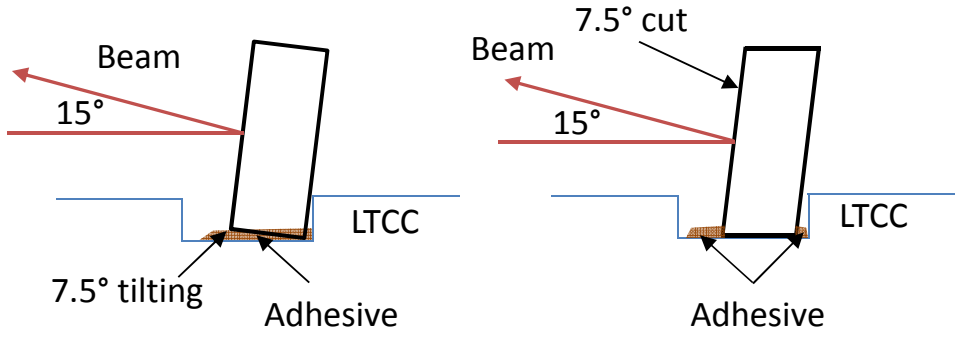

Figure 6.9 Difference in the placement of a 7.5° tilted mirror and a mirror with a cut base at the same tilted angle

However, as observed in Fig. 6.7, beams corrected by FAC lenses were displaced from their ideal position during the curing of adhesive. To compensate these displacements and reach the designed position, 3 of the mirrors were slightly tilted making it complicated to control the positioning of the mirrors during the curing of the UV Adhesive. Mirrors were placed and manipulated using the same six axis manipulator used for placement of the FAC lenses. Beams were aligned and stacked measuring the profiles projected on a spinning disk placed approximately 340 mm away from the mirrors. Mirrors were placed starting with the beam coming from laser 4. The Spiricon image in Fig. 6.10 shows the 4 beams stacked and rotated after mirrors were placed and glued to the LTCC structure.

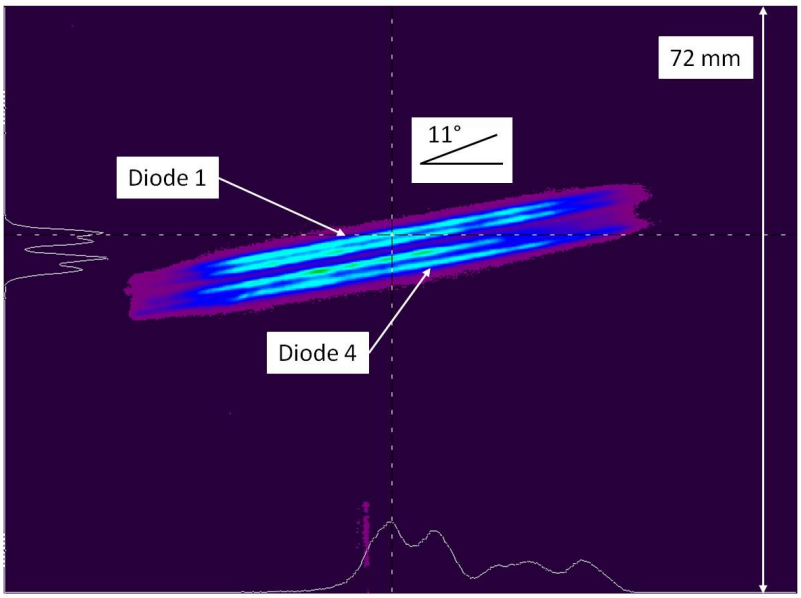

Figure 6.10 The four beams stacked and rotated after the mirrors were placed and glued to the LTCC structure

The gap observed in Fig. 6.10 between the beam 2 and 3 was the result of a disturbance of mirror 2 introduced during the adhesive curing. The placement error of steering mirrors during bonding is a problem which occurs with different substrates such as copper, and is not inherent to the use of LTCC. Figure 6.11 shows the LTCC module with the optics attached.

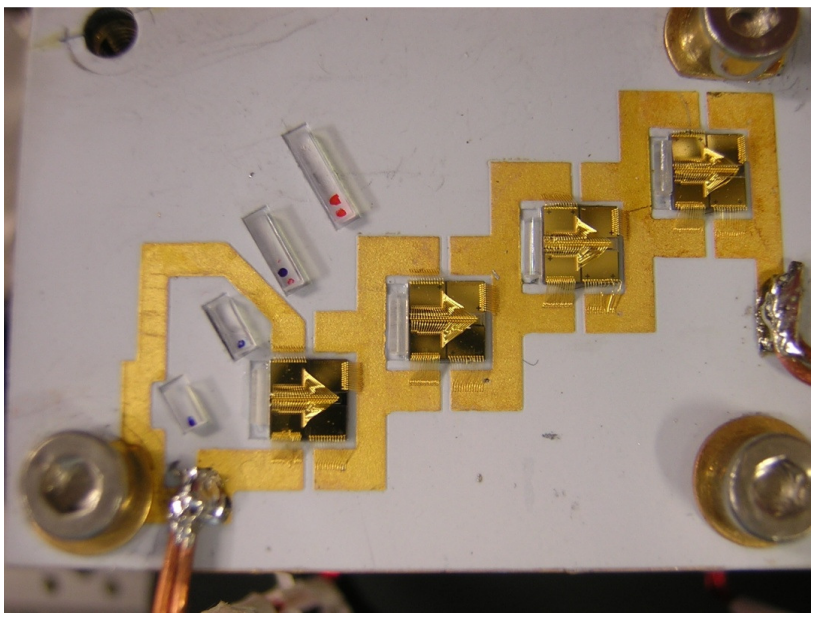

Figure 6.11 The LTCC module with the optics in position

To compensate the rotation and produce a parallel horizontal stack, a temporary fifth folding mirror giving a deflection angle of -15° was introduced in the designed position shown in Fig. 6.1. The Fig. 6.12 shows the compensating mirror in position.

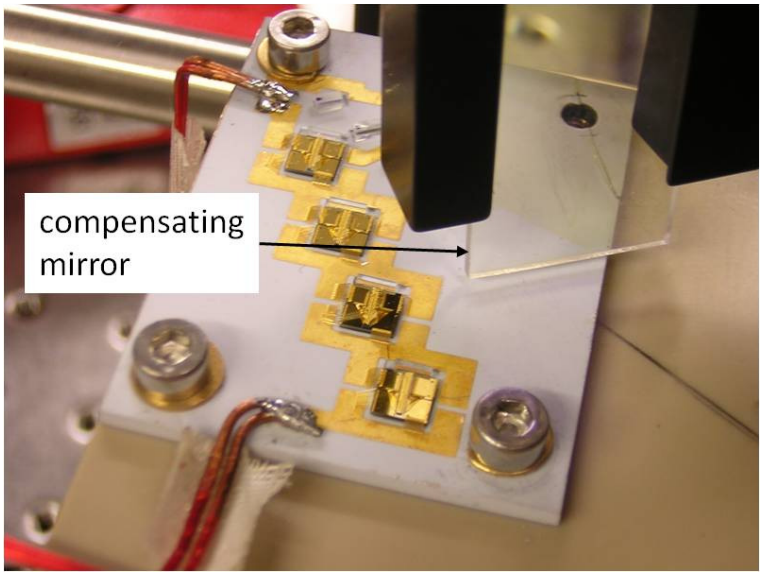

Figure 6.12 Compensating folding mirror placed on the designed position

A cylindrical lens with FL of 70 mm was placed ≈ 20mm from the edge of the LTCC structure to correct the slow-axis divergence of the 4 beams. The Fig. 6.13 shows the 4 beam stacked after being reflected by the 5th mirror and corrected by the cylindrical lens, on an IR viewing card placed 15 cm away from the mirror.

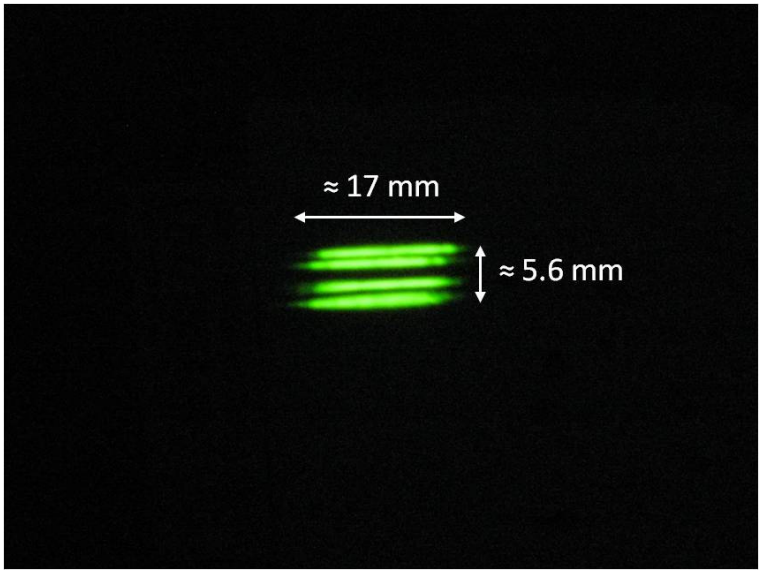

Figure 6.13 Beams after slow-axis correction, 150 mm away from the compensating mirror

The difference in dimensions in the horizontal direction with respect to the designed stack shown in the Fig. 6.2 was due to the slow-axis collimation lens being positioned away from the designed position shown in Fig. 6.1. In the future, the cylindrical mirror can be placed on the LTCC structure, closer to the mirror.

Although the stack looks acceptable in the near field as observed in Fig. 6.13, a method to measure the quality of the stack is calculating the BPP (beam parameter product) in the far field of the slow and fast direction. As the continuation of the project will involve the launching of the beam stack into a fibre, the stacking technique used must provide a lower BPP than the fibre to be used. For an excellent explanation of the BPP consult [114].

The required far field profile of the stack was measured in the focal plane of a lens with FL=1 m. It was performed at operating current of 5.9 A with a flow rate of 0.15 $lmin^{-1}$ per chip. The field profile is shown in Fig. 6.14.

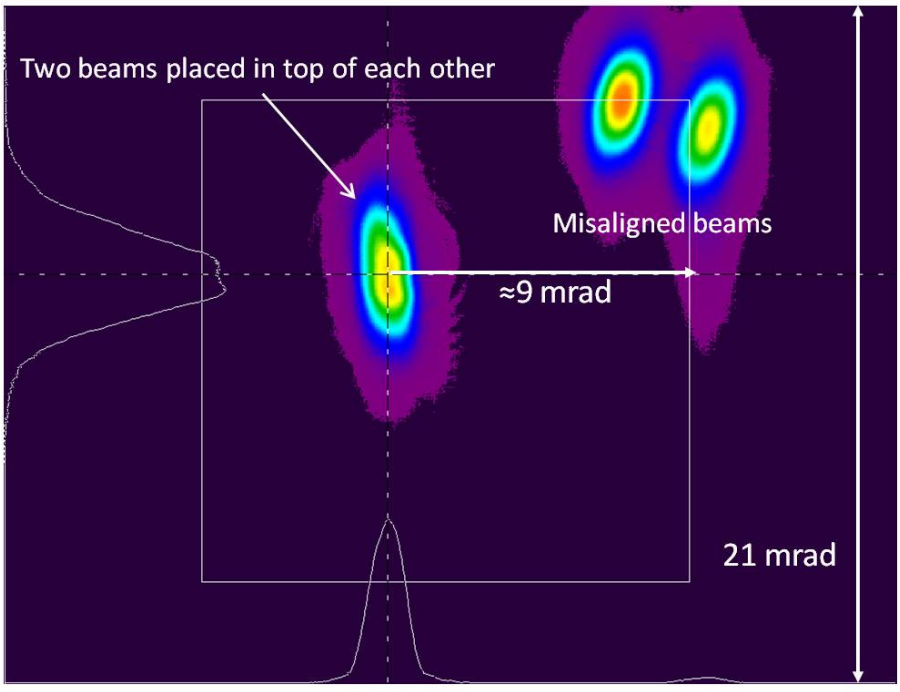

Figure 6.14 The far field profile of the stack showing 2 misaligned beams due to mainly horizontal misplacement of the "edge" mirrors

The calculation of the BPP was not possible due to the variations in the required angular pointing of two of the beams, as observed in Fig. 6.14. Although the 4 beams looked

almost parallel 150 mm away from the compensating mirrors, as observed in Fig. 6.13, the small variations in the horizontal position (slow-axis direction) resulted in a maximum misalignment of approximately of 9 mrad of two of the beams in the far field, as shown in Fig. 6.14. On the other hand, the 4 beams were deflected at the designed angle, resulting in the placing of 4 beams approximately equally spaced in the fast-axis (vertical) direction.

Apart from the errors introduced during the curing of the adhesive, the misplacement of the beams in the far field was caused mainly by a misalignment of less than 0.6° in the horizontal axis of two of the "edge" mirrors. This shows how critical is the alignment of the mirrors. As alignment of the 4 "edge" mirrors was done measuring the beam profiles just 340 mm away from the mirrors, as shown in Fig. 6.1, it was impossible to detect the misalignment. To overcome the problem will be necessary to implement a more complex measuring system capable to monitor simultaneously the near and far field profiles during the alignment of the mirrors. Additionally, the IR camera and spinning disk should be mounted in a platform tilted at the same angle at which beams are deflected by the mirrors to get 4 beams of identical dimensions at the spinning disk. On the other hand, beams were positioned successfully in the vertical direction because they were collimated and aligned in the fast-axis direction by measuring the profiles in the far field, as shown in Fig. 6.7. After being collimated the 4 beams were deflected at the same angle by the "edge" mirrors.

Although the optical results of the first prototype were not as expected, the processes that affected the performance were identified and can be modified to improve the optical performance of future devices. Unfortunately, as the maximum time allowed to finish the PhD project was reached, the changes necessary to obtain a module with the required optical characteristics must be implemented by the person who continues with the project.

6.7 Conclusions

I have pioneered successfully the use of LTCC technology for the fabrication of modules capable to allocate several BA single emitter diode lasers, with integrated micro-optics and active water cooling on board. For the diode lasers stacking, a novel out-of-plane beam shaping method using inexpensive optics, such as FAC lenses and glass coated mirrors cut at the required angles, has been presented. The fabrication of an

effective internal water manifold using nanocarbon inserts for the cooling of the 4 diode lasers with have been reported. A variation of less than 2 °C in the temperature between the 4 diodes was obtained. Failure of the diode lasers due to laser facet contamination was observed during the testing of one of the modules. To improve the lifetime of the laser diodes, modules must be assembled and tested in a “class 100” clean room and the use of solder for electrical connections should be avoided. To achieve the designed diode laser stacking, several changes must done to the actual lens and mirrors mounting processes such as the integration of a system capable to dispense adhesive with high reproducibility and positioning accuracy to minimize the displacement of the optics during the curing. A measurement system capable to observe simultaneously the near and far field profiles of the stacked beams during the positioning of the “edge” mirrors must be implemented. Finally, although a yield and cost analysis has not been done yet, considering the success of LTCC in other areas as automotive or wireless industries, we strongly believe this technology could be transferable to mass production for the laser diode industry.

CHAPTER 7

CONCLUSIONS

7.1 Overview

This thesis has covered a study of the use of low temperature co-fired ceramic (LTCC) as material for the fabrication of a multi-layer module with integrated cooling and optics, capable of accommodating several BA single emitter diode lasers on submount. The developed device addresses the recent trend in the laser industry of combining multiple BA single emitter laser diodes in a common package to reach the beam brightness and power required for pumping fibre lasers and for direct-diode industrial applications, such as welding, cutting, and etching. At the present, single emitters are packaged on Cu or CuW platforms, whose high thermal conductivities allow efficient passive cooling. However, as the number of emitters per package increases and improvement in the BA laser technology enable higher output power, the passive cooling will be insufficient. Therefore, this thesis has taken up the challenge to deal efficiently with the localised heat sources by an all new active cooling approach based on ceramic substrates. A new platform capable of removing the heat generated through impingement jet cooling has been developed. To reach the power scaling while simultaneously maintaining the high brightness, a novel out-of-plane beam combining method has been demonstrated. A complete fabrication process has been developed; this involves precise laser machining of features on the LTCC layers, the fabrication of internal structures with no distortions, the printing of silver tracks to supply high current on board and the accurate positioning of the required optics.

7.2 Conclusions

The potential of LTCC material as replacement for the fabrication multiple diode laser packages has been demonstrated in this thesis. The major contributions of this thesis are the fabrication of a LTCC substrate with internal structure, the heat removal of a diode sub-module using a jet impingement cooler and the beam combining of 4 BA single emitter diode lasers placed on a LTCC structure using a novel technique.

Fabrication of a LTCC substrate with internal structure

The fabrication of a multi-layer LTCC substrate with an internal structure has been reported. Unlike the structure reported by Northrop Grumman [69], in which the layers

were machined using mechanical methods, the substrate reported in this thesis has been formed using laser cut layers. Layers were cut with high-quality using a custom CO_2 machining laser system. The machining system was based in a novel "cold" self-cleaning technique for processing LTCC in "green" state developed previously in our research group. Internal structures without deformations were achieved placing nanocarbon inserts into the hollow spaces and using a modified hot uniaxial pressing method. Structure was laminated at 7 MPa for 10 minutes at 75 °C. This technique is faster and less prone to misalignment issues than the method proposed by Northrop Grumman, in which internal structures are formed using a progressive uniaxial lamination. Nanocarbon inserts were cut by the CO_2 laser system using similar machining conditions to those used with LTCC; this is the first time that laser machining conditions for nanocarbon have been reported. The complete removal of nanocarbon inserts during the sintering of the LTCC substrate was obtained using a modified firing profile. This profile allowed the co-firing of LTCC, nanocarbon and silver paste, resulting in a structure with no distortions, capable to manage high current and with a maximum variation from flatness of 50 µm in a length of 35 mm. This flatness allows the placement of electrical tracks and optical elements without the need of post-grinding.

Heat removal of a diode sub-module using a jet impingement cooler

The active cooling of a 7W Bookham broad area single emitter diode laser on an aluminium nitride (*AlN*) sub-mount using a water jet impingement cooler was achieved. Twenty four LTCC layers were used to form a structure capable to receive water from a cooling source and route it toward five 350 µm diameter jets trough internal channels and finally, return the water to the source. A maximum flow rate of 0.160 $lmin^{-1}$ with a pressure drop of 4.9 bar was obtained. At this flow rate, every jet had an exit velocity of 4.7 m/s, which yielded a Reynolds number of 1718.

At full output power, an overall thermal impedance of the LTCC package of 2.7°C/W at 0.160 $lmin^{-1}$ was obtained. The larger fraction of the overall thermal impedance in the LTCC cooling structure corresponded to the Bookham laser on the AlN submount, with 2.15 C°/W. With a thermal impedance of 2.7°C/W, the LTCC cooler could dissipate up to 18.5 W at 70°C junction temperature with a reference temperature of 20 °C. This value is adequate for the latest commercial broad area single emitter diode lasers which deliver up to 13 W of optical power.

As the coolant is not in electrical contact with the diode laser, the use of deionised water could be avoided, eliminating with this the problems and cost associated with the use of it. Finally, the geometry of the module can be modified easily to allocate diode laser of different dimensions.

Beam combining of 4 BA single emitter diode lasers placed on a LTCC structure using a novel technique

This is the first time that a multi BA emitter diode lasers module base on LTCC technology has been reported. It has been provided with integrated water cooling and micro-optics and is capable to allocate 4 Bookham diode lasers. To supply high current on board, silver tracks were printed and platted with a 3 µm layer of soft pure gold Type III, Grade A. Additionally, diode lasers and electrical paths were connected using 33 µm diameter gold wire bonds. The structure has been provided with an internal water manifold capable to impinge water at 0.15 $lmin^{-1}$ flow rate on the back surface of each laser with a variation of less than 2 °C in the temperature between the 4 diodes.

A manual assembly station was built up to manipulate and place the diode lasers accurately over the impingement windows. A displacement of the laser chip, especially the front part, with respect to the position of the jets could cause an increase of the thermal resistance, producing a reduction in the conversion efficiency and thermal overload of the diode laser. Lasers were successfully bonded to the structure using a two part epoxy.

The high divergence of the laser in the fast-axis direction was corrected using a FAC lens with an EFL of 0.590 mm and height of 1 mm. As the focal distance and the lateral FAC lens position had to be maintained within less than 0.5 µm and the 3 angular degrees of freedom within 0.5 to 20mrad. The manipulation and positioning of the lens was done manually using a 6 axis alignment system with a resolution of 20 nm for the three spatial axes and 0.1 arcsec resolution in the three rotational axes.The beam divergence after correction for a 90 % enclosed power was 4.2 mRad with a pointing variation of 0.1 mRad. This pointing variation is lower than the 0.5 mrad in the fast-axis reported by Karlsen [104] using a precise aligning and attaching technique developed by nLight for single emitters diode lasers.

To reach power scaling while simultaneously maintaining the high brightness, a novel out-of-plane beam shaping method using inexpensive optics was proposed. A compact arrangement was obtained using 4 tilted aligned folding mirrors, which stacked the 4 beams on top of one another in the fast-axis direction. The 4 beam stacking was unsuccessful in the "slow" direction due to a misalignment of less than 0.6° in the horizontal axis of two of the folding mirrors. This produced a horizontal pointing error of approximately 9 mrad in the far field of two of the beams. Misalignment was not detected because placement of the mirrors was done measuring the beam profiles just in the near field. Although the optical results were not as expected, the processes that affected the performance were identified and will be modified to improve the optical performance of future devices.

7.3 Future Work

To increase the reliability of the multiple BA single emitter laser diodes modules, further improvements need to be done. The needed changes are as follows:

- The region around the impingement window needs to be metalized to allow the soldering of the laser chip to the structure. This will eliminate the risk of diode laser detachment due to the high internal pressure. Additionally, it will reduce the beam pointing error caused by the displacement of the laser structure when the backsurface is impinged at high velocity.
- To reduce the misalignment of optics during the curing of the adhesive, it will be necessary to incorporate a microdrop dosage system capable to dispense adhesive with high reproducibility and positioning accuracy.
- A measurement system capable of observing simultaneously the near and far field profiles of the stacked beams during the positioning of the "edge" mirrors must be implemented.
- Modules must be assembled and tested in a "class 100" clean room to reduce the failure of the diode lasers due to laser facet contamination.

Finally, as the work developed in this thesis was a successful proof-of-concept of the use of LTCC material for the packaging of multiple BA diode lasers, future designs must incorporate a larger number of lasers per module with higher output powers to reach the power required for industrial applications.

APPENDIX 1

G-CODE TRANSLATOR SOFTWARE

As explain in Sec. 3.2.1 custom commands were created to instruct the movements of the translation stages in the CO_2 machinning system for the cutting of the required patterns in the LTCC layers. The use of custom instructions prevented us from directly converting design drawings into text files containing movement instructions, such as G-Code, which can be recognized by the motion controller. Every command for the movement of the translation stages was introduced manually in the input text file. As the complexity of the design was increased, the manual input became time-consuming and more prone to typing errors. For example, some of our text files required the input up to 1800 code lines. To speed up the process, an interpreter on the LabView platform to translate a G-code file to a text file containing instructions recognized by the control software of the machining system was created.

The flow process involved drawing the required pattern on TurboCAD 2D (IMSI Design, USA) and saving it as DXF file. A layer of the design of the LTCC water-jet cooler for a single-emitter BA laser is shown in Fig. A1.

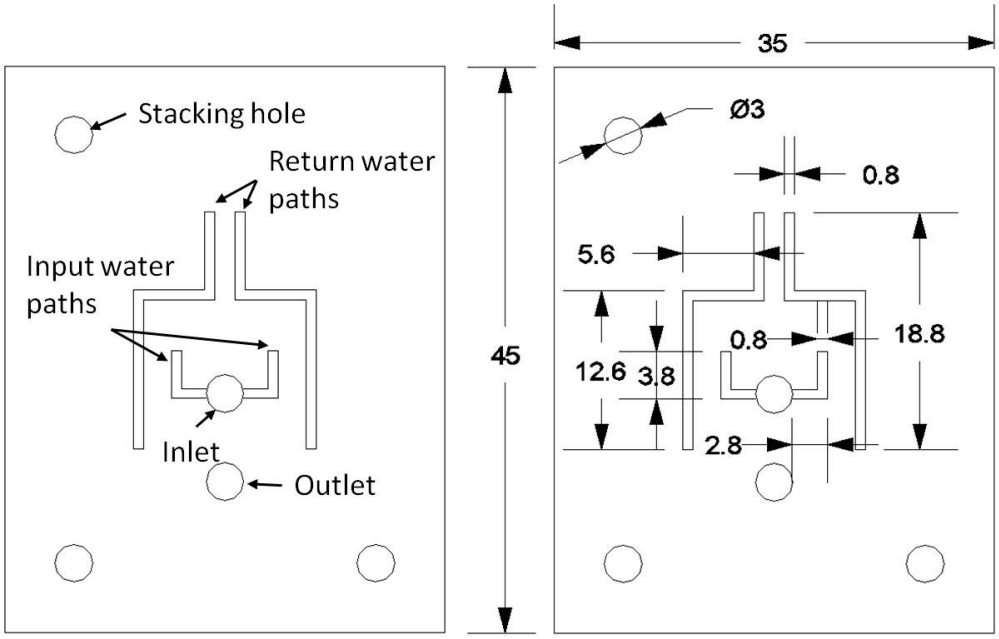

Figure A. 1. Drawing generated using TurboCAD 2D.

Next, the DXF file is converted to a G-code file using the CAM Expert (RibbonSoft, Germany) software. It generates a text file containing movement instructions. The next lines of code are the instructions needed to cut the pattern shown in Fig. A.1.

JET COOLERS IN HERAEUS.nc

```
N10 G00 Z100.000
N15 G00 X14.000 Y24.000
N20 Z2.0 F200
N25 G01 Z-0.2
N30 G03 X14.000 Y24.000 I-1.500 J0.000
N35 G00 Z2.0
N40 X38.000 Y24.000
N45 G01 Z-0.2
N50 G03 X38.000 Y24.000 I-1.500 J0.000
N55 G00 Z2.0
N60 X14.000 Y58.050
N65 G01 Z-0.2
N70 G03 X14.000 Y58.050 I-1.500 J0.000
N75 G00 Z2.0
N80 X26.000 Y37.500
N85 G01 Z-0.2
N90 G03 X26.000 Y37.500 I-1.500 J0.000
N95 G00 Z2.0
N100 X26.000 Y30.500
N105 G01 Z-0.2
N110 G03 X26.000 Y30.500 I-1.500 J0.000
N115 G00 Z2.0
N120 X7.000 Y63.500
N125 G01 Z-0.2
N130 Y18.500
N135 X42.000
N140 Y63.500
N145 X7.000
N150 G00 Z2.0
N155 X26.130 Y48.730
N160 G01 Z-0.2
N165 Y51.900
N170 X25.328
N175 Y48.730
N180 Y44.928
N185 X30.945
N190 Y33.099
N195 X31.747
N200 Y45.730
N205 X26.130
```

```
N210 Y48.730
N215 G00 Z2.0
N220 X22.880
N225 G01 Z-0.2
N230 Y45.730
N235 X17.253
N240 Y33.099
N245 X18.055
N250 Y44.928
N255 X23.682
N260 Y48.730
N265 Y51.900
N270 X22.880
N275 Y48.730
N280 G00 Z2.0
N285 X25.945 Y37.099
N290 G01 Z-0.2
N295 X28.747
N300 Y40.901
N305 X27.945
N310 Y37.901
N315 X25.945
N320 G00 Z2.0
N325 X23.055
N330 G01 Z-0.2
N335 X21.055
N340 Y40.901
N345 X20.253
N350 Y37.099
N355 X23.055
N360 G00 Z2.0
N365 M30
```

From the previous set of instructions, commands that need to be translated in order to be recognized by our software are:

- G00 XA YB, go to the position (A, B)
- XA, YB, go to the position (A, B).
- G03 XA YB IC J, it generates a full circle with centre in (A, B) and radius of C.
- XA, move the table A distance in the X direction.
- YB, move the table B distance in the Y direction.

The remaining lines are ignored. Next, the useful G-code lines are converted to recognizable instructions using our translator software and saved in a text file.

- G00 XA YB is replaced by g0 xA yB. This instruction indicates to the laser system to move the translation stages to the (A, B) position.
- XA, YB is replaced by g0 xA yB. This instruction indicates to the laser system to move the translation stages to the (A, B) position.
- G03 XA YB IC J is replaced by Arc A B C 0.000 360 1.000. This instruction indicates to the laser system to generate a full circle with centre in (A, B) and radius of C, firing a laser shot every dU mm.
- XA is replaced by LineX A. This instruction indicates to the laser system to move the translation stage X a distance of A mm, firing a laser shot every dU mm.
- YB is replaced by LineY B. This instruction indicates to the laser system to move the translation stage Y a distance of B mm, firing a laser shot every dV mm.

Additionally, the user must introduce manually the next parameters in the user interface (GUI) of the translations software:

- The name of the G-Code source file
- The focal position of the final lens mounted on the motorized vertical translation stage (“Header”)
- The speed of the translation stages (“Feed rate”)
- The pitch between laser shots in X and Y direction (“Raster pitch” dU, dV)
- Pulse width duration (“AOM pulse width”, x50 µs)
- Output power level on target (“AOM voltage”)

The Fig. A.2 shows the GUI of the translator software.

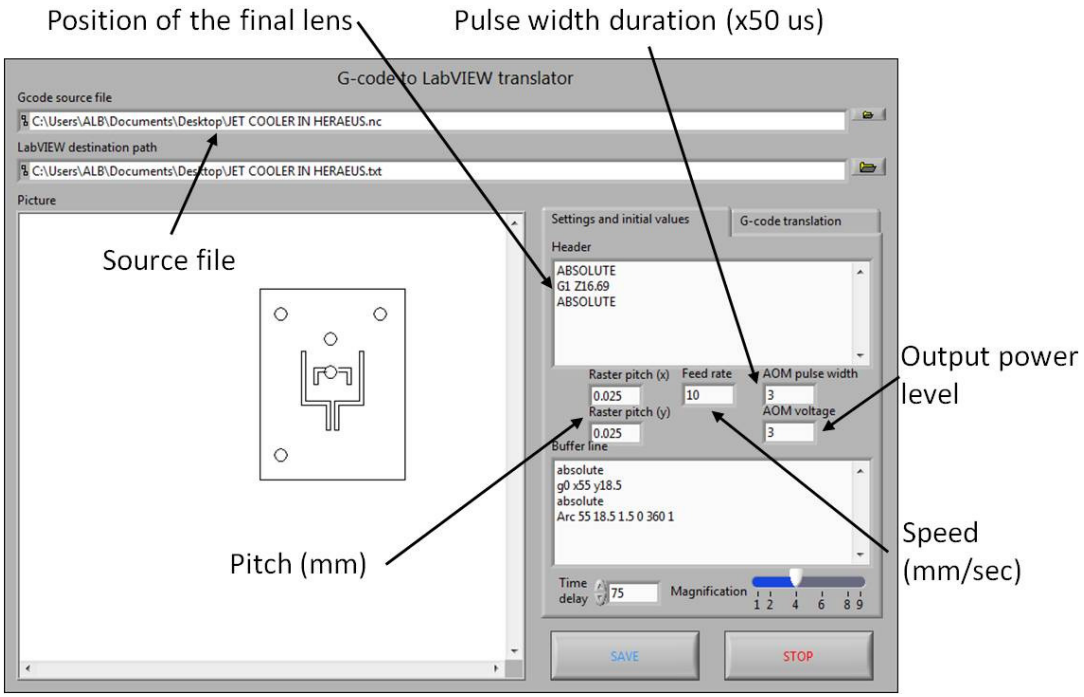

Figure A. 2. GUI of the translator software

The next lines of code are the instructions generated by the translator software. The text file is introduced in the CO_2 machining system for cutting the pattern shown in Fig. A.1.

JET COOLERS IN HERAEUS.txt

ABSOLUTE
G1 Z16.69
ABSOLUTE
RasterdU 0.025
RasterdV 0.025
FeedRate 10.000000
AOMPulseWidthTicks 3.000000
VAOM 3.000000
absolute
g0 x55 y18.5
absolute
Arc 55 18.5 1.5 0 360 1
g0 x14.000 y24.000
absolute
g0 x14.000 y24.000
Arc 12.500 24.000 1.500 0.000 360.000 1.000
Arc 12.500 24.000 1.500 0.000 360.000 1.000
g0 x38.000

absolute
g0 x38.000 y24.000
Arc 36.500 24.000 1.500 0.000 360.000 1.000
Arc 36.500 24.000 1.500 0.000 360.000 1.000
g0 x14.000 y58.050
absolute
g0 x14.000 y58.050
Arc 12.500 58.050 1.500 0.000 360.000 1.000
Arc 12.500 58.050 1.500 0.000 360.000 1.000
g0 x26.000 y37.500
absolute
g0 x26.000 y37.500
Arc 24.500 37.500 1.500 0.000 360.000 1.000
Arc 24.500 37.500 1.500 0.000 360.000 1.000
g0 y30.500
absolute
g0 x26.000 y30.500
Arc 24.500 30.500 1.500 0.000 360.000 1.000
Arc 24.500 30.500 1.500 0.000 360.000 1.000
g0 x7.000 y63.500
LineY -45.000
LineX 35.000
LineY 45.000
LineX -35.000
LineX 35.000
LineY -45.000
LineX -35.000
LineY 45.000
absolute
g0 x7.000 y63.500
g0 x26.130 y48.730
LineY 3.170
LineX -0.802
LineY -3.170
LineY -3.802
LineX 5.617
LineY -11.829
LineX 0.802
LineY 12.631
LineX -5.617
LineY 3.000
LineY -3.000
LineX 5.617
LineY -12.631
LineX -0.802
LineY 11.829
LineX -5.617

LineY 3.802
LineY 3.170
LineX 0.802
LineY -3.170
absolute
g0 x26.130 y48.730
g0 x22.880
LineY -3.000
LineX -5.627
LineY -12.631
LineX 0.802
LineY 11.829
LineX 5.627
LineY 3.802
LineY 3.170
LineX -0.802
LineY -3.170
LineY 3.170
LineX 0.802
LineY -3.170
LineY -3.802
LineX -5.627
LineY -11.829
LineX -0.802
LineY 12.631
LineX 5.627
LineY 3.000
absolute
g0 x22.880 y48.730
g0 x25.945 y37.099
LineX 2.802
LineY 3.802
LineX -0.802
LineY -3.000
LineX -2.000
LineX 2.000
LineY 3.000
LineX 0.802
LineY -3.802
LineX -2.802
absolute
g0 x25.945 y37.901
g0 x23.055
LineX -2.000
LineY 3.000
LineX -0.802
LineY -3.802

```
LineX 2.802
LineX -2.802
LineY 3.802
LineX 0.802
LineY -3.000
LineX 2.000
absolute
g0 x23.055 y37.099
END
```

Cutting instructions are repeated twice because as explain in Sec. 3.5, the optimal condition for cutting the 130 µm HL2000 tape are double pass, using 150 µs pulses spaced by 25 µm.

The use of this translation software reduced the time of generating the text file from hours to less than 15 minutes.

REFERENCES

[1] M. Behringer, "High-Power Diode Laser Technology and Characteristics," in *High Power Diode Lasers: Technology and Applications* New York: Springer, 2007, pp. 5-73.

[2] G. Erbert, A.Barwolff, J. Sebastian, and J. Tomm, "High-Power Broad-Area Diode Lasers and Laser Bars," in *High-power diode lasers: fundamentals, technology, applications*, R. Diehl, Ed. Berlin: Springer, 2000, pp. 173-223.

[3] M. M. Apter and F. Leibreich, "HIGH-POWER SEMICONDUCTOR SOURCES: High-power diode-laser bars come of age," in *Laser Focus World*. vol. 42, March 2006.

[4] R. Szweda, "Novalas - taking lasers into the 21st century," in *III-Vs Review*. vol. 11, 1998, pp. 18-21.

[5] F. Bachmann, "Present technology, industrial applications and future prospects of high power diode lasers," in *ALT'01 International Conference on Advanced Laser Technologies*, Constanta, Romania, 2002, pp. 1-15.

[6] S. Strohmaier, C. Tillkorn, P. Olschowsky, and J. Hostetler, "High-Power, High-Brightness Direct-Diode Lasers," in *OPN Optics & Photonics News*, October 2010, pp. 25-29.

[7] M. T. Knapczyk, J. H. Jacob, H. Eppich, A. K. Chin, K. D. Lang, J. T. Vignati, and R. H. Chin, "70% efficient near 1kW single 1-cm laser-diode bar at 20°C," in *High-Power Diode Laser Technology and Applications IX*, San Francisco, CA, USA, 2011, pp. 79180F-79180F.

[8] K. Paschke, S. Einfeldt, C. Fiebig, A. Ginolas, K. Häusler, P. Ressel, B. Sumpf, and G. Erbert, "10 W reliable operation of 808 nm broad-area diode lasers by near field distribution control in a multstripe contact geometry," in *High-Power Diode Laser Technology and Applications V*, San Jose, California, USA, 2007, pp. 64560H-1-64560H-5.

[9] H. Treusch, J. Harrison, R. Morris, J. J. Powers, D. Brown, and J. Martin, "Compact high-brightness and high-power diode laser source for materials processing " in *Laser Diodes and LEDs in Industrial, Measurement, Imaging, and Sensors Applications II; Testing, Packaging, and Reliability of Semiconductor Lasers V* San Jose, CA, USA, 2000.

[10] J. Sebastian, G. Beister, F. Bugge, F. Buhrandt, G. Erbert, H. G. Hänsel, R. Hülsewede, A. Knauer, W. Pittroff, R. Staske, M. Schröder, H. Wenzel, M. Weyers, and G. Tränkle, "High-Power 810-nm GaAsP–AlGaAs Diode Lasers With Narrow Beam Divergence," *IEEE J. SEL. TOP. QUANT. ,* vol. 7, pp. 334-339, 2001.

[11] T. Ebert, G. Treusch, P. Loosen, and R. Poprawe, "Optimisation of micro channel heat sinks for high power diode lasers in copper technology," in *Fabrication, Testing, Reliability, and Applications of Semiconductor Lasers III*, Bellingham, WA, USA, 1998.

[12] E. F. Stephens, "Characterization of Exotic Material Heat Sinks for Laser Diode Arrays," in *MRS Spring Meeting*, San Francisco, CA, USA, 2005.

[13] A. Yuen, "Telecom packaging improves reliability of high-power lasers," in *Laser Focus World*, July 2007.

[14] F. Amzajerdian, B. L. Meadows, N. R. Baker, B. W. Barnes, R. S. Baggott, G. E. Lockard, U. N. Singh, and M. J. Kavaya, "Improving Reliability of High Power Quasi-CW Laser Diode Arrays for Pumping Solid State Lasers," in *Lidar Remote Sensing for Environmental Monitoring VI*, San Diego, CA, USA, 2005, pp. 78-84.

[15] R. Stevenson, "nLight expands wavelength range in order to attack new markets," in *Compound Semiconductor*. vol. 12, May 2006, pp. 26-27.

[16] V. Krause, H. G. Treusch, B. DeOdorico, M. Marchiano, H. Oestreicher, F. Robert, A. Koesters, J. Biesenbach, P. Loosen, and T. Kimpel, "Microchannel coolers for high-power laser diodes in copper technology," in *Laser Diode Technology and Applications VI*, Los Angeles, CA, USA 1994, pp. 351-358.

[17] R. Beach, W. J. Benett, B. L. Freitas, D. Mundinger, B. J. Comaskey, R. W. Solan, and M. A. Emanuel, "Modular Microchannel Cooled Heatsinks for High Average Power Laser Diode Arrays," *IEEE J.Quantum Electron.,* vol. 28, pp. 966-976, 1992.

[18] P. Loosen, "Cooling and Packaging of High-Power Diode Lasers," in *High-power diode lasers: fundamentals, technology, applications*, R. Diehl, Ed. Berlin: Springer, 2000, pp. 289-301.

[19] J. M. Haake and B. O. Faircloth, "Requirements for long-life microchannel coolers for direct diode laser systems " in *High-Power Diode Laser Technology and Applications III* San Jose, CA, USA 2005.

[20] G. Treusch, R. Srinivasan, D. Brown, R. Miller, and J. Harrison, "Reliability of Water Cooled High Power Diode Laser Modules," in *High-Power Diode Laser Technology and Applications III*, San Jose, CA, USA, 2005.

[21] H. Miyajima, H. Kan, T. Kanzaki, and S. Furuta, "Jet-type, water-cooled heat sink that yields 255-W continuous-wave laser output at 808 nm from a 1-cm laser diode bar," *Opt. Lett,* vol. 29, pp. 304-306, 2004.

[22] R. Feeler, J. Junghans, G. Kemner, and E.Stephens, "Next-generation microchannel coolers," in *High-Power Diode Laser Technology and Applications VI* San Jose, CA, USA, 2008.

[23] M. Leers, T. Westphalen, and E. Liermann, "Both Sides Cooled Packages for High-Power Diode Laser Bars," in *The 60th Electronic Components and Technology Conference*, Las Vegas , NV, USA 2010, pp. 708-712.

[24] L. Zhong and X. Ma, "Recent Developments in High Power Semiconductor Diode Lasers," in *Optoelectronics - Devices and Applications*, P. Predeep, Ed. Rijeka: InTech, 2011, pp. 325-348.

[25] K. Price, F. Pfeffer, P. Leisher, S. Karlsen, and R. Martinsen, "KW-class industrial diode lasers comprised of single emitters " in *High-Power Diode Laser Technology and Applications VIII* San Francisco, CA, USA, 2010.

[26] S. J. Horowitz, D. I. Amey, B. E. Taylor, and M. Doyle, "Next-generation Packaging for Fiber Optics & MEMS," in *Advanced Packaging Magazine*. vol. 11, January 2002.

[27] K. M. Nowak, H. J. Baker, D. R. Hall, X. Liu, and A. Bell, "Low-loss passive alignment of single-mode fibres in low-temperature cofired ceramics using CO2 laser fabricated U-grooves," *Appl. Opt.,* vol. 45, pp. 9168-9175, 2006.

[28] Y. Imanaka, "Introduction," in *Multilayered Low Temperature Cofired Ceramics (LTCC) Technology* New York: Springer, 2005, pp. 1-17.

[29] W. A. Vitriol and J. I. Steinberg, "Development of a Low Temperature Cofired Multilayer Ceramic Technology," in *ISHM '83*, Philadelphia, 1983, pp. 593-598.

[30] M. R. Gongora-Rubio, P. Espinoza-Vallejos, L. Sola-Laguna, and J. J. Santiago-Aviles, "Overview of low temperature co-fired ceramics tape technology for meso-system technology (MsST)," *Sensors and Actuators A: Physical* vol. 89, pp. 222-241, 2001.

[31] J. H. Alexander and A. S. Shaikh, "The Use of Silver And Silver Plus Gold Conductors with the Ferro Low Temperature Tape," in *IEEE 43rd Electronic Components and Technology Conference*, Orlando, FL, USA, 1993, pp. 888-892.

[32] Y. Imanaka, "Casting," in *Multilayered Low Temperature Cofired Ceramics (LTCC) Technology* New York, USA: Springer, 2005, pp. 113-144.

[33] H. Jantunena, R. Rautioahob, A. Uusimäkia, and S. Leppävuori, "Compositions of MgTiO3–CaTiO3 ceramic with two borosilicate glasses for LTCC technology " *Journal of the European Ceramic Society,* vol. 20, pp. 2331-2336, 2000.

[34] D. Suvorov and M. Valant, "Bi-Based Compounds for Glass-Free LTCC Technology," *J. Ceram. Soc. Jap,* vol. 112-1, pp. S1557-S1562, 2004.

[35] J. H. Jean, S. C. Lin, and C. R. Chang, "Low-Temperature, Low-Dielectric, Crystallizable Glass Composite," *IEEE Trans. Compon., Packag., Manuf. Technol. B,* vol. 18, pp. 751-754, 1995.

[36] J. H. Jean and T. K. Gupta, "Liquid-phase sintering in the glass-cordierite system " *Journal of Materials Science* vol. 27, pp. 1575-1584, 1992.

[37] M. F. Zawrah and E. M. A. Hamzawyb, "Effect of cristobalite formation on sinterability, microstructure and properties of glass/ceramic composites " *Ceramics International,* vol. 28, pp. 123-130, 2002.

[38] R. M. German, P. Suri, and S. J. Park, "Review: liquid phase sintering " *Journal of Materials Science* vol. 44, pp. 1-39, 2009.

[39] D. Hotza and P. Greilb, "Review: aqueous tape casting of ceramic powders," *Materials Science and Engineering A,* vol. 202, pp. 206-217, 1995.

[40] W. K. Jones, Y. Liu, B. Larsen, P. Wang, and M. Zampino, "Chemical, Structural, and Mechanical Properties of the LTCC Tapes," *Int. J. Microcircuits Electron. Packag.,* vol. 23, pp. 469-473, 2000.

[41] Y. Cho, J. R. Rellick, and K. W. Hang, "LTCC TAPE COMPOSITION ", E. P. Office, Ed.: E.I. DU PONT DE NEMOURS AND COMPANY 2009, p. 15.

[42] J. P. Bertinet, E. Leleux, J. P. Cazenave, J. P. Ganne, M. Pate, R. Lebourgeois, E. Mueller, and F. Bechtold, "Filtering capacitors embedded in LTCC substrates for RF and microwave applications," *Microwave Journal,* vol. 50, pp. 72-87, 2007.

[43] Y. Imanaka, "Printing and Laminating," in *Multilayered Low Temperature Cofired Ceramics (LTCC) Technology* New York: Springer, 2005, pp. 145-166.

[44] M. A. Piwonski and A. Roosen, "Low pressure lamination of ceramic green tapes by gluing at room temperature," *Journal of the European Ceramic Society,* vol. 19, pp. 263-270, 1999.

[45] A. Rosen, "New lamination technique to join ceramic green tapes for the manufacturing of multilayer devices " *Journal of the European Ceramic Society,* vol. 21, pp. 1993-1996, 2001.

[46] D. Jurkow, H. Roguszczaka, and L. Golonkaa, "Cold chemical lamination of ceramic green tapes " *Journal of the European Ceramic Society,* vol. 2009, pp. 703-709, 2009.

[47] W. K. Jones, Y. Liu, and M. Gao, "Micro heat pipes in low temperature cofire ceramic (LTCC) substrates " *IEEE Trans. Compon. Packag. Technol.,* vol. 26, pp. 110-115, 2003.

[48] W. Smetanaa, B. Ballucha, G. Stangla, S. Lüftlc, and S. Seidlerc, "Processing procedures for the realization of fine structured channel arrays and bridging elements by LTCC-Technology " *Microelectronics Reliability,* vol. 49, pp. 592-599, 2009.

[49] H. Birol, T. Maeder, and P. Ryser, "Processing of graphite-based sacrificial layer for microfabrication of low temperature co-fired ceramics (LTCC)," *Sensors and Actuators A: Physical,* vol. 130-131, pp. 560-567, 2006.

[50] D. Schulze and W. A. Schiller, "Burnout of Organic Components of Glass Ceramic Composite Tapes: Thermoanalytical investigations " *Journal of Thermal Analysis and Calorimetry* vol. 52, pp. 211-219, 1998.

[51] L. Chai, A. Shaikh, and V. Stygar, "Self Adhesive Metallization (SAM) - A New Concept in LTCC Technology," in *The 34th Internationl Symposium on Microelectronics*, Baltimore, MD, USA, 2001.

[52] Y. Imanaka, "Conducting material," in *Multilayered Low Temeprature Cofired Ceramics (LTCC) Technology* New York, USA: Springer, 2005, pp. 59-81.

[53] L. Chai, "New Wire Bondable Gold Thick Film Conductors For LTCC Applications," in *The 33th Internationl Symposium on Microelectronics*, Boston, MA, USA, 2000, pp. 702-705.

[54] M. Girardi, G. Barner, C. Lopez, B. Duncan, and L. Zawicki, "Response Predicting LTCC Firing Shiringake: A response Surface Analysis Study," in *The 41st International Symposium on Microelectronics*, Providence, RI, USA, 2008, pp. 330-335.

[55] M. Hintz, H. Thust, and E. Polzer, "Generic investigation on 0-shrinkage processed LTCC," in *IMAPS Nordic 2002 Conference*, Stockholm, Sweden, 2002.

[56] F. Lautzenhiser and E. Amaya, "HeraLock^{TM} 2000 Self-constrained LTCC Tape," in *International Conference on Advanced Packaging and Systems*, Reno, NV, USA, 2002, pp. 143-149.

[57] F. Lautzenhiser, E. Amaya, and J. T. Hochheimer, "Self-constrained low temperature glass-ceramic unfired tape for microelectronics and methods for making and using the same." vol. US 6,743,534 B2 USA: Heraeus Incorporated, West Conshohocken, PA, USA, 2004.

[58] C. Q. Scrantom and J. C. Lawson, "LTCC Technology Where we are and where we're going - II," in *1999 IEEE MTT-S Symposium on Technologies for Wireless Applications*, Vancouver, BC, Canada, 1999, pp. 193-200.

[59] K. Imen and S. D. Allen, "Pulse CO_2 Laser Drilling of Green Alumina Ceramic," *IEEE Trans. Adv. Packag,* vol. 22, pp. 620-623, 1999.

[60] A. Slocombe, J. Clarke, and L. Li, "The effect of pigment addition in diode laser ablation machining of ceramic/polymer composite material " *Appl. Surf. Sci. ,* vol. 168, pp. 21-24, 2000.

[61] J. Kita, A. Dziedzic, L. J. Golonka, and T. Zawada, "Laser treatment of LTCC for 3D structures and elements fabrication," *Microelectronics International,* vol. 19, pp. 14-18, 2002.

[62] L. Rebenklau, K. J. Wolter, and G. Hagen, "Realization of µ-Vias in LTCC Tape," in *ISSE 2006 29th International Spring Seminar on Electronics Technology*, St.Marienthal, Germany, 2006, pp. 55-63.

[63] K. M. Nowak, H. J. Baker, and D. R. Hall, "Cold processing of green state LTCC with a CO2 laser " *Appl. Phys. A,* vol. 84, pp. 267-270, 2006.

[64] K. M. Nowak, H. J. Baker, and D. R. Hall, "A model for “cold” laser ablation of green state ceramic materials," *Appl. Phys. A: Mater. Sci. Process.,* vol. 91, pp. 341-348, 2008.

[65] L. J. Golonka, "New application of LTCC technology," in *ISSE 2005 28th International Spring Seminar on Electronics Technolog*, Wiener Neustadt, Austria, 2005, pp. 162-166.

[66] Y. L. Low, R. E. Scotti, D. A. Ramsey, C. A. Bolle, S. P. O’Neill, and K. C. Nguyen, "Packaging of Optical MEMS Devices," *J. Electron. Packag.,* vol. 125, pp. 325-328, 2003.

[67] J. Heilala, K. Keränen, J.-T. Mäkinen, O. Väätäinen, K. Kautio, P. Voho, and P. Karioja, "LTCC technology for cost-effective packaging of photonic modules," *Assembly Automation,* vol. 25, pp. 30-37, 2005.

[68] J. Youngsman, B. Marx, M. Schimpf, S. Wolter, J. Glass, and A. Moll, "Low temperature co-fired ceramics for micro-fluidics," in *56th Electronic Components & Technology Conference*, San Diego, CA, USA, 2006, pp. 699-704.

[69] F. Barlow, J. Wood, A. Elshabini, E. F. Stephens, R. Feeler, G. Kemner, and J. Junghans, "Fabrication of Precise Fluidic Structures in LTCC," *INT. J. APPL. CERAM. TEC.,* vol. 6, pp. 18-23, 2009.

[70] K. Malecha and L. J. Golonka, "Three-dimensional structuration of zero-shrinkage LTCC ceramics for microfluidic applications," *Microelectronics Reliability,* vol. 49, pp. 585-591, 2009.

[71] K. Malecha, D. Jurków, and L. J. Golonka, "Comparison of solvent and sacrificial volume-material-based lamination processes of low-temperature co-fired ceramics tapes " *J. Micromech. Microeng.,* vol. 19, pp. 1-10, 2009.

[72] F. Tuinstra and J. L. Koening, "Raman Spectrum of Graphite," *J. Chem. Phys.,* vol. 53, pp. 1126-1130, 1970.

[73] R. A. Friedel and G. L. Carlson, "Infrared Spectra of Ground Graphite," *J. of Phys. Chem.,* vol. 75, pp. 1149-1151, 1971.

[74] E. N. Wang, L. Zhang, L. Jiang, J.-M. Koo, J. G. Maveety, E. A. Sanchez, K. E. Goodson, and T. W. Kenny, "Micromachined jets for liquid impingement cooling of VLSI chips," *J. Microelectromech. Syst. ,* vol. 13, pp. 833-842, 2004.

[75] C. Glynn, T. O'Donovan, and D. B. Murray, "Jet Impingement Cooling," in *UK National Heat Transfer Conference*, Manchester, UK, 2005, pp. PS3-01 - PS3-09.

[76] W. A. Vitriol, "Thick Film & Ceramic Technologies for Hybrid MCMs," in *Multichip Module Technologies and Alternatives: The Basics*, D. A. Doane and P. D. Franzon, Eds. New York: Springer, 1992, pp. 215-253.

[77] R. K. Yamamoto, R. S. Pessoa, M. R. Gongora-Rubio, and H. S. Maciel, "Development of a Microsystem for Plasma Generation," in *6th Ibero-American Congress on Sensors IBERSENSOR 2008* São Paulo, Brazil 2008, pp. 450-455.

[78] X. Shan, Y. C. Soh, C. W. P. Shi, C. K. Tay, K. M. Chua, and C. W. Lu, "Large-area patterning of multilayered green ceramic substrates using micro roller embossing," *J. Micromech. Microeng.,* vol. 18, pp. 1-8, 2008.

[79] L. E. Khoong, Y. M. Tan, and Y. C. Lam, "Study of deformation and porosity evolution of low temperature co-fired ceramic for embedded structures fabrication," *J. Eur. Ceram. Soc.,* vol. 29, pp. 2337-2745, 2009.

[80] L. E. Khoong, Y. M. Tan, and Y. C. Lam, "Carbon burnout and densification of self-constrained LTCC for fabrication of embedded structures in a multi-layer platform," *J. Eur. Ceram. Soc.,* vol. 29, pp. 457-463, 2009.

[81] R. Manepalli, F. Stepniak, S. A. Bidstrup-Allen, and P. A. Kohl, "Silver Metallization for Advanced Interconnects," *IEEE Trans. Adv. Packag.,* vol. 22, pp. 4-8, 1999.

[82] M. E. Ferguson, C. D. Fieselman, and M. A. Elkins, "Manufacturing Concerns When Soldering with Gold Plated Component Leads or Circuit Board Pads," *IEEE Trans. Compon. Packag. Manuf. Technol. C,* vol. 20, pp. 188-193, 1997.

[83] M. Kondo, "Dispensable Adhesive Benchmarking," in *Nepcon West 2000*, Anaheim CA, USA, 2000.

[84] G. E. Servais and S. D. Brandenburg, "Wire Bonding – A Closer Look," in *The 17th International Symposium for Testing & Failure Analysis*, Los Angeles, CA, USA, 1991, pp. 525-529.

[85] S. J. Hu, G. E. Lim, T. L. Lim, and K. P. Foong, "Study of Temperature Parameter on the Thermosonic Gold Wire Bonding of High-speed CMOS," *IEEE Trans. Compon. Hybrids, Manufact. Technol.,* vol. 14, pp. 855-858, 1991.

[86] S. J. Hu, R. K. S. Lim, and G. Y. Sow, "Gold Wire Weakening in the Thermosonic Bonding of the First Bond," *IEEE Trans. Compon. Packag. Manuf. Technol. A,* vol. 18, pp. 230-234, 1995.

[87] S. V. Garimella and R. A. Rice, "Confined and Submerged Liquid Jet Impingement Heat Transfer," *J. Heat Transfer,* vol. 117, pp. 871-877, 1995.

[88] J. Stevens and B. W. Webb, "Local Heat Transfer Coefficients Under an Axisymmetric, Single-Phase Liquid Jet," *J. Heat Transfer,* vol. 113, pp. 71-78, 1991.

[89] N. Zuckerman and N. Lior, "Jet Impingement Heat Transfer: Physics, Correlations, and Numerical Modeling," *Adv. Heat Transfer,* vol. 39, pp. 565-631, 2006.

[90] B. Köhler, T. Brand, M. Haag, and J. Biesenbach, "Wavelength stabilized high-power diode laser modules," in *High-Power Diode Laser Technology and Applications VII*, San Jose, CA, USA, 2009, pp. 719810-1 719810-12.

[91] A. Moser, A. Oosenbrug, E. E. Latta, T. Forster, and M. Gasser, "High-power operation of strained InGaAs/AlGaAs single quantum well lasers " *Appl. Phys. Lett. ,* vol. 59, pp. 2642-2644, 1991.

[92] M. Voss, C. Lier, U. Menzel, A. Barwolff, and T. Elsaessera, "Time-resolved emission studies of GaAs/AlGaAs laser diode arrays on different heat sinks," *J. Appl. Phys.,* vol. 79, pp. 1170-1172, 1996.

[93] F. Klopf, S. Deubert, J. P. Reithmaier, and A. Forchel, "Correlation between the gain profile and the temperature-induced shift in wavelength of quantum-dot lasers," *Appl. Phys. Lett.,* vol. 81, pp. 217-219, 2002.

[94] G. Ropars, M. Vallet, M. Brunel, A. L. Floch, and G. P. Agrawa, "Asymmetric Russian-Doll Model for Semiconductor Lasers," *IEEE Photonic Tech. L.,* vol. 17, pp. 747-749, 2005.

[95] X. Liu, L. C. Hughes, M. H. Rasmussen, M. H. Hu, V. A. Bhagavatula, R. W. Davis, S. Coleman, R. Bhat, and C. Zah, "Packaging and Performance of 980nm Broad Area Semiconductor Lasers," in *6th International Conference on Electronic Packaging Technology*, Shenzhen, China, 2005, pp. 67-73.

[96] V. Gapontsev, I. Berishev, G. Ellis, A. Komissarov, N. Moshegov, O. Raisky, P. Trubenko, V. Ackermann, E. Shcherbakov, J. Steinecke, and A. Ovtchinnikov, "High-efficiency 970-nm multimode pumps," in *High-Power Diode Laser Technology and Applications III* San Jose, CA, USA, 2005.

[97] S. O'Brien, H. Zhao, and R. J. Lang, "High power wide aperture AIGaAs-based lasers at 870nm," *Electron. Lett. ,* vol. 34, pp. 184-186, 1998.

[98] A. Campos-Zatarain, A. McKay, H. J. Baker, D. R. Hall, and M. Desmulliez, "High-Quality CO_2 Laser Machining of LTCC Structures for Thermal Management of a Group of Single-Emitter Laser Diodes," in *IMAPS 2009 42nd International Symposium on Microelectronics* San Jose, CA, USA, 2009, pp. 452-458.

[99] M. Szymański, "Two-dimensional model of heat flow in broad-area laser diode: Discussion of the upper boundary condition," *Microelectronics Journal,* vol. 38, pp. 771-776, 2007.

[100] U. Brauch, P. Loosen, and H. Opower, "High-Power Diode Lasers for Direct Applications," in *High-Power Diode Lasers: Fundamentals, Technology, Applications*, R. Diehl, Ed. Germany: Springer, 2000.

[101] C. Gaertner, V. Bluemel, B. Hoefer, A. Kraeplin, T. Possner, and P. Schreiber, "Assembly processes for micro-optical beam transformation systems for high power diode laser bars and stacks," in *MOEMS and Miniaturized Systems*, Santa Clara, CA, USA, 2000, pp. 147-155.

[102] P. Loosen and A. Knitsch, "Accuracy of Alignment of FAC-Lenses," in *High power diode lasers : Technology and applications*, F. Bachmann, P. Loosen, and R. Poprawe, Eds.: Springer, 2007, pp. 131-135.

[103] J. F. Monjardin, K. M. Nowak, H. J. Baker, and D. R. Hall, "Correction of beam errors in high power laser diode bars and stacks," *OPT. EXPRESS* vol. 14, pp. 8178-8183, 2006.

[104] S. R. Karlsen, R. K. Kirk, M. Reynolds, A. Brown, R. Mehl, S. Patterson, and R. J. Martinsen, "100-W, 105-µm, 0.15NA Fiber Coupled Laser Diode Module," in *High-Power Diode Laser Technology and Applications VII* San Jose, CA, USA, 2009, p. 71980T.

[105] T. Hausken, "Battle heats up between bars and single-emitter diodes," in *Laser Focus World*. vol. 42, August 2006, pp. 69-70.

[106] R. Duesterberg, L. Xu, J. A. Skidmore, J. Guo, J. Cheng, J. Du, B. Johnson, D. L. Vecht, N. Guerin, B. Huang, D. Yin, P. Cheng, R. Raju, K. W. Lee, J. Cai, V. Rossin, and E. P. Zucker, "100W high-brightness multi-emitter laser pump " in *High-Power Diode Laser Technology and Applications IX* San Francisco, CA, USA, 2011, pp. 79180V1 - 79180V-8

[107] X. Qiu, Y. Dai, M. Au, J. Guo, V. Wong, V. Rossin, D. Venables, J. Skidmore, and E. Zucker, "A High Power, High-Brightness Multi-Single-Emitter Laser Pump Platform," in *High-Power Diode Laser Technology and Applications VII*, San Jose, CA, USA 2009, pp. 71980Z-1 - 71980Z-6.

[108] M. Werner, C. Wessling, S. Hengesbach, M. Traub, and H.-D. Hoffmann, "100 W / 100 µm passively cooled, fiber coupled diode laser at 976 nm based on multiple 100 µm single emitters," in *High-Power Diode Laser Technology and Applications VII*, San Jose, CA, USA, 2009, pp. 71980P-1 - 71980P-7.

[109] D. Wilson, R. Duesterberg, L. Xu, and J. Skidmore, "LASER BEAM COMBINING: Beam-combining improvements optimize laser-diode pump sources," in *Laser Focus Wold*. vol. 47, August 2011, pp. 45-48.

[110] M. Levy, N. Rapaport, D. Yanson, Y. Karni, M. Shamay, R. Tessler, and Y. Don, "High power single emitters for fiber coupled diode packages," in *High-Power Diode Laser Technology and Applications X* San Francisco, CA, USA: SPIE, 2012.

[111] L. Bao, M. A. Devito, M. Grimshaw, P. O. Leisher, H. Zhou, W. Dong, X. Guan, S. Zhang, R. J. Martinsen, and J. Haden, "High performance diode lasers emitting at 780-820 nm " in *High-Power Diode Laser Technology and Applications X* San Francisco, CA, USA SPIE, 2012.

[112] S. J. McGinily, R. H. Abram, E. Riis, and A. I. Ferguson, "Efficient coupling of several broad area laser diodes into an optical fiber," *Rev. Sci. Instrum,* vol. 77, pp. 116101-1 - 116101-3 2006.

[113] M. Haag, B. Köhler, J. Biesenbach, and T. Brand, "Novel high-brightness fiber coupled diode laser device," in *High-Power Diode Laser Technology and Applications V*, San Jose, CA., USA, 2007, pp. 64560T-1 - 64560T-8.

[114] Z. Wang, A. Segref, T. Koenning, and R. Pandey, "Fiber Coupled Diode Laser Beam Parameter Product Calculation and Rules for Optimized Design," in *High-Power Diode Laser Technology and Applications IX*, San Francisco, CA, USA, 2011, pp. 7918-8-1 - 7918-8-10.